EXAMINATION OF MITOCHONDRIAL MORPHOLOGY AND MOVEMENT WITHIN SKELETAL MUSCLE

SOBIA IQBAL

A DISSERTATION SUBMITTED TO THE FACULTY OF GRADUATE STUDIES IN PARTIAL FULFILMENT OF THE REQUIREMENTS FOR THE DEGREE OF

DOCTOR OF PHILOSOPHY

GRADUATE PROGRAMME IN KINESIOLOGY AND HEALTH SCIENCE
YORK UNIVERSITY
TORONTO, ONTARIO

January 2014

ABSTRACT

Mitochondria are vital organelles, critical for energy supply and cell survival. Such functional versatility is paralleled by the structural complexity of the organelle. Mitochondria are dynamic and can continuously alter their morphology. The movement of these organelles is controlled by their interaction with the cytoskeleton. To date, the morphology and movement of mitochondria in muscle has yet to be fully explored. Thus, the overall purpose of this Dissertation was to: 1) examine the effects of chronic muscle use and disuse on mitochondrial morphology and regularity protein expression, 2) investigate the cytoskeletal filaments responsible for governing mitochondrial movement within skeletal muscle cells, and 3) elucidate the effects of oxidative stress on organelle moment and morphology.

The mitochondrial network within cells is mediated by opposing fission and fusion processes. In Manuscript #1, we investigated the expression of the proteins responsible for these events during conditions of altered oxidative capacity within rat skeletal muscle. The results demonstrate that chronic muscle use increases the ratio of fusion:fission proteins, leading to reticular mitochondria, whereas muscle disuse and aging result in a decrease in this ratio, culminating in a disruption of the mitochondrial network, and fragmented organelles.

Manuscript #2 focuses on determining the cytoskeletal elements that are primarily responsible for mitochondrial movements in muscle cells, and asks whether calcium can influence organelle motility. Dynein and kinesins motor proteins use microtubules to transport cargo throughout the cell. The ability of mitochondria to respond to calcium has previously been found to be mediated by motor protein/adaptor complexes in neurons. Using live-cell imaging, we monitored

mitochondrial motility and found that they move primarily along microtubules tracks. Moreover, displacement of mitochondria is regulated by calcium, which inhibits organelle movements through the microtubule motor protein adapter, Milton. By understanding the regulation of these movements we elucidated the underlying basis for organelle interactions that lead to the formation of the mitochondrial reticulum, and the distribution of energy in muscle cells.

The focus of Manuscript #3 was to determine whether mitochondrial dynamics are altered after an acute exposure to oxidative stress. In addition, we elucidated the interplay between mitochondrial morphology and stress responses. Mitochondrial stress is speculated to result in the activation of at least three cellular responses, including mitophagy, and the mitochondrial- and the ER-unfolded protein responses. We found that oxidative stress halts mitochondrial movement and induces mitochondrial fragmentation in myoblasts. The observed oxidative stress-induced mitochondrial fragmentation is mediated by Drp1. Moreover, we demonstrated that the unfolded protein responses are activated prior to the initiation of mitophagy during oxidative stress.

Collectively, our data illustrate that mitochondrial morphology is affected during conditions of chronic muscle use and disuse, and the movement of mitochondria in muscle cells is influenced by both oxidative stress and calcium signalling.

ACKNOWLEDGMENTS

TABLE OF CONTENTS

LIST OF FIGURES

LIST OF ABBREVIATIONS

$\Delta\psi_m$	mitochondrial membrane potential
ADP	adenosine diphosphate
AMPK	ATP-dependent protein kinase
ATG7	autophagy related protein 7
ATP	adenosine triphosphate
Arp	actin related protein
BAX	Bcl-2 associated X protein
Bcl-2	B-cell lymphoma protein 2
C2C12	Mouse myoblast cell line
C	Celsius
CCA	chronic contractile activity
Ca^{2+}	calcium
CaM	calmodulin
CaMK	calmodulin-dependent protein kinase
CaMKII	calmodulin-dependent protein kinase II
CaMKIV	calmodulin-dependent protein kinase IV
CAMKKβ	calmodulin-dependent protein kinase kinase-beta
CHOP	C/EBP-homologous protein
COS-7	cell line from African green monkey kidney fibroblasts
COX	cytochrome c oxidase
CS	citrate synthase
C-terminal	carboxyl-terminus
DNA	deoxyribonucleic nucleic acid
Drp1	dynamin-related protein 1
ER	endoplasmic reticulum
ETC	electron transport chain
F344BN	Fischer 344 x Brown Norway rats
F-actin	filamentous actin
Fis1	fission 1
G-actin	globular actin
GFP	green fluorescent protein
GLUT4	glucose transporter
HeLa	Henrietta Lacks' cervical cancer cell line
H_2O_2	hydrogen peroxide
hours	hr
HSPs	heat shock proteins
Hz	frequency unit per second
IMM	inner mitochondrial membrane
IMF	intermyofibrillar
kDa	kilodalton
Kif	kinesin
LC3	light chain protein
Liquid N_2	liquid nitrogen
LKB1	liver kinase B1
MAC	mitochondrial apoptosis-inducing channel

MAPKs	mitogen-activated protein kinases
Mfn1	mitofusin 1
Mfn2	mitofusin 2
Mge1	mitochondrial heat shock protein interacting factor
min	minutes
Miro	mitochondrial Rho GTPase
mM	milli-Molar (concentration, 10^{-3})
MnSOD	manganese superoxide dismutase
mRNA	messenger ribonucleic acid
mt	mitochondria
mtDNA	mitochondrial DNA
mtPTP	mitochondrial permeability transition pore
MHC	myosin heavy chain
n	sample size
NADH	nicotinamide adenine dinucleotide phosphate
nDNA	nuclear DNA
NRF-1	nuclear respiratory factor-1
NRF-2	nuclear respiratory factor-2
N-terminal	nitrogen associated terminal of protein
NUGEMPs	nuclear genes encoding mitochondrial proteins
O_2	oxygen
Opa1	optic atrophy 1
OMM	outer mitochondrial membrane
PERK	
PGC-1α	peroxisome proliferator activated receptor-gamma coactivator 1 alpha
PKA	cyclic AMP-dependent protein kinase
RNA	ribonucleic acid
ROS	reactive oxygen species
RT	room temperature
Tfam	mitochondrial transcription factor A
Ser	Serine
Sirt1	Sirtuin 1
SDH	succinate dehydrogenase
SS	subsarcolemmal
Tak1	transforming growth factor-β-activated kinase-1
T2D	type 2 diabetes
Thr	Threonine
ULK1	unc-51-like kinase 1
UPR	unfolded protein response
VDAC	voltage dependent anion channel
μM	micro-Molar, (concentration, 10^{-6})

CHAPTER 1:

LITERATURE REVIEW

1.0 INTRODUCTION

The maintenance of mitochondrial size depends on reaching an equilibrium between the fission and fusion states. The fusion process involves the mixing of mitochondrial material, whereas the fission process divides the organelle into smaller components. Disruptions in either of these opposing processes can lead to developmental defects and disease (178), suggesting that proper maintenance of mitochondrial morphology is critical for normal cell function. Skeletal muscle mitochondrial morphology has been demonstrated to be altered under various disease conditions, including diabetes (9; 82) and obesity (9; 10), as well as during development (11), aging (75), and exercise (87). Mitochondria are maintained in a dynamic state as a quality control mechanism. Mitochondrial fusion allows for the formation of a networked reticulum. Fusion of mitochondria also enables complementation to occur, and acts as a cellular defence mechanism (123). Two mitochondrial genomes are able to complement potential defects through inter-mitochondrial mixing, and can prevent the expression of disease phenotypes that may arise from mtDNA defects. In addition to the advantages of an extended reticulum, some disadvantages may also exist. If local damage was to occur within a portion of the mitochondria, it may be postulated that this damage would influence the entire reticulum; however mitochondrial fission is able to negate those potential detrimental effects. Under detrimental conditions such as apoptosis, fragmented, smaller mitochondrial structures have been observed (45; 46; 77; 93). Moreover, recently it has been established that dysfunctional mitochondria have to be segregated and processed into smaller, fragmented components in order to be engulfed by

autophagosomes during autophagy (163). These observations suggest that there may be a compensatory mechanism in place to isolate the damaged portion of the mitochondrial network from its unaffected parts.

Traditionally, mitochondria have been thought to be static in nature. Modern imaging techniques reveal that these organelles are quite dynamic, capable of altering their shape and distribution within the cell. The location of these organelles within skeletal muscle is thought to influence the likelihood of a fusion or fission event occurring. Positioning of mitochondria to specific sites within the cell is dependent on a cytoskeletal based transportation system. In neurons, microtubules are the primary tracks governing mitochondrial movement in mammals. However, the cytoskeletal system governing mitochondrial movement within skeletal muscle has yet to be examined.

2.0 MITOCHONDRIA

In 1890 Altmann first characterized mitochondria based on their morphological resemblance to bacteria, and termed them “bioblasts” (6). It was Carl Benda who described the structures and coined the name mitochondria (mito-tread, chondrion-granule). The morphology of these organelles began to be detailed in 1915 by Lewis and Lewis (95). They noted that “in living cells these bodies are never quiet, but continually changing in shape, size, and position.”

2.1. The geography of mitochondria in skeletal muscle

In 1966, Gauthier and Padykula used electron microscopy to note the heterogeneity that exists in mitochondria within the diaphragm (53). They described “a conspicuous feature…of large mitochondria beneath the sarcolemma…they are large and more or less spherical”. Whereas, “the interior of the fiber, large mitochondria form chains running longitudinally among myofibrils” (53). Bakeeva *et al* (12) and Kirkwood *et al* (86) expanded upon this knowledge of muscle mitochondrial morphologies by demonstrating the presence of a mitochondrial reticulum, akin to the sarcoplasmic reticulum, and representing a network of interconnected organelles. Ogata and Yamasaki and Kayar *et al* provided further detailed characterizations of mitochondrial morphologies within muscle fibers possessing different oxidative capacities in the rat (118), horse (81) and human (119). They noted the distinction between mitochondria localized in proximity to myonuclei and adjacent to the sarcolemma (subsarcolemmal (SS) mitochondria), as well as those situated between the myofibrils (intermyofibrillar

(IMF) mitochondria). Historically, these morphological measurements using electron microscopy techniques allowed for the first evidence of structural and "geographical" heterogeneity within mitochondrial subfractions of muscle. However, these studies also observed that the distinction between SS and IMF mitochondria was not absolute; continuity in the network could exist between the two subfactions, suggesting that one subfraction might arise from the synthesis of mitochondria in another region, and that processes of organelle fission, fusion and movement were likely to be important in determining mitochondrial location and morphology.

2.1.1. Properties of SS and IMF mitochondria

Adopting subcellular fractionation techniques first developed for heart muscle (124), Krieger *et al* (90) and Cogswell *et al* (34) separated the two mitochondrial subfractions and noted differences in mitochondrial respiration, enzyme activities, lipid composition, protein synthesis and adaptation to muscle use and disuse. Thus, when isolated from muscle, these mitochondrial subfractions exhibit somewhat subtle, but distinct biochemical properties, which may parallel their divergent morphological characteristics. SS mitochondria are located just below the sarcolemma, while IMF mitochondria are found between the myofibrils. SS and IMF mitochondria possess distinctive biochemical properties. In terms of respiration, IMF mitochondria exhibit a greater state 3 rate than SS mitochondria, and they possess greater cytochrome c oxidase activity (34). Compositional differences among these subfractions exists in terms of

phospholipid content and protein-to-lipid ratios, as evident by the greater proportion of cardiolipin in SS relative to IMF mitochondria (34).

Currently, it is unknown whether one subfraction is a precursor of the other, or whether SS and IMF mitochondria are actually physically interconnected. Is it possible for continuous membrane networks within cells to possess divergent functional characteristics, given the fluidity of membrane bilayers? Certainly this appears to be true at the neuromuscular junction, where specialized synaptic proteins are localized in distinction from the rest of the sarcolemma. The interface between the lateral sac of the SR and the t-tubule is another example, where voltage-sensitive proteins promote the release of calcium, in contrast to the longitudinal portion of the SR where calcium uptake is favoured. These situations provide evidence of protein heterogeneity within a continuous lipid bilayer. It seems reasonable to assume that divergences could also exist within the mitochondrial network, particularly in view of the more "labile" nature of the SS subfraction in response to chronic muscle use or disuse, as well as their proximity to myonuclei in comparison to more continuous IMF mitochondria.

2.2. Existence of mitochondrial reticulum

The distribution, volume and shape of mitochondria within muscle fibres are a reflection of the balance between the activities of mitochondria morphology proteins, possibly regulated by the requirement for metabolite transport, energy demand, and oxygen diffusion. The beneficial aspects of a continuous membrane network would be apparent in instances where the energy requirement and substrates are not

homogeneously distributed within a fibre. A reticular mitochondrial structure could rapidly compensate for any deficits, serving to maintain an electrical potential along the membranes for extended distances, and reducing diffusion times for lipid soluble metabolites and oxygen (12). In contrast, the dismantling of the mitochondrial network into fragmented parts, as produced by chronic muscle disuse, likely decreases the efficiency of substrate transport, and produces mitochondria that are functionally heterogeneous with respect to membrane potential and mtDNA content. The loss of mitochondrial fusion results in a pathogenic profile in skeletal muscle, whereby mtDNA mutations are severely elevated (30). Romanello *et al* (135) also found that increases in mitochondrial fragmentation contribute to muscle loss, and that the inhibition of organelle fission protects from muscle atrophy. Disruptions in organelle dynamics have also been tied to obesity and type 2 diabetes (97). These studies suggest that mitochondrial morphology is linked in the pathophysiology of various diseases.

2.3. Machinery involved in mitochondrial reticulum formation

Changes in mitochondrial dynamics are regulated by opposing fusion and fission processes. Fusion of smaller organelles promotes the intermixing of mitochondrial material and an expansion of the mitochondrial reticulum as a result of endurance training, an observation made by Kirkwood *et al* some years ago (87). Fission, on the other hand, divides mitochondria into smaller pieces. Essential mammalian skeletal muscle fusion proteins involved in these processes are displayed in Figure 1.

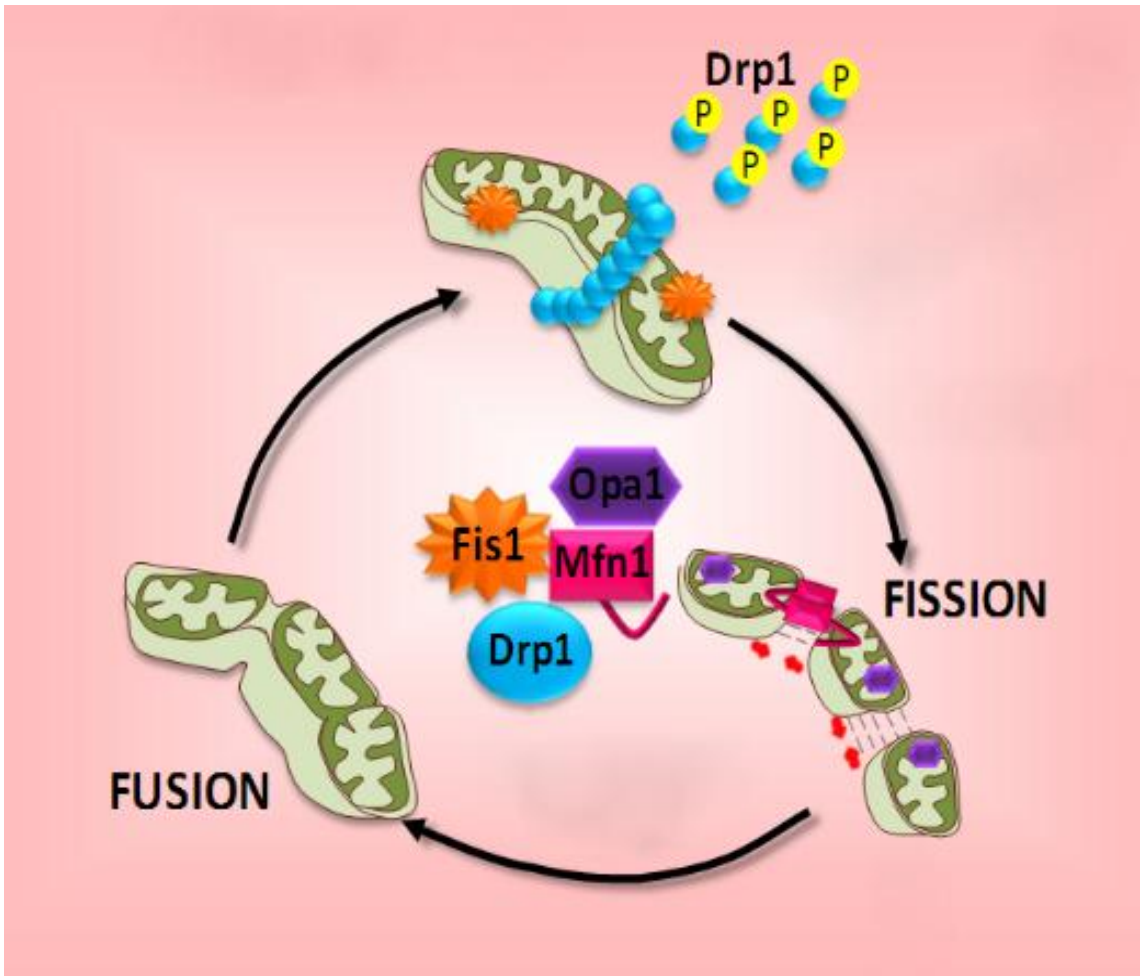

Figure 1: The maintenance of mitochondrial shape is dependent on reaching an equilibrium between the fission and fusion states. The fusion process involves the mixing of mitochondrial material, whereas the fission process divides the organelle into smaller components. Mitochondrial fusion is governed by the proteins Opa1 and Mfn1/2. Opa1 coordinates the fusion of the inner mitochondrial member (IMM). Whereas, Mfn1/2 tethers adjacent organelles and brings them into close proximity to one another to allow for the fusion of the outer mitochondrial membranes (OMM). Fission events are mediated by Fis1 and Drp1. Fis1 resides on the OMM and Drp1 is found in the cytosol in a phosphorylated state. During division, Drp1 is dephosphorylated and recruited to the mitochondrion. Drp1 forms a ring-like structure around the organelle, constricts, and divides the mitochondrion.

Mitofusin 2 (Mfn2), which behaves as an anchor, bringing adjacent mitochondria into close enough proximity to fuse their outer membranes, as well as the inner mitochondrial membrane protein optical atrophy 1 (Opa1). Mitochondrial membrane fission is mediated by dynamin related peptide 1 (Drp1), in combination with fission protein 1 (Fis1). Fis1 is involved in outer membrane fission, whereas Drp1 must be recruited from the cytosol to the outer surface of the organelle, whereupon it wraps around the constriction points of diving mitochondria to promote the division of organelles.

2.3.1. Mfn2

The double membrane nature of mitochondria makes it essential to consider both components when discussing mitochondrial morphology. Inner and outer membrane fusion events within mitochondria are separable, and involve different morphology machinery proteins. Outer member fusion is regulated by the mitofusions, Mfn1 and Mfn2 (134). The mitofusions contain a GTP-binding domain, a transmembrane domain, two coiled-coil regions, upstream and downstream of the transmembrane domain, allowing for anchorage of the protein in the outer membrane (138). The mitofusions have N- and C-terminal domains exposed towards the cytosol. This topology implies that the hydrophobic domains span the outer membrane twice (134). The mitofusions tether adjacent mitochondria through a dimeric anti-parallel coiled-coiled structure, either through homotypic (Mfn2-Mfn2) or heterotypic (Mfn1-Mfn2) means (89), thus allowing for adjacent organelles to be brought into close proximity to one another for a fusion event to occur.

Although structurally similar, the functional roles of the mitofusions are divergent. Mfn2 is presumed to have mostly a regulatory role, while Mfn1 is mainly responsible for tethering adjacent mitochondria (76). Moreover, Mfn1 can only promote mitochondrial fusion in the presence of Opa1, whereas Mfn2 can act independently (33). The expression patterns of the mitofusions are tissue specific, whereby Mfn2 is highly expressed in skeletal muscle as compared to Mfn1 (137).

2.3.2. Opa1

Inner mitochondrial membrane fusion is mediated by the dynamin-related protein, Opa1. Opa1 is weakly anchored to the inner mitochondrial membrane, with the N-terminus exposed to the matrix and the bulk of the C-terminal domain exposed to the intermembrane space (44; 122). Mammalian Opa1 exists as eight isoforms as a result of alternative splicing and proteolytic processing (40), which may indicate functional diversity of the protein, however the differences in function and processing mechanisms have yet to be fully identified. Separately, the Opa1 isoforms have little activity, but when coexpressed the long and short and isoforms functionally complement each other (44). Furthermore, the yeast homologue, Mgm1, exists in two lengths, the large Mgm1 (l-Mgm1) and the small isoform (s-Mgm1), and both forms are required for the proper maintenance of mitochondrial DNA and morphology (67).

Over-expression of Opa1 promotes an elongated mitochondrial reticulum, whereas knockdown of the protein results in fragmented organelles (33). Blockage of the protein in mammalian cells eliminates all mitochondrial fusion, and results in poor cell

growth and decreased respiration (28). In addition to its role in inner mitochondrial membrane fusion, Opa1 is also essential for mitochondrial cristae organization and function. In cells devoid of the protein, mitochondria exhibit disorganized cristae structures (121).

2.3.3. Drp1

Similar to mitochondrial fusion, the fission processes are also regulated by specific morphology proteins. Mitochondrial fission was first observed as a process orchestrated by Drp1 (17; 148). Drp1 belongs to a family of large GTPase of the dynamin family, possessing highly conserved N-terminal and a putative helical domains (148). All dynamin members are structurally similar, but functionally diverse GTP-binding proteins. Drp1 polymerizes into a ring-like structure around mitochondria. Cross-bridging of the GTPase domains of adjacent Drp1 proteins results in GTP hydrolysis, constriction, and ultimately severing of mitochondria (152). The phosphorylation status of Drp1 is an important determinant of its localization and effect on mitochondrial structure. Phosphorylation of Drp1 at Ser^{637} results in inhibition of its GTPase activity and an inability of Drp1 to translocate from the cytosol to the sites of mitochondrial division, resulting in an attenuation of mitochondrial fission (27; 35). Because Drp1 lacks a mitochondrial targeting sequence, it is thought that a protein(s) may be responsible for mediating the recruitment of Drp1 to mitochondria. Whether or not the other well characterized fission protein, Fis1 is involved is still controversial.

The mechanisms by which Drp1 is regulated are only beginning to be established. Drp1 is modified post-translationally by protein phosphorylation, sumoylation and ubiquitylation. As previously mentioned, dephosphorylation of Drp1 is required for the translocation and subsequent activation of Drp1. Cyclic AMP-dependent protein kinase (PKA)-dependent phosphorylation of Drp1 at Ser^{637} results in inhibition of its GTPase activity and mitochondrial division (27; 35). Additionally, in response to ATP depletion, de-phosphorylation of Drp1 at Ser^{637} is upregulated, but becomes re-phosphorylated when cells are returned to a high ATP environment, indicating that Drp1 phosphorylation is ATP-dependent (32). ATP depletion results in Drp1 activation and contributes to mitochondrial fragmentation (32). Moreover, it has been shown that calcineurin regulates Drp1 dephosphorylation, allowing for its translocation to mitochondria (25; 35). Knockdown of calcineurin results in an accumulation of P-Drp1 in the cytosol, coinciding with reduced Drp1 localization to mitochondria and attenuated mitochondrial fragmentation (169).

Drp1 is expressed at the highest levels in the brain, followed by skeletal and cardiac muscles (148). Depletion of Drp1 in HeLa cells leads to the loss of mtDNA, a decrease in mitochondrial respiration, coupled to an increase in the levels of cellular reactive oxygen species (125). Moreover, inhibition of Drp1 prevents DNA fragmentation, indicative of reduced apoptotic cell death (46). Therefore, these results suggest that mitochondrial fission is required to isolate damaged regions through fragmentation.

2.3.4. Fis1

The C-terminal domain of Fis1 contains a single transmembrane domain that anchors the protein in the mitochondrial outer membrane, leaving the bulk of the protein exposed to the cytosol. The N-terminal cytosolic domain contains six α-helices that are responsible for the fission activity of Fis1 (43; 144; 157). The transmembrane segment of Fis1 directs the import of the protein post-translationally from the cytosol into the outer membrane of mitochondria (83).

Over-expression of Fis1 results in fragmented mitochondria, whereas the knockdown of the protein leads to an increase in organelle networks and interconnected mitochondria (151). Taken together these findings propose that multiple members of the mitochondria fusion-fission machinery are involved in controlling mitochondrial morphology and that there is a complex interplay between the regulators.

2.3. Models of mitochondrial reticulum alterations in skeletal muscle

Mitochondria are vital contributors not only to cellular life, but also to the death process. Disruptions in mitochondrial dynamics can lead to developmental defects and diseases (178), suggesting that proper maintenance of mitochondrial morphology is critical for normal cell function. Skeletal muscle mitochondrial morphology has been demonstrated to be altered under various disease conditions, such as diabetes (9; 82), and denervation (108), as well as during development (11), aging (75), and exercise (87; 129).

2.4.1. Alterations in mitochondria morphology with development and age

Immediately following birth, a progressive increase in the formation of interconnected mitochondrial networks occurs (11). During this phase of muscle development, mitochondria begin to take on the appearance of mature reticula. They begin to contain mitochondrial junctions with branched tubular networks (11). It is speculated that mitochondrial fusion during this process is important for life, since mice deficient in Mfn2 experience severe placental disruptions development, and a homozygous Mfn2 deficiency is embryonic lethal (29).

Mitochondrial dynamics are not only important during early development, but also during the aging process. Age affects the size of mitochondria in skeletal muscle, with mitochondrial area being larger in infancy, and gradually becoming smaller with age in humans (79). Poggi *et al.* found similar results in their humans study, whereby mitochondrial size and mitochondrial percentage per fibre area decreasing with age (132). We have also found that the SS mitochondrial content is reduced in senescent Fisher 344 Brown Norway rats as compared to their younger counterparts (75).

Aging is a multidimensional process that involves a decline in the ability of the muscle to adapt to stress, damage and disease. A decline in muscle mass and strength are prominent features of aged skeletal muscle, a condition known as sarcopenia. During aging this decrease in muscle mass has been attributed to reductions in muscle fibre number and fibre atrophy (96). Skeletal muscle mass is determined by the rate of muscle protein synthesis and breakdown. A reduction in muscle mass may occur if degradation rates exceed synthesis, or conversely a decrease in muscle protein synthesis occurs. With

advanced age, the synthesis of myosin heavy chain (MHC) declines in humans, and correlates with measures of muscle strength (15). The age-related declines in MHC may indicate a compromised ability of muscle to remodel.

Several mechanisms have been proposed that cause sarcopenia, including increased reactive oxygen species (ROS) and oxidative stress (26; 168), an accumulation of mitochondrial abnormalities such as mtDNA mutations (99; 168), as well as an increased susceptibility to apoptosis (26; 42). The free radical theory of aging postulates that the accumulation of ROS is a key determinant of an organism's life span (64). Although the mechanisms by which ROS contributes to aging and reduced lifespan are still unclear, there is evidence that increased oxidative stress damages DNA, proteins, and lipids (14). Oxidative stress can damage mtDNA and impair mitochondrial function, resulting in an accumulation of ROS and exacerbated intracellular ROS-induced damage. Moreover, mitochondria isolated from senescent skeletal muscle have shown an increased production of ROS, in addition to enhanced apoptotic susceptibility (26; 102). Increased ROS production can activate the apoptotic signaling cascade and cell death mechanisms. In aged skeletal muscle, an enhanced susceptibility towards the opening of the mitochondrial permeability transition pore (mtPTP) has been demonstrated (26). Opening of the mtPTP leads to the release of pro-apoptotic proteins, such as cytochrome c and endonuclease G, both proteins are upregulated in aged rats compared to their younger counterparts and result in increased mitochondrial apoptotic susceptibility (26).

The mutation rates in mtDNA are substantially higher than in nuclear DNA (167). This is due to the lack of protective histones and lower number of repair enzymes within

mitochondria. Examination of 34-year old rhesus monkeys (99) and 36-month old rats (21; 66) revealed an age associated accumulation of ETC enzyme abnormalities and mtDNA mutations.

2.4.2. Alterations in mitochondria morphology with denervation

Similar to the effects of aging, chronic muscle disuse, induced through denervation, is a potent stimulus that reduces mitochondrial content in the muscle (3; 108; 147). The molecular basis mediating this alteration has been attributed to, at least in part, the decreased expression of nuclear genes encoding mitochondrial proteins (147), reductions in protein import (147), increased ROS production (117), and/or increased mitochondrially mediated cell death (3).

Denervation occurs when the nerve supply to muscle is severed. Denervation can be achieved through mechanical means (i.e. surgical sectioning or crushing), chemical blocking (i.e. tetrodotoxin), or injury (113). This condition results in the elimination of nerve-muscle communication. A predominant feature of denervation is muscle atrophy and a loss of muscle strength (172). Moreover, denervation can lead to changes in the ultrastructure of muscle, including alterations to the number and size of mitochondria, sarcomere disorganization, and myofibrillar disruptions (105). Mitochondrial content, as well as protein levels within tissue are balanced between the rate of synthesis and degradation. With denervation there is a decrease in mitochondrial biogenesis and enhanced mitochondrially mediated degradation through apoptosis (172). Since mitochondria possess their own transcription and translational machinery, they have the

ability to synthesize a number of their own proteins. However, the majority of mitochondrial proteins are nuclear encoded and are imported into the organelle, with denervation mitochondrial import machinery components and import rates are reduced (147). As a result of denervation, mitochondrial enzyme activities of cytochrome c oxidase (COX), citrate synthase (CS), and succinate dehydrogenase (SDH) are attenuated (172). Concomitantly, denervation results in coordinated decreases in the expression of the mitochondrially-encoded subunit III and nuclear-encoded subunit VIc components of COX (172) and contributes to the reduced COX activity observed under these conditions.

The exact mechanisms governing the loss in muscle mass with denervation have yet to be fully elucidated, although there is increasing evidence suggesting an upregulation in the rate of muscle protein degradation and the activation of mitochondrially specific autophagy (termed mitophagy). For this process to occur it is thought that mitochondria must first be processed into smaller, fragmented components in order to be engulfed by autophagosomes during the mitophagy process. In diaphragm muscle following denervation, it has been observed that mitochondria are smaller in structure, in contrast to control muscle that contain long, reticular organelles (108). Mitochondrial fragmentation has been observed to occur following denervation, however, the link between the shape of the organelle and mitophagy still needs to be fully explored.

2.4.3. Alterations in mitochondria morphology with mitochondrial biogenesis

Skeletal muscle has the remarkable ability to adapt to increased metabolic demands, such as exercise, by increasing the size and number or mitochondria. This

process is termed mitochondrial biogenesis and involves the coordination of both mitochondrial and nuclear genomes (72). Changes in mitochondria biogenesis are due to multiple molecular events. These pathways include the activation of signaling kinases, the induction of transcription factors, changes in mRNA stability, post-translational modifications, alterations in protein import rates, and/or the rate of protein folding (72).

In response to exercise, the mRNA and protein expression of the transcriptional coactivator, PGC-1α, and transcription factors, such as mitochondrial transcription factor A (Tfam) are upregulated (5; 58; 91). Activation of mitochondrial transcriptional factors regulates the expression of nuclear genes encoding mitochondrial proteins (NUGEMPs), as well as the transcription and mRNA expression of PGC-1α (73). Moreover, PGC-1α binds to transcription factors and regulates the expression of NUGEMPs (130). Subsequently, the mRNA products are translated and imported through specialized import machinery into the organelle. These proteins will either be used as transcription factors for mtDNA, or be integrated into the subunits of the electron transport chain (73). The coordination of both the nuclear and mitochondrial genomes allows for the expansion of the mitochondrial reticulum and alterations in the composition of the mitochondrion (70; 87).

Chronic muscle use can be induced through a variety of models, including treadmill and voluntary wheel training, as well as chronic contractile activity (CCA). Chronic activity through these protocols can cause changes in the expression of mitochondrial proteins (72). Previous studies have demonstrated the effectiveness of CCA model for studying the phenotypic changes in skeletal muscle elicited by contractile

activity (159). Chronic low-frequency indirect muscle stimulation has been shown to lead to alterations in mitochondrial gene expression and enzyme activities, in addition to an increased concentration of the mitochondrial phospholipid cardiolipin (158).

The mitochondrial reticular network is known to expand as a result of endurance training (87; 129). Kirkwood *et al* originally demonstrated that mitochondria in skeletal muscle adapted to chronic exercise by increasing the extensiveness of the mitochondrial reticulum (87). This suggests that chronic exercise shifts the expression of fission and fusion machinery towards that of enhanced fusion.

The alterations in mitochondrial biogenesis are driven, in part, by PGC-1α, a major regulator of mitochondrial biogenesis (61). Mice deficient in PGC-1α have a reduced expression of Mfn2 mRNA (177). Conversely, an up-regulation in PGC-1α, from a single bout of cycling exercise, stimulated ERRα binding at the -413/-398 motifs on the Mfn2 promoter, resulting in an increase in Mfn2 mRNA during the recovery phase (24). Similar observations were seen by Ding *et al* (41), whereby Mfn2 mRNA content increased during recovery from acute exercise. Moreover, Garnier *et* al (52) also found a coordinate increase in mitochondrial biogenesis, specifically PGC-1α, and Mfn2 transcriptional levels.

2.4.4. Alterations in mitochondria morphology with diabetes

Diabetes is defined as a group of metabolic disorders, characterized by abnormally elevated plasma glucose concentrations, due to insufficient insulin secretion or abnormal insulin response. The most common form is Type 2 diabetes (T2D), and comprises of

approximately 90% of all diabetics cases around the world (1). T2D is associated with insulin resistance, and high levels of blood glucose, also known as hyperglycemia. Following a meal, the concentration of glucose is elevated, which drives the insulin oscillations (57). The increase in glucose post-meal, drives β-cell release of insulin (57). In the post-absorptive state the concentrations of glucose and insulin return to basal levels. However, in T2D individuals, the uptake of glucose by insulin sensitive tissues is impaired. Consequently, β-cells try to compensate for the insulin resistance by increasing insulin secretion, to little avail in the circulating glucose concentrations. The maintenance of normal glucose homeostasis depends on a variety of tissues, such as skeletal muscle, a predominant site of insulin-mediated glucose uptake (38; 39). Moreover, the skeletal muscle of T2D patients display impaired mitochondrial functioning (82).

Several mechanisms regulate the reduction in mitochondrial activity in insulin-resistant patients, such as a reduction in mitochondrial content. In this regard, mitochondria from the skeletal muscle of T2D patients have been found to be smaller in size than in muscle from lean individuals (82). The size of mitochondria correlated with insulin sensitivity and glucose disposal rates (82). Upon closer examination at the level of the proteins involved in mitochondrial morphology, a positive correlation was found between levels of Mfn2 expression and insulin sensitivity in T2D patients (9). T2D patients display reduced Mfn2 mRNA levels, relative to their lean counterparts (9). Moreover, the repression of Mfn2 has been shown to reduce glucose oxidation (10).

2.5. Signaling pathways

Skeletal muscle is highly malleable and responds by increasing or decreasing its mitochondrial content in response to physiological stimuli. Major signaling transduction pathways involved in these adaptations include those initiated by 1) AMP-activated kinase (AMPK), 2) calcium, and/or 3) reactive oxygen species (ROS), as displayed in Figure 2.

2.5.1. AMPK-activated protein kinase (AMPK)

AMPK is a heterotrimer protein comprises of an α-catalytic subunit and βγ-regulatory subunits. Isoforms for all three subunits have been identified (α1, α2, β1, β2, γ1, γ2, and γ3) (150). AMPK is a critical energy sensor in the cell that reacts to fluctuations in the AMP/ATP ratio. AMPK is activated by the allosteric binding of AMP, in addition to the phosphorylation of Thr^{172} within its catalytic subunit by upstream kinases. To date, three upstream mammalian kinases for AMPK have been identified, 1) liver kinase B1 (LKB1) (98), 2) calmodulin-dependent protein kinase kinase-beta (CAMKKβ) (173), 3) transforming growth factor-β-activated kinase-1 (Tak1 kinase) (176).

AMPK is a metabolic sensor that can regulate the energy status of the cell. Its activation represses many anabolic processes, such as triglyceride, cholesterol, fatty acid, and protein synthesis (150). Conversely, AMPK stimulates several catabolic processes that generate ATP, such as fatty acid oxidation and glycolysis (150). In response to exercise,

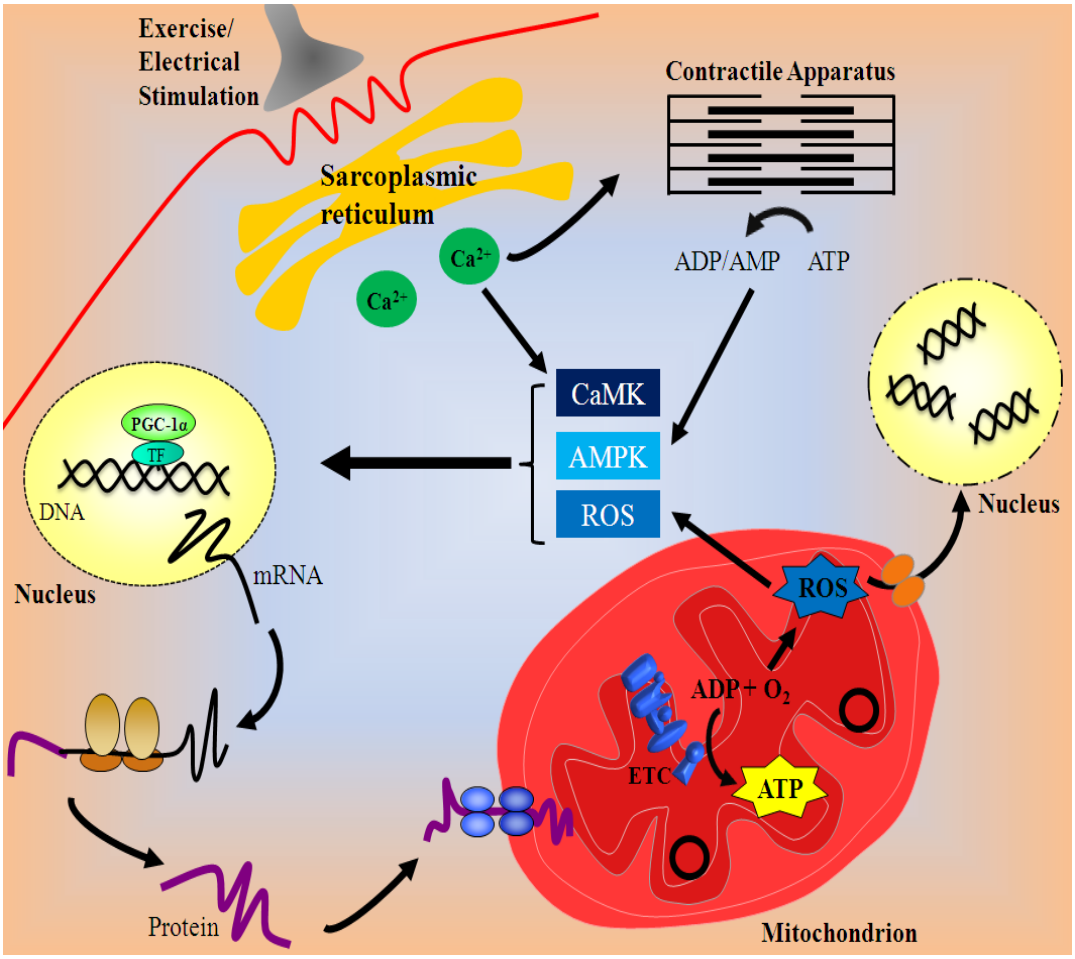

Figure 2: Overview of major signaling pathways regulating mitochondrial content in skeletal muscle cells. Signals originating from the neuromuscular junction include propagating action potentials to the post-synaptic membrane. As the action potential travels across the sarcolemma membrane, it causes the release of calcium ($Ca2^{+}$) from the sarcoplasmic reticulum. Calcium interacts with the contractile machinery to initiate muscle contractions. Calcium also activates kinases such as $Ca2^{+}$/calmodulin-dependent protein kinase (CaMK). Furthermore, contractile activity breaks down adenine triphosphate (ATP) to produce adenine diphosphate (ADP), and subsequently adenine monophosphate (AMP). Thus increasing the AMP/ADP to ATP ratio and activating AMP-dependent protein kinase (AMPK). Moreover, mitochondria are the primary source of reactive oxygen species (ROS), Elevated ROS levels can lead to a signaling cascade that can result in apoptosis. CaMK, AMPK, and ROS signaling cascades regulate the transcription of nuclear genes encoding mitochondrial proteins. These mRNAs are subsequently translated into proteins and imported into mitochondria, thus increasing mitochondrial activity and content.

skeletal muscle undergoes rapid ATP turnover. Whereby, AMP and ADP levels increase with exercise, resulting in the activation of AMPK (51). AMPK activation allows for ATP levels to remain relatively constant, despite the large fluctuations in energy demands.

Once stimulated, AMPK phosphorylates downstream targets aimed at conserving existing ATP levels. AMPK activation has been shown to induce the expression of PGC-1α, GLUT4, and mitochondrial genes (78). Furthermore, AMPK was found to directly phosphorylate PGC-1α, thus allowing for increased PGC-1α-dependent induction of the PGC-1α promoter (78). Moreover, AMPK upregulates Sirtuin 1 (SIRT1) activity, resulting in the deacetylation and modulation of downstream SIRT1 targets, such as PGC-1α (23). Although all the targets of AMPK have yet to be fully elucidated, AMPK activation appears to influence mitochondrial content through PGC-1α, a key regulatory protein in mitochondrial biogenesis.

2.5.2. Calcium

In response to stimuli such as muscular contractions, calcium (Ca^{2+}) is released from the sarcoplasmic reticulum, increasing the concentration of cytosolic Ca^{2+} and leading to the activation of Ca^{2+}-induced kinases, such as calcium/calmodulin (CaM) kinases (CaMKs), and protein kinases C (PKC), in addition to the phosphatase calcineurin. The ubiquitous Ca^{2+} sensor CaM serves as the primary intracellular receptor for Ca^{2+}. CaM is a small 148 amino acid protein, capable of binding Ca^{2+} ions at a stoichiometry of 4 to 1 (103). Binding of Ca^{2+} to CaM produces a conformational change

allowing for its interaction with target enzymes (103). The Ca^{2+} /CaM complex can bind to a variety of proteins, including CaMKs.

The CaMK family consists of CaM-dependent protein kinase I (CaMKI), CaMKII and CaMKIV, as well as the CaMKK members. CaMKII is the predominant isoform found within skeletal muscle (136). CaMKII members (CaMKII-α, -β, -γ, -δ), are activated by Ca^{2+}/CaM binding, in response to elevated $[Ca^{2+}]_i$. Subsequently, this binding results in a conformational change of the protein, allowing for the exposure of the ATP- and substrate-binding sites in the catalytic domains, as well as Thr^{287} in the inhibitory domain. Phosphorylation of Thr^{287} allows for an enhanced affinity for CaM (104). After finally disassociating from CaM, the modified subunit remains partly active. This results in the autonomous (independent of Ca^{2+} /CaM) CaMKII activation and phosphorylation at Thr^{287} (136). CaMKII activation occurs rapidly, and persists even when $[Ca^{2+}]_i$ decreases and return to basal levels, thus propagating the Ca^{2+} response. Thus, autophosphorylation may be a mechanism in skeletal muscle to accelerate the activation of CaMKII with contractions. Calcium signaling regulates protein kinases, as well as the activity of transcription factors, such as the early growth response gene-1 (Erg-1). Calcium-induced activation of Erg-1 is thought to be involved in Ca^{2+}-mediated signal leading to mitochondrial biogenesis (49).

During basal conditions, $[Ca^{2+}]_i$ in isolated single muscle fibres is 30 – 50 nM (171). In response to muscle contractions $[Ca^{2+}]_i$ reach 100 nM to 2 μM (31; 171). Increases in Ca^{2+} levels within skeletal muscle can also be achieved through the addition of the Ca^{2+} ionophore A-23187, ionomycin, caffeine, or thapsigargin. These treatments

have been shown to increase $[Ca^{2+}]_i$ and induce the expression of genes involved in mitochondrial biogenesis in skeletal muscle (47; 48). Moreover, rises in $[Ca^{2+}]_i$, through the activation of CaMKII, result in the increase of PGC-1α protein and mitochondrial biogenesis (174).

2.5.3. Reactive oxygen species (ROS)

Mitochondria are the primary source of ROS generation (36; 88). Within these organelles, low levels of ROS are constantly produced during normal respiration when the oxygen consumed undergoes a one-electron reduction, at complexes I and III in the electron transport chain (16). Approximately 2 – 5% of electrons in the electron transport chain are prematurely donated to oxygen during cellular respiration (18; 100), producing the free radical superoxide. Superoxide is quickly transformed into hydrogen peroxide (H_2O_2) by superoxide dismutase (MnSOD). Subsequently, H_2O_2 is reduced to water by glutathione peroxidase or catalase, or converted to the highly reactive hydroxyl radical (·OH) in the presence of reduced iron or copper (22). Mitochondria are not the only source of ROS within skeletal muscle. Additional sources of ROS production include phospholipase A2 (179), xanthine oxidase in the cytosol of skeletal muscle cells (56), and nicotinamide adenine dinucleotide phosphate (NADPH) oxidases (NOXs) located within the sarcoplasmic reticulum, transverse tubules, and the sarcolemma (128).

ROS molecules were once considered as solely detrimental, causing damage to proteins, lipids, and DNA. Indeed, ROS are involved in the pathogenesis of conditions such as inherited muscular dystrophy (112), denervation (3) and aging (26). However,

accumulating evidence indicates that moderate levels of ROS have a positive role in skeletal muscle. For example, ROS can have adaptive effects during muscle injury and repair (162). Similarly, ROS generation during exercise promotes mitochondrial biogenesis through the expression of NRF-1 and PGC-1α (145; 156).

2.6. Mitochondrially-mediated apoptosis

Apoptosis is the process of programmed cell death, it occurs when a cell is no longer required or damaged. Ultrastructural features of apoptosis include DNA fragmentation, plasma membrane blebbing, loss of membrane integrity, cell shrinkage, and chromatin condensation (84). The elimination of cells is a finely controlled process regulated by the activation of pro- and anti-apoptotic proteins. Mitochondrial outer membrane permeability leads to the loss of mitochondrial membrane potential and allows for the release of apoptotic factors, such as cytochrome c to the cytosol. Outer membrane permeability is regulated by the BCL-2 family of proteins. Anti-apoptotic BCL-2 family members that help to maintain the integrity of the membrane include Bcl-2 and Bcl-xL (2). Whereas pro-apoptotic BCL-2 proteins promote the release of cytochrome c include Bax, Bak and BH3-only proteins such as Bid and Bim (2). The release of pro-apoptotic proteins from the mitochondria is facilitated by specialized pores, termed the mtPTP and the mitochondrial apoptosis-inducing channel (MAC). MACs are composed of oligomerized Bax and/or Bak, and are localized to the outer membrane of mitochondria.

The connection between mitochondrial fission and fusion processes and apoptosis is intriguing. During apoptosis the mitochondrial network became fragmented in S.

Cerevisiae, C. elegans, COS-7 and HeLa cells (45; 46; 77; 93). Perhaps compromised levels of mitochondrial fusion or enhanced levels of fission can potentially sensitize cells to apoptotic stimuli. In support of these finding, an overexpression in fusion machinery components has been shown to inhibit apoptotic mitochondrial fragmentation, and delay Bax/Bak activation and cytochrome c release (155). Conversely, downregulation of the fission machinery proteins prevents mitochondrial fragmentation, and reduces apoptotic cell death (46). Moreover, Opa1 has been found to alter mitochondrial cristae junctions, thus allowing for the regulation of cytochrome c release during apoptosis (50; 92).

2.7. Autophagy

Autophagy involves the sequestering of cytoplasmic material, its encapsulation and eventual digestion through delivery to the lysosome in response to stressful conditions, as a means of removal of damaged or superfluous organelles and proteins (60). Autophagy can promote cell survival and maintain homeostasis, but it can also promote cell death through excessive self-digestion. During general autophagy induction, the pro-autophagy proteins Beclin1, ULK1 and ATG7 initiate the formation of the autophagosome. Selective removal of dysfunctional mitochondria (i.e. mitophagy) is induced as a result of elevated mitochondrial ROS production (140), as well as the dissipation of the mitochondrial membrane potential (133; 163). During this process, the cytosolic E3 ubiquitin ligase, Parkin, is recruited to dysfunctional organelles with reduced membrane potential in a PINK1-dependent manner, thereby promoting mitophagy (115). p62 binds to the ubiquitinated mitochondria, and acts as an adaptor for the organelles to be

recognized by the autophagic marker LC3 (120). Subsequently, LC3II, a processed form of LC3, is localized in the membranes participating in the mitophagy process, and its content reflects the number of autophagosomes present in the tissue (80). Upon encapsulation of the dysfunctional mitochondria, the autophagosome delivers this material to the lysosome for degradation, where lysosomal proteinases such as cathepsin D participate in their degradation (164).

Mitochondrial morphology is closely integrated with mitophagy. For example, Parkin is an important component of the mitophagy process, and it also plays a critical role in modulating the morphology of mitochondria, such that inhibition of mitochondrial fission has been demonstrated to reduce Parkin-mediated mitophagy (160). Moreover, Mfn1/2 are ubiquitinated in a PINK1/Parkin-dependent manner upon induction of mitophagy (54). Therefore, the PINK1/Parkin pathway is thought to be the intermediate step between mitochondrial remodeling and mitophagy. Mitophagy is dependent on the reduced fusion and the presence of fission, since Fis1 and Drp1 knockdown, and Opa1 overexpression all reduce the levels of mitophagy (163). For mitophagy to occur, dysfunctional organelles have to be segregated and processed into smaller, fragmented components in order to be engulfed by autophagosomes during the mitophagy process (163). This alteration in mitochondrial shape involves fission and fusion machinery components.

2.8. Unfolded protein response

The endoplasmic reticulum (ER) and mitochondria (mt) are exposed to newly synthesized protein and are responsible for their proper folding and assembly. Homeostasis is achieved by balancing the nascent protein load with the folding capacity of the organelle. When the ability to do so is compromised, ER and mitochondrial stress ensues. The adaptive responses to this imbalance, termed the ER-unfolded protein response (UPR) and mt-UPR, coincide with the upregulation of molecular chaperones allowing for the increased folding capacity of the cell. If the cellular stress is too extensive and cannot be alleviated, the UPR activates cell destructive responses including apoptosis and the mitophagy pathway (127).

ER stress triggers three ER transmembrane proteins, inositol requiring 1 (IRE1), double stranded RNA activated protein kinase (PKR)-like endoplasmic reticulum kinase (PERK), and activating transcription factor 6 (ATF6). Once these stress sensors become activated they initiate the UPR by effecting downstream targets. IRE1, PERK, and ATF6 are maintained in an inactive state through interactions with the ER chaperone protein Binding Ig Protein (BiP). In response to ER stress, PERK is liberated from BiP, thus allowing for its autophosphorylation and activation. Subsequently, PERK phosphorylates eukaryotic initiation factor 2 (eIF2α), leading to inhibition of global protein translation (63; 143). Additional downstream targets of PERK include C/EBP-homologous protein (CHOP) (62). CHOP is a transcription factor that binds to and activates the promoter of stress response genes, such as c-Jun N-terminal Kinase (JNK) (74). As such, CHOP is

capable of propagating the UPR signal. Furthermore, it is also known that CHOP activates the transcription of mtUPR chaperone genes, such as mtHSP60 (127).

In addition to the protective effects of the ER-UPR, the mechanisms governing the mitochondrial protein folded environment are beginning to be elucidated. The majority of mitochondrially-destined proteins are encoded by nucleus and imported into the mitochondria in an unfolded state. Failure of these proteins to fold properly can result in ROS accumulation (13). ROS generation, in response to mitochondrially-specific stress activates general control nonrepressed 2 (GCN2), which phosphorylates eIF2α to reduce general translation of proteins (13). A complementary pathway to that of GCN-2 and eIF2α, involves transcription factor associated with stress–1 (ATFS-1), which upregulates mitochondrial chaperones to offset the accumulation of unfolded proteins (13; 116). Recent microarray experiments from Nargund *et al* have found that mitochondrial fission genes are involved in the mtUPR in *C. elegans* (116), however more work is required to better understand its influence on mitochondrial morphology.

3.0 CYTOSKELETON

Mitochondria are vital organelles, critical for energy supply and cell survival. Such functional versatility is paralleled by the structural complexity of the organelle. Mitochondria can compensate for alterations in energy requirements by adjusting their size and distribution within skeletal muscle (37). It is their interaction with the cytoskeleton that is used to control their position, movement and anchorage within cells (161). As displayed in Figure 3, the three cytoskeletal elements, actin, microtubules and intermediate filaments act to vary the degree of scaffolding along which mitochondria are capable of moving.

3.1. Microtubules

Microtubules are used to support intracellular transport and cell organization. They are long rigid filaments, approximately 25 nm in diameter. Microtubules are composed of α- and β-tubulin subunits, that link together in a heterodimer arrangement. Growth of microtubules occurs by the addition of these GTP-tubulin dimers. During the addition of tubulin to the microtubule ends, the energy provided by the hydrolysis of tubulin bound GTP initiates a conformational change, resulting in the dynamic instability of the filament (109). Dynamic instability allows for a plus-end, where the net addition of α/β-tubulin dimers occurs, and a depolymerizing minus-end, where there is a net loss of the tubulin dimers. The growing plus-ends radiate out from the centre of the cell towards the periphery, whereas the minus-ends are located in the cell centre. The movement of motor proteins along microtubules takes advantage of the dynamic

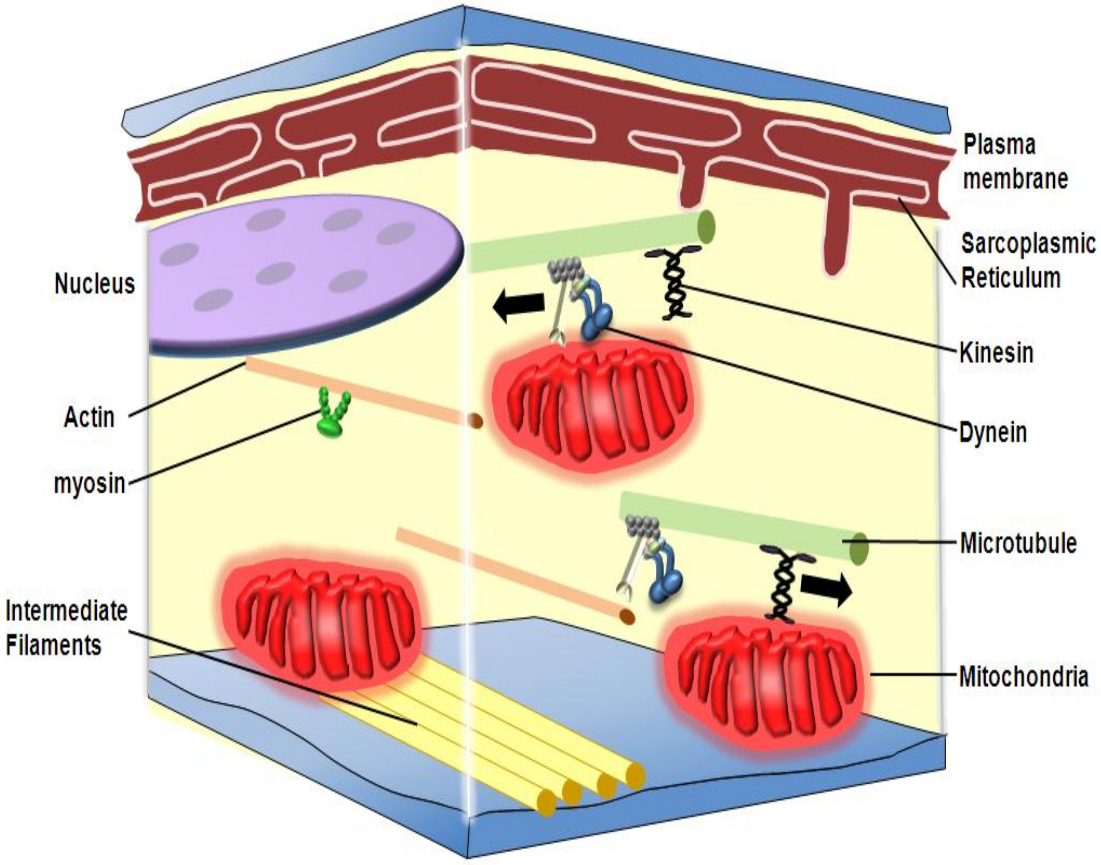

Figure 3: Pictorial representation of mitochondrial movement within the cell, as governed by cytoskeletal elements. Actin, microtubules, and intermediate filaments constitute the cellular cytoskeleton, whereas dynein and kinesin are the motor proteins for microtubules. Mitochondrial movement towards the nucleus is mainly governed by dynein, whereas motility away from the nucleus is predominately regulated by kinesins. Myosin motor protein direct movement along actin.

instability of the tubulin polymer. Growth of microtubules allows for the continued expansion of the cytoskeleton. Conversely, the ability of microtubules to shrink is thought to be important for morphological changes in the cell, and in the reorientation of microtubules during the locomotion of organelles (109; 110).

3.1.1. Kinesin motor protein

Intracellular transport of cargo, such as mitochondria, to specific locations within the cell involves molecular motors that bind directly to cargo, such as mitochondria, and the cytoskeletal track. Dynein and kinesins are the motor proteins responsible for motility along microtubules. In neurons, movement along microtubules occurs either towards the cell body using cytoplasmic dynein, or away, using kinesins. There are 14 kinesin superfamilies encoded by the human and mouse genomes, consisting of more than 45 members (68; 107). Molecular motors convert the chemical energy derived from the hydrolysis of ATP into mechanical energy. Kinesin molecules move in discrete 8 nm steps along microtubules (141). The kinesins motor protein is composed of a catalytic core domain, also termed the “head”, followed by the stalk region, and finally the “tail” domain. The catalytic core contains the ATP- and microtubule-binding motifs, and is responsible for the movement generated by the hydrolysis of ATP (106). This domain is conserved among kinesins, since they move across microtubules in a similar manner, however the stalk and tail domains are highly divergent, allowing for specification during cargo selection.

In neurons, Kinesin-1 and Kinesin-3 have been identified to regulate mitochondrial movements (114; 131). Kinesin-1, also known as conventional kinesin, consists of three distinct members, Kif5A, Kif5B and Kif5C. Kif5A and Kif5C are neuron-specific, whereas Kif5B is ubiquitously expressed (4; 8). Inhibition of Kinesin-1 in *Drosophila* halts mitochondrial movement and alters mitochondrial positioning in motor axons (131), and in non-neuronal cells (161; 175).

3.1.1.1. Milton-Miro adaptor complex

Recently, adaptor proteins that respond to intracellular signals are beginning to be identified. Motor protein/adaptor complexes can mediate the transport of mitochondria in response to Ca^{2+}. The core of this complex is composed of the Kinesin-1 motor protein along with two mitochondrial-specific adaptors, mitochondrial Rho GTPase (Miro) and Milton (170). Milton binds directly to Kinesin-1 (149), whereas Miro serves as an anchor linking Milton and Kinesin-1 to mitochondria (55). The Milton-Miro complex has been recognized in *Drosophila* (19), rats and humans (20). Mutations in either Miro or Milton result in disruptions to mitochondrial distribution in *Drosophila* (55; 59). Miro and Milton proteins are also involved in Ca^{2+}-dependent mitochondrial movement along microtubules (101; 170). Elevated Ca^{2+} binds to the EF hands of Miro inducing a conformational change in the protein and allowing for its dissociation from microtubules, thus arresting mitochondrial movements (101; 170).

3.1.2. Dynein motor protein

Cytoplasmic dynein is another microtubule-based motor protein that governs organelle movement towards the direction of the centre of the cell. The dynein complex is composed of a carboxy-terminal motor "head" domain, consisting of a microtubule binding domain and an ATPase domain, which powers motility along microtubules, an amino-terminal tail domain, which consists of several noncatalytic subunits, and a linker region connecting the head and tail regions. The amino-terminal domain of dynein homodimerizes and acts as the scaffolding for the assembly of the noncatalytic subunits which regulate dynein motility. One of the subunits of the tail domain is dynactin. Dynein and dynactin form a multi-subunit complex that direct movement along microtubules towards the cell centre (85). Although dynein alone can generate force and move along microtubules, it cannot bind to cargo on its own and requires dynactin as a linker between dynein and its cargo (85; 94). The dynactin complex is composed of eleven different subunits, the largest ones being the actin related protein (Arp1) polymer, and $p150^{Glued}$ (71; 139). $p150^{Glued}$ binds directly to microtubules and dynein, and allows for proper transport of cargo throughout the cell (85).

3.2. Actin

Microfilaments, also known as actin filaments, are composed of actin monomers and average 8 nm in diameter (142). The globular actin (G-actin) monomers polymerize to form filamentous actin (F-actin). Two filaments twist to form helical actin. Actin has a fast growing end, where there is a net addition of subunits, and a slow growing end,

with a net loss of actin subunits. G-actin monomers are added to the growing filament end as ATP-actin. ATP bound to actin is dephosphorylated to ADP during polymerization (153). ADP and phosphate (P_i) both remain bound to actin, and after a long delay P_i is released, resulting in ADP bound actin (166). The regulation of actin growth is determined not only by assembly and depolymerization steps, but also by branching and capping events. Actin filaments alternate between capped and uncapped states. Capping is important because it inhibits the disassembly of actin (166). Furthermore, cross-linking of actin filaments is regulated primarily by the actin related protein (Arp2/3) complex. The Arp2/3 complex binds to the side of existing actin filaments and initiates the polymerization of a new actin branch (166).

Mammals possess at least six isoforms of actin. Four muscle actins have been identified: α-skeletal, α-cardiac, α-smooth, and γ-smooth muscle actins, all have very similar structures (165). Two cytoplasmic cytoskeletal actins (β- and γ-non-muscle) have also been found (165).

In *S. cerevisiae* the positioning of mitochondria is reliant on actin-based transportation (146). Furthermore, in cultured neurons, mitochondria use both microtubules and actin filaments for transport, although the motile behaviour of mitochondria are different between the two cytoskeletal filaments. Whereby movement across actin occurs slower than along microtubules (111).

3.2.1. Myosin motor proteins

Myosin motor proteins use actin filaments to transport cargo throughout the cell. To date, very limited work has been done to determine the role of myosin motors in regulating mitochondrial movement along actin. The best candidates for mitochondrial movement are members of the myosin I, II, V, and VI families, as these motor proteins have been associated with movement of a variety of organelles (69). Myosin V has been shown to play a role in mitochondrial movement in budding yeast (7). Pathak *et al* found that mitochondrial motility away from the cell body was disrupted by myosin V, while movement towards the cell body was altered by both myosin V and VI (126).

3.3. Intermediate filaments

Intermediate filaments are flexible structures, ranging from 10-12 nm in diameter (154). They are primarily used as structural support within animal cytoplasm and nuclei. There are five different categories of intermediate filaments, four are cytosolic and one is located in the nucleus (65). To date there is no known motor proteins for intermediate filaments and they not thought to be involved in organelle movement.

4.0 PURPOSES:

Based on the literature review, we have designed experiments with the following purposes in mind:

1. To determine how mitochondrial morphology is altered during muscle use and disuse.
2. To determine which cytoskeletal components are primary responsible for mitochondrial movement in muscle cells;
3. To investigate the influence of calcium and ROS signaling on mitochondrial dynamics in myoblasts.

Reference List

1. World Health Organization [Online]. 2011.
2. **Adams V, Gielen S, Hambrecht R and Schuler G**. Apoptosis in skeletal muscle. *Front Biosci* 6: D1-D11, 2001.
3. **Adhihetty PJ, O'Leary MF, Chabi B, Wicks KL and Hood DA**. Effect of denervation on mitochondrially mediated apoptosis in skeletal muscle. *J Appl Physiol* 102: 1143-1151, 2007.
4. **Aizawa H, Sekine Y, Takemura R, Zhang Z, Nangaku M and Hirokawa N**. Kinesin family in murine central nervous system. *J Cell Biol* 119: 1287-1296, 1992.
5. **Akimoto T, Pohnert SC, Li P, Zhang M, Gumbs C, Rosenberg PB, Williams RS and Yan Z**. Exercise stimulates Pgc-1alpha transcription in skeletal muscle through activation of the p38 MAPK pathway. *J Biol Chem* 280: 19587-19593, 2005.
6. **Altmann R**. *Die Elementarorganismen Und Ihre Beziehungen Zu Den Zellen.* Leipzig: Veit & comp, 1890.
7. **Altmann K, Frank M, Neumann D, Jakobs S and Westermann B**. The class V myosin motor protein, Myo2, plays a major role in mitochondrial motility in Saccharomyces cerevisiae. *J Cell Biol* 181: 119-130, 2008.
8. **Argyropoulos G, Stutz AM, Ilnytska O, Rice T, Teran-Garcia M, Rao DC, Bouchard C and Rankinen T**. KIF5B gene sequence variation and response of cardiac stroke volume to regular exercise. *Physiol Genomics* 36: 79-88, 2009.
9. **Bach D, Naon D, Pich S, Soriano FX, Vega N, Rieusset J, Laville M, Guillet C, Boirie Y, Wallberg-Henriksson H, Manco M, Calvani M, Castagneto M, Palacin M, Mingrone G, Zierath JR, Vidal H and Zorzano A**. Expression of Mfn2, the Charcot-Marie-Tooth neuropathy type 2A gene, in human skeletal muscle: effects of type 2 diabetes, obesity, weight loss, and the regulatory role of tumor necrosis factor alpha and interleukin-6. *Diabetes* 54: 2685-2693, 2005.
10. **Bach D, Pich S, Soriano FX, Vega N, Baumgartner B, Oriola J, Daugaard JR, Lloberas J, Camps M, Zierath JR, Rabasa-Lhoret R, Wallberg-Henriksson H, Laville M, Palacin M, Vidal H, Rivera F, Brand M and Zorzano A**. Mitofusin-2 determines mitochondrial network architecture and mitochondrial metabolism. A novel regulatory mechanism altered in obesity. *J Biol Chem* 278: 17190-17197, 2003.
11. **Bakeeva LE, Chentsov YS and Skulachev VP**. Ontogenesis of mitochondrial reticulum in rat diaphragm muscle. *Eur J Cell Biol* 25: 175-181, 1981.
12. **Bakeeva LE, Chentsov Y and Skulachev VP**. Mitochondrial framework (reticulum mitochondriale) in rat diaphragm muscle. *Biochim Biophys Acta* 501: 349-369, 1978.
13. **Baker BM, Nargund AM, Sun T and Haynes CM**. Protective coupling of mitochondrial function and protein synthesis via the eIF2alpha kinase GCN-2. *PLoS Genet* 8: e1002760, 2012.

14. **Balaban RS, Nemoto S and Finkel T**. Mitochondria, oxidants, and aging. *Cell* 120: 483-495, 2005.
15. **Balagopal P, Rooyackers OE, Adey DB, Ades PA and Nair KS**. Effects of aging on in vivo synthesis of skeletal muscle myosin heavy-chain and sarcoplasmic protein in humans. *Am J Physiol* 273: E790-E800, 1997.
16. **Barja G**. Mitochondrial oxygen radical generation and leak: sites of production in states 4 and 3, organ specificity, and relation to aging and longevity. *J Bioenerg Biomembr* 31: 347-366, 1999.
17. **Bleazard W, McCaffery JM, King EJ, Bale S, Mozdy A, Tieu Q, Nunnari J and Shaw JM**. The dynamin-related GTPase Dnm1 regulates mitochondrial fission in yeast. *Nat Cell Biol* 1: 298-304, 1999.
18. **Boveris A and Chance B**. The mitochondrial generation of hydrogen peroxide. General properties and effect of hyperbaric oxygen. *Biochem J* 134: 707-716, 1973.
19. **Brickley K, Smith MJ, Beck M and Stephenson FA**. GRIF-1 and OIP106, members of a novel gene family of coiled-coil domain proteins: association in vivo and in vitro with kinesin. *J Biol Chem* 280: 14723-14732, 2005.
20. **Brickley K and Stephenson FA**. Trafficking kinesin protein (TRAK)-mediated transport of mitochondria in axons of hippocampal neurons. *J Biol Chem* 286: 18079-18092, 2011.
21. **Bua EA, McKiernan SH, Wanagat J, McKenzie D and Aiken JM**. Mitochondrial abnormalities are more frequent in muscles undergoing sarcopenia. *J Appl Physiol (1985)* 92: 2617-2624, 2002.
22. **Camello-Almaraz C, Gomez-Pinilla PJ, Pozo MJ and Camello PJ**. Mitochondrial reactive oxygen species and Ca2+ signaling. *Am J Physiol Cell Physiol* 291: C1082-C1088, 2006.
23. **Canto C, Gerhart-Hines Z, Feige JN, Lagouge M, Noriega L, Milne JC, Elliott PJ, Puigserver P and Auwerx J**. AMPK regulates energy expenditure by modulating NAD+ metabolism and SIRT1 activity. *Nature* 458: 1056-1060, 2009.
24. **Cartoni R, Leger B, Hock MB, Praz M, Crettenand A, Pich S, Ziltener JL, Luthi F, Deriaz O, Zorzano A, Gobelet C, Kralli A and Russell AP**. Mitofusins 1/2 and ERRalpha expression are increased in human skeletal muscle after physical exercise. *J Physiol* 567: 349-358, 2005.
25. **Cereghetti GM, Stangherlin A, Martins de BO, Chang CR, Blackstone C, Bernardi P and Scorrano L**. Dephosphorylation by calcineurin regulates translocation of Drp1 to mitochondria. *Proc Natl Acad Sci U S A* 105: 15803-15808, 2008.
26. **Chabi B, Ljubicic V, Menzies KJ, Huang JH, Saleem A and Hood DA**. Mitochondrial function and apoptotic susceptibility in aging skeletal muscle. *Aging Cell* 7: 2-12, 2008.
27. **Chang CR and Blackstone C**. Cyclic AMP-dependent protein kinase phosphorylation of Drp1 regulates its GTPase activity and mitochondrial morphology. *J Biol Chem* 282: 21583-21587, 2007.

28. **Chen H, Chomyn A and Chan DC**. Disruption of fusion results in mitochondrial heterogeneity and dysfunction. *J Biol Chem* 280: 26185-26192, 2005.
29. **Chen H, Detmer SA, Ewald AJ, Griffin EE, Fraser SE and Chan DC**. Mitofusins Mfn1 and Mfn2 coordinately regulate mitochondrial fusion and are essential for embryonic development. *J Cell Biol* 160: 189-200, 2003.
30. **Chen H, Vermulst M, Wang YE, Chomyn A, Prolla TA, McCaffery JM and Chan DC**. Mitochondrial fusion is required for mtDNA stability in skeletal muscle and tolerance of mtDNA mutations. *Cell* 141: 280-289, 2010.
31. **Chin ER and Allen DG**. The role of elevations in intracellular [Ca2+] in the development of low frequency fatigue in mouse single muscle fibres. *J Physiol* 491 (Pt 3): 813-824, 1996.
32. **Cho SG, Du Q, Huang S and Dong Z**. Drp1 dephosphorylation in ATP depletion-induced mitochondrial injury and tubular cell apoptosis. *Am J Physiol Renal Physiol* 299: F199-F206, 2010.
33. **Cipolat S, Martins de BO, Dal ZB and Scorrano L**. OPA1 requires mitofusin 1 to promote mitochondrial fusion. *Proc Natl Acad Sci U S A* 101: 15927-15932, 2004.
34. **Cogswell AM, Stevens RJ and Hood DA**. Properties of skeletal muscle mitochondria isolated from subsarcolemmal and intermyofibrillar regions. *Am J Physiol* 264: C383-C389, 1993.
35. **Cribbs JT and Strack S**. Reversible phosphorylation of Drp1 by cyclic AMP-dependent protein kinase and calcineurin regulates mitochondrial fission and cell death. *EMBO Rep* 8: 939-944, 2007.
36. **Davies KJ, Quintanilha AT, Brooks GA and Packer L**. Free radicals and tissue damage produced by exercise. *Biochem Biophys Res Commun* 107: 1198-1205, 1982.
37. **De Vos KJ, Allan VJ, Grierson AJ and Sheetz MP**. Mitochondrial function and actin regulate dynamin-related protein 1-dependent mitochondrial fission. *Curr Biol* 15: 678-683, 2005.
38. **DeFronzo RA, Gunnarsson R, Bjorkman O, Olsson M and Wahren J**. Effects of insulin on peripheral and splanchnic glucose metabolism in noninsulin-dependent (type II) diabetes mellitus. *J Clin Invest* 76: 149-155, 1985.
39. **DeFronzo RA and Tripathy D**. Skeletal muscle insulin resistance is the primary defect in type 2 diabetes. *Diabetes Care* 32 Suppl 2: S157-S163, 2009.
40. **Delettre C, Griffoin JM, Kaplan J, Dollfus H, Lorenz B, Faivre L, Lenaers G, Belenguer P and Hamel CP**. Mutation spectrum and splicing variants in the OPA1 gene. *Hum Genet* 109: 584-591, 2001.
41. **Ding H, Jiang N, Liu H, Liu X, Liu D, Zhao F, Wen L, Liu S, Ji LL and Zhang Y**. Response of mitochondrial fusion and fission protein gene expression to exercise in rat skeletal muscle. *Biochim Biophys Acta* 1800: 250-256, 2010.
42. **Dirks AJ and Leeuwenburgh C**. Aging and lifelong calorie restriction result in adaptations of skeletal muscle apoptosis repressor, apoptosis-inducing factor, X-linked inhibitor of apoptosis, caspase-3, and caspase-12. *Free Radic Biol Med* 36: 27-39, 2004.

43. **Dohm JA, Lee SJ, Hardwick JM, Hill RB and Gittis AG**. Cytosolic domain of the human mitochondrial fission protein fis1 adopts a TPR fold. *Proteins* 54: 153-156, 2004.
44. **Ehses S, Raschke I, Mancuso G, Bernacchia A, Geimer S, Tondera D, Martinou JC, Westermann B, Rugarli EI and Langer T**. Regulation of OPA1 processing and mitochondrial fusion by m-AAA protease isoenzymes and OMA1. *J Cell Biol* 187: 1023-1036, 2009.
45. **Fannjiang Y, Cheng WC, Lee SJ, Qi B, Pevsner J, McCaffery JM, Hill RB, Basanez G and Hardwick JM**. Mitochondrial fission proteins regulate programmed cell death in yeast. *Genes Dev* 18: 2785-2797, 2004.
46. **Frank S, Gaume B, Bergmann-Leitner ES, Leitner WW, Robert EG, Catez F, Smith CL and Youle RJ**. The role of dynamin-related protein 1, a mediator of mitochondrial fission, in apoptosis. *Dev Cell* 1: 515-525, 2001.
47. **Freyssenet D, Connor MK, Takahashi M and Hood DA**. Cytochrome c transcriptional activation and mRNA stability during contractile activity in skeletal muscle. *Am J Physiol* 277: E26-E32, 1999.
48. **Freyssenet D, Di CM and Hood DA**. Calcium-dependent regulation of cytochrome c gene expression in skeletal muscle cells. Identification of a protein kinase c-dependent pathway. *J Biol Chem* 274: 9305-9311, 1999.
49. **Freyssenet D, Irrcher I, Connor MK, Di CM and Hood DA**. Calcium-regulated changes in mitochondrial phenotype in skeletal muscle cells. *Am J Physiol Cell Physiol* 286: C1053-C1061, 2004.
50. **Frezza C, Cipolat S, Martins de BO, Micaroni M, Beznoussenko GV, Rudka T, Bartoli D, Polishuck RS, Danial NN, De SB and Scorrano L**. OPA1 controls apoptotic cristae remodeling independently from mitochondrial fusion. *Cell* 126: 177-189, 2006.
51. **Fujii N, Hayashi T, Hirshman MF, Smith JT, Habinowski SA, Kaijser L, Mu J, Ljungqvist O, Birnbaum MJ, Witters LA, Thorell A and Goodyear LJ**. Exercise induces isoform-specific increase in 5'AMP-activated protein kinase activity in human skeletal muscle. *Biochem Biophys Res Commun* 273: 1150-1155, 2000.
52. **Garnier A, Fortin D, Zoll J, N'Guessan B, Mettauer B, Lampert E, Veksler V and Ventura-Clapier R**. Coordinated changes in mitochondrial function and biogenesis in healthy and diseased human skeletal muscle. *FASEB J* 19: 43-52, 2005.
53. **Gauthier GF and Padykula HA**. Cytological studies of fiber types in skeletal muscle. A comparative study of the mammalian diaphragm. *J Cell Biol* 28: 333-354, 1966.
54. **Gegg ME, Cooper JM, Chau KY, Rojo M, Schapira AH and Taanman JW**. Mitofusin 1 and mitofusin 2 are ubiquitinated in a PINK1/parkin-dependent manner upon induction of mitophagy. *Hum Mol Genet* 19: 4861-4870, 2010.
55. **Glater EE, Megeath LJ, Stowers RS and Schwarz TL**. Axonal transport of mitochondria requires milton to recruit kinesin heavy chain and is light chain independent. *J Cell Biol* 173: 545-557, 2006.

56. **Gomez-Cabrera MC, Borras C, Pallardo FV, Sastre J, Ji LL and Vina J**. Decreasing xanthine oxidase-mediated oxidative stress prevents useful cellular adaptations to exercise in rats. *J Physiol* 567: 113-120, 2005.
57. **Goodner CJ, Walike BC, Koerker DJ, Ensinck JW, Brown AC, Chideckel EW, Palmer J and Kalnasy L**. Insulin, glucagon, and glucose exhibit synchronous, sustained oscillations in fasting monkeys. *Science* 195: 177-179, 1977.
58. **Gordon JW, Rungi AA, Inagaki H and Hood DA**. Effects of contractile activity on mitochondrial transcription factor A expression in skeletal muscle. *J Appl Physiol* 90: 389-396, 2001.
59. **Guo X, Macleod GT, Wellington A, Hu F, Panchumarthi S, Schoenfield M, Marin L, Charlton MP, Atwood HL and Zinsmaier KE**. The GTPase dMiro is required for axonal transport of mitochondria to Drosophila synapses. *Neuron* 47: 379-393, 2005.
60. **Gustafsson AB and Gottlieb RA**. Recycle or die: the role of autophagy in cardioprotection. *J Mol Cell Cardiol* 44: 654-661, 2008.
61. **Handschin C and Spiegelman BM**. Peroxisome proliferator-activated receptor gamma coactivator 1 coactivators, energy homeostasis, and metabolism. *Endocr Rev* 27: 728-735, 2006.
62. **Harding HP, Novoa I, Zhang Y, Zeng H, Wek R, Schapira M and Ron D**. Regulated translation initiation controls stress-induced gene expression in mammalian cells. *Mol Cell* 6: 1099-1108, 2000.
63. **Harding HP, Zhang Y and Ron D**. Protein translation and folding are coupled by an endoplasmic-reticulum-resident kinase. *Nature* 397: 271-274, 1999.
64. **HARMAN D**. Aging: a theory based on free radical and radiation chemistry. *J Gerontol* 11: 298-300, 1956.
65. **Helfand BT, Chang L and Goldman RD**. Intermediate filaments are dynamic and motile elements of cellular architecture. *J Cell Sci* 117: 133-141, 2004.
66. **Herbst A, Pak JW, McKenzie D, Bua E, Bassiouni M and Aiken JM**. Accumulation of mitochondrial DNA deletion mutations in aged muscle fibers: evidence for a causal role in muscle fiber loss. *J Gerontol A Biol Sci Med Sci* 62: 235-245, 2007.
67. **Herlan M, Vogel F, Bornhovd C, Neupert W and Reichert AS**. Processing of Mgm1 by the rhomboid-type protease Pcp1 is required for maintenance of mitochondrial morphology and of mitochondrial DNA. *J Biol Chem* 278: 27781-27788, 2003.
68. **Hirokawa N, Noda Y, Tanaka Y and Niwa S**. Kinesin superfamily motor proteins and intracellular transport. *Nat Rev Mol Cell Biol* 10: 682-696, 2009.
69. **Hollenbeck PJ and Saxton WM**. The axonal transport of mitochondria. *J Cell Sci* 118: 5411-5419, 2005.
70. **Holloszy JO**. Biochemical adaptations in muscle. Effects of exercise on mitochondrial oxygen uptake and respiratory enzyme activity in skeletal muscle. *J Biol Chem* 242: 2278-2282, 1967.

71. **Holzbaur EL, Hammarback JA, Paschal BM, Kravit NG, Pfister KK and Vallee RB**. Homology of a 150K cytoplasmic dynein-associated polypeptide with the Drosophila gene Glued. *Nature* 351: 579-583, 1991.
72. **Hood DA**. Invited Review: contractile activity-induced mitochondrial biogenesis in skeletal muscle. *J Appl Physiol (1985)* 90: 1137-1157, 2001.
73. **Hood DA, Uguccioni G, Vainshtein A and D'souza D**. Mechanisms of exercise-induced mitochondrial biogenesis in skeletal muscle: implications for health and disease. *Compr Physiol* 1: 1119-1134, 2011.
74. **Horibe T and Hoogenraad NJ**. The chop gene contains an element for the positive regulation of the mitochondrial unfolded protein response. *PLoS One* 2: e835, 2007.
75. **Huang JH, Joseph AM, Ljubicic V, Iqbal S and Hood DA**. Effect of age on the processing and import of matrix-destined mitochondrial proteins in skeletal muscle. *J Gerontol A Biol Sci Med Sci* 65: 138-146, 2010.
76. **Ishihara N, Eura Y and Mihara K**. Mitofusin 1 and 2 play distinct roles in mitochondrial fusion reactions via GTPase activity. *J Cell Sci* 117: 6535-6546, 2004.
77. **Jagasia R, Grote P, Westermann B and Conradt B**. DRP-1-mediated mitochondrial fragmentation during EGL-1-induced cell death in C. elegans. *Nature* 433: 754-760, 2005.
78. **Jager S, Handschin C, St-Pierre J and Spiegelman BM**. AMP-activated protein kinase (AMPK) action in skeletal muscle via direct phosphorylation of PGC-1alpha. *Proc Natl Acad Sci U S A* 104: 12017-12022, 2007.
79. **Jerusalem F, Engel AG and Peterson HA**. Human muscle fiber fine structure: morphometric data on controls. *Neurology* 25: 127-134, 1975.
80. **Kabeya Y, Mizushima N, Ueno T, Yamamoto A, Kirisako T, Noda T, Kominami E, Ohsumi Y and Yoshimori T**. LC3, a mammalian homologue of yeast Apg8p, is localized in autophagosome membranes after processing. *EMBO J* 19: 5720-5728, 2000.
81. **Kayar SR, Hoppeler H, Mermod L and Weibel ER**. Mitochondrial size and shape in equine skeletal muscle: a three-dimensional reconstruction study. *Anat Rec* 222: 333-339, 1988.
82. **Kelley DE, He J, Menshikova EV and Ritov VB**. Dysfunction of mitochondria in human skeletal muscle in type 2 diabetes. *Diabetes* 51: 2944-2950, 2002.
83. **Kemper C, Habib SJ, Engl G, Heckmeyer P, Dimmer KS and Rapaport D**. Integration of tail-anchored proteins into the mitochondrial outer membrane does not require any known import components. *J Cell Sci* 121: 1990-1998, 2008.
84. **Kerr JF, Wyllie AH and Currie AR**. Apoptosis: a basic biological phenomenon with wide-ranging implications in tissue kinetics. *Br J Cancer* 26: 239-257, 1972.
85. **King SJ and Schroer TA**. Dynactin increases the processivity of the cytoplasmic dynein motor. *Nat Cell Biol* 2: 20-24, 2000.
86. **Kirkwood SP, Munn EA and Brooks GA**. Mitochondrial reticulum in limb skeletal muscle. *Am J Physiol* 251: C395-C402, 1986.

87. **Kirkwood SP, Packer L and Brooks GA**. Effects of endurance training on a mitochondrial reticulum in limb skeletal muscle. *Arch Biochem Biophys* 255: 80-88, 1987.
88. **Koren A, Sauber C, Sentjurc M and Schara M**. Free radicals in tetanic activity of isolated skeletal muscle. *Comp Biochem Physiol B* 74: 633-635, 1983.
89. **Koshiba T, Detmer SA, Kaiser JT, Chen H, McCaffery JM and Chan DC**. Structural basis of mitochondrial tethering by mitofusin complexes. *Science* 305: 858-862, 2004.
90. **Krieger DA, Tate CA, Millin-Wood J and Booth FW**. Populations of rat skeletal muscle mitochondria after exercise and immobilization. *J Appl Physiol* 48: 23-28, 1980.
91. **Lai RY, Ljubicic V, D'souza D and Hood DA**. Effect of chronic contractile activity on mRNA stability in skeletal muscle. *Am J Physiol Cell Physiol* 299: C155-C163, 2010.
92. **Landes T, Emorine LJ, Courilleau D, Rojo M, Belenguer P and rnaune-Pelloquin L**. The BH3-only Bnip3 binds to the dynamin Opa1 to promote mitochondrial fragmentation and apoptosis by distinct mechanisms. *EMBO Rep* 11: 459-465, 2010.
93. **Lee YJ, Jeong SY, Karbowski M, Smith CL and Youle RJ**. Roles of the mammalian mitochondrial fission and fusion mediators Fis1, Drp1, and Opa1 in apoptosis. *Mol Biol Cell* 15: 5001-5011, 2004.
94. **Levy JR and Holzbaur EL**. Cytoplasmic dynein/dynactin function and dysfunction in motor neurons. *Int J Dev Neurosci* 24: 103-111, 2006.
95. **Lewis MR and Lewis WH**. Mitochondria (and other cytoplasmic structures) in tissue cultures. *Am J Anat* 17: 339-401, 1915.
96. **Lexell J, Taylor CC and Sjostrom M**. What is the cause of the ageing atrophy? Total number, size and proportion of different fiber types studied in whole vastus lateralis muscle from 15- to 83-year-old men. *J Neurol Sci* 84: 275-294, 1988.
97. **Liesa M, Palacin M and Zorzano A**. Mitochondrial dynamics in mammalian health and disease. *Physiol Rev* 89: 799-845, 2009.
98. **Lizcano JM, Goransson O, Toth R, Deak M, Morrice NA, Boudeau J, Hawley SA, Udd L, Makela TP, Hardie DG and Alessi DR**. LKB1 is a master kinase that activates 13 kinases of the AMPK subfamily, including MARK/PAR-1. *EMBO J* 23: 833-843, 2004.
99. **Lopez ME, Van Zeeland NL, Dahl DB, Weindruch R and Aiken JM**. Cellular phenotypes of age-associated skeletal muscle mitochondrial abnormalities in rhesus monkeys. *Mutat Res* 452: 123-138, 2000.
100. **Loschen G, Azzi A, Richter C and Flohe L**. Superoxide radicals as precursors of mitochondrial hydrogen peroxide. *FEBS Lett* 42: 68-72, 1974.
101. **Macaskill AF, Rinholm JE, Twelvetrees AE, rancibia-Carcamo IL, Muir J, Fransson A, Aspenstrom P, Attwell D and Kittler JT**. Miro1 is a calcium sensor for glutamate receptor-dependent localization of mitochondria at synapses. *Neuron* 61: 541-555, 2009.

102. **Mansouri A, Muller FL, Liu Y, Ng R, Faulkner J, Hamilton M, Richardson A, Huang TT, Epstein CJ and Van RH**. Alterations in mitochondrial function, hydrogen peroxide release and oxidative damage in mouse hind-limb skeletal muscle during aging. *Mech Ageing Dev* 127: 298-306, 2006.
103. **Means AR, VanBerkum MF, Bagchi I, Lu KP and Rasmussen CD**. Regulatory functions of calmodulin. *Pharmacol Ther* 50: 255-270, 1991.
104. **Meyer T, Hanson PI, Stryer L and Schulman H**. Calmodulin trapping by calcium-calmodulin-dependent protein kinase. *Science* 256: 1199-1202, 1992.
105. **Midrio M**. The denervated muscle: facts and hypotheses. A historical review. *Eur J Appl Physiol* 98: 1-21, 2006.
106. **Miki H, Okada Y and Hirokawa N**. Analysis of the kinesin superfamily: insights into structure and function. *Trends Cell Biol* 15: 467-476, 2005.
107. **Miki H, Setou M, Kaneshiro K and Hirokawa N**. All kinesin superfamily protein, KIF, genes in mouse and human. *Proc Natl Acad Sci U S A* 98: 7004-7011, 2001.
108. **Miledi R and Slater CR**. Some mitochondrial changes in denervated muscle. *J Cell Sci* 3: 49-54, 1968.
109. **Mitchison T and Kirschner M**. Dynamic instability of microtubule growth. *Nature* 312: 237-242, 1984.
110. **Mitchison T and Kirschner M**. Microtubule assembly nucleated by isolated centrosomes. *Nature* 312: 232-237, 1984.
111. **Morris RL and Hollenbeck PJ**. Axonal transport of mitochondria along microtubules and F-actin in living vertebrate neurons. *J Cell Biol* 131: 1315-1326, 1995.
112. **Murphy ME and Kehrer JP**. Activities of antioxidant enzymes in muscle, liver and lung of chickens with inherited muscular dystrophy. *Biochem Biophys Res Commun* 134: 550-556, 1986.
113. **Musacchia XJ, Steffen JM and Fell RD**. Disuse atrophy of skeletal muscle: animal models. *Exerc Sport Sci Rev* 16: 61-87, 1988.
114. **Nangaku M, Sato-Yoshitake R, Okada Y, Noda Y, Takemura R, Yamazaki H and Hirokawa N**. KIF1B, a novel microtubule plus end-directed monomeric motor protein for transport of mitochondria. *Cell* 79: 1209-1220, 1994.
115. **Narendra D, Tanaka A, Suen DF and Youle RJ**. Parkin is recruited selectively to impaired mitochondria and promotes their autophagy. *J Cell Biol* 183: 795-803, 2008.
116. **Nargund AM, Pellegrino MW, Fiorese CJ, Baker BM and Haynes CM**. Mitochondrial import efficiency of ATFS-1 regulates mitochondrial UPR activation. *Science* 337: 587-590, 2012.
117. **O'Leary MF and Hood DA**. Effect of prior chronic contractile activity on mitochondrial function and apoptotic protein expression in denervated muscle. *J Appl Physiol* 105: 114-120, 2008.
118. **Ogata T and Yamasaki Y**. Scanning electron-microscopic studies on the three-dimensional structure of mitochondria in the mammalian red, white and intermediate muscle fibers. *Cell Tissue Res* 241: 251-256, 1985.

119. **Ogata T and Yamasaki Y**. Ultra-high-resolution scanning electron microscopy of mitochondria and sarcoplasmic reticulum arrangement in human red, white, and intermediate muscle fibers. *Anat Rec* 248: 214-223, 1997.
120. **Okatsu K, Saisho K, Shimanuki M, Nakada K, Shitara H, Sou YS, Kimura M, Sato S, Hattori N, Komatsu M, Tanaka K and Matsuda N**. p62/SQSTM1 cooperates with Parkin for perinuclear clustering of depolarized mitochondria. *Genes Cells* 15: 887-900, 2010.
121. **Olichon A, Baricault L, Gas N, Guillou E, Valette A, Belenguer P and Lenaers G**. Loss of OPA1 perturbates the mitochondrial inner membrane structure and integrity, leading to cytochrome c release and apoptosis. *J Biol Chem* 278: 7743-7746, 2003.
122. **Olichon A, Emorine LJ, Descoins E, Pelloquin L, Brichese L, Gas N, Guillou E, Delettre C, Valette A, Hamel CP, Ducommun B, Lenaers G and Belenguer P**. The human dynamin-related protein OPA1 is anchored to the mitochondrial inner membrane facing the inter-membrane space. *FEBS Lett* 523: 171-176, 2002.
123. **Ono T, Isobe K, Nakada K and Hayashi JI**. Human cells are protected from mitochondrial dysfunction by complementation of DNA products in fused mitochondria. *Nat Genet* 28: 272-275, 2001.
124. **Palmer JW, Tandler B and Hoppel CL**. Biochemical properties of subsarcolemmal and interfibrillar mitochondria isolated from rat cardiac muscle. *J Biol Chem* 252: 8731-8739, 1977.
125. **Parone PA, Da CS, Tondera D, Mattenberger Y, James DI, Maechler P, Barja F and Martinou JC**. Preventing mitochondrial fission impairs mitochondrial function and leads to loss of mitochondrial DNA. *PLoS One* 3: e3257, 2008.
126. **Pathak D, Sepp KJ and Hollenbeck PJ**. Evidence that myosin activity opposes microtubule-based axonal transport of mitochondria. *J Neurosci* 30: 8984-8992, 2010.
127. **Pellegrino MW, Nargund AM and Haynes CM**. Signaling the mitochondrial unfolded protein response. *Biochim Biophys Acta* 1833: 410-416, 2013.
128. **Piao YJ, Seo YH, Hong F, Kim JH, Kim YJ, Kang MH, Kim BS, Jo SA, Jo I, Jue DM, Kang I, Ha J and Kim SS**. Nox 2 stimulates muscle differentiation via NF-kappaB/iNOS pathway. *Free Radic Biol Med* 38: 989-1001, 2005.
129. **Picard M, Gentil BJ, McManus MJ, White K, St LK, Gartside SE, Wallace DC and Turnbull DM**. Acute exercise remodels mitochondrial membrane interactions in mouse skeletal muscle. *J Appl Physiol (1985)* 2013.
130. **Pilegaard H, Saltin B and Neufer PD**. Exercise induces transient transcriptional activation of the PGC-1alpha gene in human skeletal muscle. *J Physiol* 546: 851-858, 2003.
131. **Pilling AD, Horiuchi D, Lively CM and Saxton WM**. Kinesin-1 and Dynein are the primary motors for fast transport of mitochondria in Drosophila motor axons. *Mol Biol Cell* 17: 2057-2068, 2006.
132. **Poggi P, Marchetti C and Scelsi R**. Automatic morphometric analysis of skeletal muscle fibers in the aging man. *Anat Rec* 217: 30-34, 1987.

133. **Priault M, Salin B, Schaeffer J, Vallette FM, di Rago JP and Martinou JC**. Impairing the bioenergetic status and the biogenesis of mitochondria triggers mitophagy in yeast. *Cell Death Differ* 12: 1613-1621, 2005.
134. **Rojo M, Legros F, Chateau D and Lombes A**. Membrane topology and mitochondrial targeting of mitofusins, ubiquitous mammalian homologs of the transmembrane GTPase Fzo. *J Cell Sci* 115: 1663-1674, 2002.
135. **Romanello V, Guadagnin E, Gomes L, Roder I, Sandri C, Petersen Y, Milan G, Masiero E, Del PP, Foretz M, Scorrano L, Rudolf R and Sandri M**. Mitochondrial fission and remodelling contributes to muscle atrophy. *EMBO J* 29: 1774-1785, 2010.
136. **Rose AJ, Kiens B and Richter EA**. Ca2+-calmodulin-dependent protein kinase expression and signalling in skeletal muscle during exercise. *J Physiol* 574: 889-903, 2006.
137. **Santel A, Frank S, Gaume B, Herrler M, Youle RJ and Fuller MT**. Mitofusin-1 protein is a generally expressed mediator of mitochondrial fusion in mammalian cells. *J Cell Sci* 116: 2763-2774, 2003.
138. **Santel A and Fuller MT**. Control of mitochondrial morphology by a human mitofusin. *J Cell Sci* 114: 867-874, 2001.
139. **Schafer DA, Gill SR, Cooper JA, Heuser JE and Schroer TA**. Ultrastructural analysis of the dynactin complex: an actin-related protein is a component of a filament that resembles F-actin. *J Cell Biol* 126: 403-412, 1994.
140. **Scherz-Shouval R, Shvets E, Fass E, Shorer H, Gil L and Elazar Z**. Reactive oxygen species are essential for autophagy and specifically regulate the activity of Atg4. *EMBO J* 26: 1749-1760, 2007.
141. **Schnitzer MJ and Block SM**. Kinesin hydrolyses one ATP per 8-nm step. *Nature* 388: 386-390, 1997.
142. **Schutt CE, Myslik JC, Rozycki MD, Goonesekere NC and Lindberg U**. The structure of crystalline profilin-beta-actin. *Nature* 365: 810-816, 1993.
143. **Seo HY, Kim YD, Lee KM, Min AK, Kim MK, Kim HS, Won KC, Park JY, Lee KU, Choi HS, Park KG and Lee IK**. Endoplasmic reticulum stress-induced activation of activating transcription factor 6 decreases insulin gene expression via up-regulation of orphan nuclear receptor small heterodimer partner. *Endocrinology* 149: 3832-3841, 2008.
144. **Serasinghe MN and Yoon Y**. The mitochondrial outer membrane protein hFis1 regulates mitochondrial morphology and fission through self-interaction. *Exp Cell Res* 314: 3494-3507, 2008.
145. **Silveira LR, Pilegaard H, Kusuhara K, Curi R and Hellsten Y**. The contraction induced increase in gene expression of peroxisome proliferator-activated receptor (PPAR)-gamma coactivator 1alpha (PGC-1alpha), mitochondrial uncoupling protein 3 (UCP3) and hexokinase II (HKII) in primary rat skeletal muscle cells is dependent on reactive oxygen species. *Biochim Biophys Acta* 1763: 969-976, 2006.

146. **Simon VR, Karmon SL and Pon LA**. Mitochondrial inheritance: cell cycle and actin cable dependence of polarized mitochondrial movements in Saccharomyces cerevisiae. *Cell Motil Cytoskeleton* 37: 199-210, 1997.
147. **Singh K and Hood DA**. Effect of denervation-induced muscle disuse on mitochondrial protein import. *Am J Physiol Cell Physiol* 300: C138-C145, 2011.
148. **Smirnova E, Shurland DL, Ryazantsev SN and van der Bliek AM**. A human dynamin-related protein controls the distribution of mitochondria. *J Cell Biol* 143: 351-358, 1998.
149. **Smith MJ, Pozo K, Brickley K and Stephenson FA**. Mapping the GRIF-1 binding domain of the kinesin, KIF5C, substantiates a role for GRIF-1 as an adaptor protein in the anterograde trafficking of cargoes. *J Biol Chem* 281: 27216-27228, 2006.
150. **Steinberg GR and Kemp BE**. AMPK in Health and Disease. *Physiol Rev* 89: 1025-1078, 2009.
151. **Stojanovski D, Koutsopoulos OS, Okamoto K and Ryan MT**. Levels of human Fis1 at the mitochondrial outer membrane regulate mitochondrial morphology. *J Cell Sci* 117: 1201-1210, 2004.
152. **Strack S and Cribbs JT**. Allosteric modulation of Drp1 mechanoenzyme assembly and mitochondrial fission by the variable domain. *J Biol Chem* 287: 10990-11001, 2012.
153. **STRAUB FB and FEUER G**. [Adenosine triphosphate, the functional group of actin]. *Kiserl Orvostud* 2: 141-151, 1950.
154. **Strelkov SV, Herrmann H and Aebi U**. Molecular architecture of intermediate filaments. *Bioessays* 25: 243-251, 2003.
155. **Sugioka R, Shimizu S and Tsujimoto Y**. Fzo1, a protein involved in mitochondrial fusion, inhibits apoptosis. *J Biol Chem* 279: 52726-52734, 2004.
156. **Suliman HB, Carraway MS, Welty-Wolf KE, Whorton AR and Piantadosi CA**. Lipopolysaccharide stimulates mitochondrial biogenesis via activation of nuclear respiratory factor-1. *J Biol Chem* 278: 41510-41518, 2003.
157. **Suzuki M, Jeong SY, Karbowski M, Youle RJ and Tjandra N**. The solution structure of human mitochondria fission protein Fis1 reveals a novel TPR-like helix bundle. *J Mol Biol* 334: 445-458, 2003.
158. **Takahashi M and Hood DA**. Chronic stimulation-induced changes in mitochondria and performance in rat skeletal muscle. *J Appl Physiol* 74: 934-941, 1993.
159. **Takahashi M, Rana A and Hood DA**. Portable electrical stimulator for use in small animals. *J Appl Physiol* 74: 942-945, 1993.
160. **Tanaka A, Cleland MM, Xu S, Narendra DP, Suen DF, Karbowski M and Youle RJ**. Proteasome and p97 mediate mitophagy and degradation of mitofusins induced by Parkin. *J Cell Biol* 191: 1367-1380, 2010.
161. **Tanaka Y, Kanai Y, Okada Y, Nonaka S, Takeda S, Harada A and Hirokawa N**. Targeted disruption of mouse conventional kinesin heavy chain, kif5B, results in abnormal perinuclear clustering of mitochondria. *Cell* 93: 1147-1158, 1998.

162. **Tidball JG**. Inflammatory processes in muscle injury and repair. *Am J Physiol Regul Integr Comp Physiol* 288: R345-R353, 2005.
163. **Twig G, Elorza A, Molina AJ, Mohamed H, Wikstrom JD, Walzer G, Stiles L, Haigh SE, Katz S, Las G, Alroy J, Wu M, Py BF, Yuan J, Deeney JT, Corkey BE and Shirihai OS**. Fission and selective fusion govern mitochondrial segregation and elimination by autophagy. *EMBO J* 27: 433-446, 2008.
164. **Uchiyama Y**. Autophagic cell death and its execution by lysosomal cathepsins. *Arch Histol Cytol* 64: 233-246, 2001.
165. **Vandekerckhove J and Weber K**. At least six different actins are expressed in a higher mammal: an analysis based on the amino acid sequence of the amino-terminal tryptic peptide. *J Mol Biol* 126: 783-802, 1978.
166. **Vavylonis D, Yang Q and O'Shaughnessy B**. Actin polymerization kinetics, cap structure, and fluctuations. *Proc Natl Acad Sci U S A* 102: 8543-8548, 2005.
167. **Wallace DC**. Mitochondrial genetics: a paradigm for aging and degenerative diseases? *Science* 256: 628-632, 1992.
168. **Wanagat J, Cao Z, Pathare P and Aiken JM**. Mitochondrial DNA deletion mutations colocalize with segmental electron transport system abnormalities, muscle fiber atrophy, fiber splitting, and oxidative damage in sarcopenia. *FASEB J* 15: 322-332, 2001.
169. **Wang JX, Jiao JQ, Li Q, Long B, Wang K, Liu JP, Li YR and Li PF**. miR-499 regulates mitochondrial dynamics by targeting calcineurin and dynamin-related protein-1. *Nat Med* 17: 71-78, 2011.
170. **Wang X and Schwarz TL**. The mechanism of Ca2+ -dependent regulation of kinesin-mediated mitochondrial motility. *Cell* 136: 163-174, 2009.
171. **Westerblad H and Allen DG**. Changes of myoplasmic calcium concentration during fatigue in single mouse muscle fibers. *J Gen Physiol* 98: 615-635, 1991.
172. **Wicks KL and Hood DA**. Mitochondrial adaptations in denervated muscle: relationship to muscle performance. *Am J Physiol* 260: C841-C850, 1991.
173. **Woods A, Dickerson K, Heath R, Hong SP, Momcilovic M, Johnstone SR, Carlson M and Carling D**. Ca2+/calmodulin-dependent protein kinase kinase-beta acts upstream of AMP-activated protein kinase in mammalian cells. *Cell Metab* 2: 21-33, 2005.
174. **Wright DC, Geiger PC, Han DH, Jones TE and Holloszy JO**. Calcium induces increases in peroxisome proliferator-activated receptor gamma coactivator-1alpha and mitochondrial biogenesis by a pathway leading to p38 mitogen-activated protein kinase activation. *J Biol Chem* 282: 18793-18799, 2007.
175. **Wu Q, Sandrock TM, Turgeon BG, Yoder OC, Wirsel SG and Aist JR**. A fungal kinesin required for organelle motility, hyphal growth, and morphogenesis. *Mol Biol Cell* 9: 89-101, 1998.
176. **Xie M, Zhang D, Dyck JR, Li Y, Zhang H, Morishima M, Mann DL, Taffet GE, Baldini A, Khoury DS and Schneider MD**. A pivotal role for endogenous TGF-beta-activated kinase-1 in the LKB1/AMP-activated protein kinase energy-sensor pathway. *Proc Natl Acad Sci U S A* 103: 17378-17383, 2006.

177. **Zechner C, Lai L, Zechner JF, Geng T, Yan Z, Rumsey JW, Collia D, Chen Z, Wozniak DF, Leone TC and Kelly DP**. Total skeletal muscle PGC-1 deficiency uncouples mitochondrial derangements from fiber type determination and insulin sensitivity. *Cell Metab* 12: 633-642, 2010.
178. **Zuchner S, Mersiyanova IV, Muglia M, Bissar-Tadmouri N, Rochelle J, Dadali EL, Zappia M, Nelis E, Patitucci A, Senderek J, Parman Y, Evgrafov O, Jonghe PD, Takahashi Y, Tsuji S, Pericak-Vance MA, Quattrone A, Battaloglu E, Polyakov AV, Timmerman V, Schroder JM and Vance JM**. Mutations in the mitochondrial GTPase mitofusin 2 cause Charcot-Marie-Tooth neuropathy type 2A. *Nat Genet* 36: 449-451, 2004.
179. **Zuo L, Christofi FL, Wright VP, Bao S and Clanton TL**. Lipoxygenase-dependent superoxide release in skeletal muscle. *J Appl Physiol (1985)* 97: 661-668, 2004.

CHAPTER 2:

MITOCHONDRIAL FISSION AND FUSION IN SKELETAL MUSCLE

Rationale for Manuscript #1

Skeletal muscle is characterized by its high mitochondrial content and its ability to adapt to metabolic stressors. Under conditions of chronic muscle use or disuse the content and morphology of mitochondria is known to be altered. The mitochondrial network within cells is mediated by fission and fusion processes. We investigated the expression of the proteins responsible for these events during conditions of altered oxidative capacity.

We hypothesized that chronic activity would induce alterations in the expression of mitochondrial fission and fusion machineries, and that fusion protein expression would outweigh the expression of fission machinery components. Conversely, during conditions of chronic muscle disuse (aging, denervation), we hypothesized that the expression of mitochondrial fission proteins would be enhanced as compared to the fusion proteins.

SI and DAH conceived and designed the experiments, interpreted the data and wrote the manuscript. SI performed all of the data collection, except for some of the western blots towards the aging portion of the study, which were performed by AMJ. OO performed the *in vivo* stimulation of the animals and the COX activity measurements. KS performed the denervation surgeries.

Expression of Mitochondrial Fission and Fusion Regulatory Proteins in Skeletal Muscle during Chronic Use and Disuse

Sobia Iqbal, Olga Ostojic, Kaustabh Singh, Anna-Maria Joseph and David A. Hood

School of Kinesiology and Health Science, and the Muscle Health Research Centre
York University, Toronto, Ontario M3J 1P3, Canada

Running title: Mitochondrial fission and fusion in skeletal muscle

To whom correspondence should be addressed:

David A. Hood, PhD
School of Kinesiology and Health Science
York University, Toronto, Ontario
M3J 1P3, Canada
Tel: (416) 736-2100 ext: 66640
Fax: (416) 736-5698
E-mail: dhood@yorku.ca

Accepted for publication to: Muscle and Nerve, 2013, Dec 48(6): 963-70.

Abstract

INTRODUCTION: The mitochondrial network within cells is mediated by fission and fusion processes. We investigated the expression of the proteins responsible for these events during conditions of altered oxidative capacity. RESULTS: With chronic contractile activity, the mitochondrial reticulum increased in size, along with concomitant increases in the fusion proteins Opa1 and Mfn2 (by 36% and 53%, $p<0.05$). When we induced muscle disuse through denervation for 7-days, fragmented mitochondria were observed, along with significant decreases in the expression of Mfn2 and Opa1 (by 84% and 70%). To assess the effects of aging on mitochondrial morphology, young (5 month) and aged (35 month) Fisher344 Brown Norway rats were used. Aged animals also possessed smaller mitochondria and displayed increased levels of fission proteins. CONCLUSIONS: Chronic muscle use increases the ratio of fusion:fission proteins, leading to reticular mitochondria, whereas muscle disuse and aging result in a decrease in this ratio, culminating in fragmented organelles.

Introduction

Skeletal muscle is characterized by its high mitochondrial content and its ability to adapt to metabolic stressors. Under conditions of chronic muscle use or disuse, this adaptation process involves coordination of several physiological events such as oxygen delivery, substrate utilization, capillary to muscle fiber ratio, and mitochondrial biogenesis. Although these alterations have been well studied, the effects of muscle use and disuse on mitochondrial morphology and the mechanisms governing the formation of these organelles has yet to be fully established.

In skeletal muscle, mitochondria have been found to exist in varying morphologies, ranging from small individual organelles, to extended reticular networks. Mitochondrial morphology is altered during muscle development (6) and in various disease conditions, including diabetes (4; 26) and obesity (4; 5). These changes in morphology are mediated by a balance of organelle fusion and fission events. The double membrane nature of the mitochondria makes it vital to consider both the inner and outer membranes during mitochondrial fusion. Essential mammalian skeletal muscle fusion proteins involved in these processes include mitofusin 2 (Mfn2), which is necessary for outer membrane fusion, and the inner mitochondrial membrane protein optical atrophy 1 (Opa1) (10; 31). Mitochondrial membrane fission is mediated by dynamin related peptide 1 (Drp1), in combination with fission protein 1 (Fis1) (17; 23). Fis1 regulates outer membrane fission, whereas Drp1 lacks a mitochondrial targeting sequence and must be recruited from the cytosol to the outer surface of the organelle, where it participates in organelle division (29). Disruptions in these key proteins have

been associated with neurological conditions such as Charcot-Marie-Tooth type 2A, and Parkinson, Alzheimer, and Huntington Diseases. In several disease models, the alterations of mitochondrial fission and fusion proteins are associated with disease phenotypes (41).

The distribution and volume of mitochondria within muscle fibers is thought to reflect a balance between the distance required for metabolite and oxygen diffusion from capillaries to the mitochondria (24) and the energy supply from mitochondria to myofibrils. The mitochondrial reticulum likely serves as a system for the transport of lipid-soluble substrates and oxygen while maintaining an electrical potential along the membranes over extended distances (7). Altering membrane topology has been shown to change the rate of metabolite transport and organelle function (11). Evidence of such a relationship between mitochondrial function and morphology has been demonstrated under conditions where mitochondrial ATP synthase and the electron transport chain were inhibited (14). Inhibition of these key components resulted in a dismantling of the mitochondrial network, with the organelle becoming smaller and more punctate in shape (14). Upon removal of these inhibitors, the mitochondria resumed their elongated reticular structure (14). In addition, during apoptosis the mitochondrial network becomes fragmented (16; 17; 22; 29). Inhibition of fission proteins such as Drp1 or Fis1 has been shown to prevent mitochondrial fragmentation and reduce apoptotic cell death (17). These results support the idea that mitochondrial function is tied to morphology.

Kirkwood *et al* originally demonstrated that mitochondria in skeletal muscle adapted to chronic exercise by increasing the extensiveness of the mitochondrial

reticulum (27). In contrast, chronic muscle disuse, induced through denervation, has been shown to reduce mitochondrial content and organelle size (2; 32). Similar results have been observed with age, whereby mitochondrial volume density decreases with age without a change in organelle number (34), reflecting greater mitochondrial fragmentation. These studies demonstrate that mitochondrial morphology is altered during conditions of muscle use and disuse, a process governed by fission and fusion machinery. The purpose of this study was to provide a descriptive evaluation of mitochondrial morphology in muscle of varying oxidative capacities in response to changes in organelle biogenesis. Our study provides the necessary foundation to warrant further investigations on the molecular and regulatory aspects of fission and fusion proteins within muscle of differing oxidative capacities.

Experimental Procedures

Animals and surgeries

Fiber Types: Normal male Sprague-Dawley rats aged 3-months were used. The soleus, red gastrocnemius and quadriceps, and white gastrocnemius and quadriceps muscles were used as representative slow-twitch red, fast-twitch red, and fast-twitch white muscles, respectively. Whole muscle extracts were prepared for all fiber types.

Chronic Contractile Activity (CCA): Male Sprague-Dawley rats (Charles River, St. Comstant, Quebec, Canada) aged 6-months were used for the stimulation studies. The stimulation protocol was approved by the York University Animal Care Committee, in accordance with the Canadian Council on Animal Care as described previously (38). Briefly, a portable stimulator unit was fastened to the back of the animals with cloth tape. Under aseptic conditions, the electrodes from the stimulator unit were passed subcutaneously from the back of the neck to the thigh and sutured to either side of the common fibular nerve that innervates the tibialis anterior (TA) and extensor digitorum longus (EDL) muscles. The skin was stapled, sterile ampicillin was injected to minimize the risk of infection, and the animals were allowed to recover for 7-days. The TA and EDL muscles were subjected to electrical stimulation (10Hz, 3 hrs/day for 7 days), while the contralateral limb served as the non-stimulated internal control. Whole muscle extracts, as well as subsarcolemmal (SS) mitochondria and cytosolic fractions were prepared.

Denervation: Denervation surgery was conducted as described previously (2) and approved by the York University Animal Care Committee in accordance with Canadian

Council of Animal Care guidelines. Briefly, to induce unilateral denervation of the TA and EDL muscles of male Sprague-Dawley rats (6-months of age), a small portion of the common fibular nerve was excised from 1 limb of the animals while under anesthetic, and the contralateral limb served as the internal control. The animals underwent denervation for 7-days, followed by tissue removal, as well as SS mitochondria and cytosole isolations

Aging: Male Fischer 344 Brown Norway rats aged 5-months and 35-months were obtained from the National Institute of Aging (Bethesda, MD, USA). The Fisher 344 Brown Norway rats are a well established animal model of aging due to their longer maximal life span and increased period of time pathology-free (30). The animals were provided food and water *ad libitum*. The TA and EDL muscles from the animals were excised and used for analysis.

Tissue extraction and mitochondrial isolation

Following muscle excision, the TA muscles were trimmed of excessive fat and connective tissue, minced thoroughly, homogenized briefly, and subjected to differential centrifugation as described previously (13) to fractionate subsarcolemmal (SS) mitochondria and cytosole extracts. We chose the SS mitochondrial subfraction for protein analyses, because they represent the most labile pool of organelles in response to muscle use and disuse (1). The EDL muscles were clamp frozen in liquid nitrogen following excision from the animals. These samples were used to assess whole muscle levels of mitochondrial morphology machinery and COX activity. The EDL muscles

from Fisher 344 Brown Norway rats were used for EM analyses. Protein concentrations of the samples were determined using the Bradford method.

Enzyme activities

Cytochrome c oxidase (COX) activity was measured in EDL muscle samples as previously described (42), by determining the maximal rate of oxidation of fully reduced cytochrome c by measuring the change in absorbance at 550 nm in a multidetection microplate reader (Synergy HT; Bio-Tek Instruments, Winooski, VT, USA) at 30^{o}C.

Immunoblotting

Whole muscle homogenates, isolated SS mitochondria, and cytosolic protein extracts were prepared from TA muscles as described above. Protein extracts were separated using 10-15% SDS-PAGE and subsequently transferred onto nitrocellulose membranes. Membranes were then blocked (1 or 1.5 hr) with a solution of 5% skim milk in 1x TBS-Tween20 (Tris-buffered saline–Tween-20: 25 mM Tris–HCl, pH 7.5, 1 mM NaCl and 0.1% Tween-20) at room temperature, followed by incubation in blocking solution with antibodies directed towards Fis1 (1:500; Alexis Biochemical), Drp1 (1:500, BD Transduction Laboratories), Opa1 (1:500; BD Transduction Laboratories), Mfn2 (1:250; Sigma), Aciculin (1:200; DSHB University of Iowa), Porin (1:3000; Abcam), and GAPDH (1:20,000; Abcam) overnight at 4°C. Samples were corrected for loading using GAPDH and Porin, for cytosolic and SS mitochondrial fractions, respectively. Aciculin was used as the loading control for whole muscle tissue. Following incubation with the primary antibodies, membranes were washed 3x 5-min with TBS-Tween20, followed by

incubation at room temperature (1 hr) with the appropriate secondary antibody conjugated to horseradish peroxidase and washed again 3x 5-min each with TBS-Tween20. Membranes were developed using Western Blot Luminol Reagent (Santa Cruz Biotechnology), and films were subsequently scanned and quantified via densitometric analysis of signal intensity with SigmaScanPro software (version 5, Jandel Scientific, San Rafael, CA, USA).

Transmission Electron Microscopy

Samples from the EDL muscles of young control, young stimulated, young denervated and aged Fisher 344 Brown Norway rats were prepared and analyzed as previously described (20). Briefly, muscle samples were incubated on ice in 3% glutaraldehyde buffered with 0.1 M sodium cacodylate for 1 hr. Muscle sections were then washed 3 x 15-min with 0.1 M sodium cacodylate, followed by incubation in 1% osmium tetroxide in 0.1 M sodium cacodylate at room temperature. After sections were fixed for proteins and lipids, samples were subjected to gradient dehydration of 30%, 50%, 80% and 100% anhydrous ethanol. Next, sections were embedded in a 1:1 solution of fresh Spurr embedding resin and anhydrous ethanol overnight. Groups of muscle fibers were then dissected from the sections and embedded in fresh Spurr embedding resin and incubated at 60°C for 48 hrs. Ultrathin sections (60 nm) were cut, placed on copper grids, and post-stained with uranyl acetate and lead citrate. Electron micrographs were imaged on a Philips EM201 electron microscope (FEI, Hillsboro, OR, USA).

The average area of individual intermyofibrillar (IMF) mitochondria and maximal SS depth were assessed based on EM images taken at 20, 000 – 45, 000X magnifications. In order to determine the maximal depth of SS mitochondria, a line was drawn from the outer edge of the most peripheral mitochondria to the edge of the myofibril. The line was placed perpendicular to the myofibril. The maximal distance between the mitochondria and myofibril was chosen in each case.

Statistical Analyses

Data were analyzed with GraphPad 4.0 software and expressed as means ± SE. Where appropriate, paired *t*-tests and one-way analyses of variance (ANOVA) were performed, followed by the Bonferroni *post hoc* test. Differences were considered statistically significant if $P < 0.05$.

Results

Expression of mitochondrial morphology proteins and cytochrome c oxidase (COX) activity in muscle fiber types. COX activity was significantly greater in slow-twitch red (STR) and fast-twitch red (FTR) muscle by 1.9-fold and 2.7-fold, respectively, compared with fast-twitch white muscle (FTW) (Fig. 1A). These findings are similar to other assessments of mitochondrial enzyme activity within low- and high-oxidative skeletal muscle fibers (3). Representative immunoblots of Fis1, Drp1, Opa1, and Mfn2, key mitochondrial morphology proteins are shown in Fig. 1B. Quantification of repeated experiments revealed that FTW fibers possessed the lowest protein expression of Fis1, Drp1, Opa1, and Mfn2. The expression of Fis1 was identical in both STR and FTR fibers, and was 2.4-fold greater than in FTW whole muscle extracts. The fission protein Drp1 was greatest in the STR fibers, followed by FTR fibers, and these values were 1.7 – 2-fold greater than levels found in FTW. The fusion proteins Opa1 and Mfn2 also displayed the greatest level of expression in the highly oxidative STR and FTR fibers. Both of these proteins were 1.5 – 2.1-fold ($P<0.05$) greater in STR and FTR muscle, compared with FTW muscle sections.

CCA-induced alterations in mitochondrial content and morphology: Transmission electron microscopy (TEM) analysis allowed us to assess changes in mitochondrial content and morphology in response to CCA (Fig. 2B), denervation (Fig. 2C) and aging (Fig. 2D) in skeletal muscle of Fisher 344 Brown Norway rats. Animals subjected to chronic contractile activity (Fig. 2B) displayed increased thickness of the SS

mitochondrial layer by 58% ($p<0.05$), as compared to young control animals (Fig. 2A). Additionally, following CCA, individual IMF mitochondria were 75% larger (Fig. 2F) and appeared to be more reticular (Fig. 2B) than in the young control animals (Fig. 2A). This was accompanied by an approximately 30% increase in COX enzyme activity (Fig. 3A), indicative of an increase in mitochondrial content. This increase with CCA is in line with observations previously reported from our laboratory (1). Within isolated SS mitochondria, expression of the fusion proteins Opa1 and Mfn2 increased significantly by 36% and 53%, respectively (Fig. 3B). Expression of the fission protein Drp1 decreased by 13% ($P<0.05$), whereas no significant difference was detected for Fis1. Whole muscle levels reflected a similar pattern (data not shown). Thus, these data suggest that CCA favors the expression and localization of fusion, rather than fission proteins.

Expression of mitochondrial remodeling proteins and mitochondrial morphology as a result of denervation: Transmission electron microscopy revealed that muscle subjected to denervation displayed a 64% reduction in the SS mitochondrial layer (Figs. 2C, 2E). The IMF mitochondrial network appeared to be sparse. IMF mitochondria tended to be smaller and more fragmented in size as compared to those organelles in muscle of young control animals (Figs. 2A, 2F). Similar to results previously reported with 7-days of denervation by our laboratory, (42) COX activity was reduced by 35% compared to the contralateral control muscle (Fig. 4A). In the SS mitochondrial and cytosolic subfractions we observed dramatic decreases in the fusion proteins Opa1 and Mfn2 by 84% and 70%, respectively (Fig. 4B). In contrast, we observed a more moderate decline

of Fis1 by 46% in mitochondrial fraction from denervated muscle, while no difference existed for Drp1. These observations suggest that denervation downregulates the fusion proteins to a greater extent than the fission proteins.

Effect of aging on mitochondrial morphology proteins and COX activity: We observed a 46% decrease in the thickness of the SS mitochondrial layer, disruptions in the distribution of normal IMF mitochondria, and a 37% ($P<0.05$) reduction in the size of individual IMF mitochondria (Figs. 2D, 2E, 2F) with age. The mitochondria were distributed irregularly among the myofibrils, and disruptions in the alignment of the sarcomeres were visible in the aged animals (Fig. 2D). COX activity was 39% lower ($P<0.05$) in senescent animals compared to their younger counterparts (Fig. 5A), similar to results previously reported by our laboratory (9). Fis1 protein levels were 92% higher in the SS mitochondrial subfraction of senescent animals, while Drp1 protein was 2.5-fold higher in the cytosol of aged animals (Fig. 5B). In contrast to increased expression of fission proteins in the senescent animals, we observed a 44% lower expression of the fusion protein Mfn2, while Opa1 was unchanged with age. These data illustrate upregulation of the fission proteins with age, while the proteins governing mitochondrial fusion are suppressed.

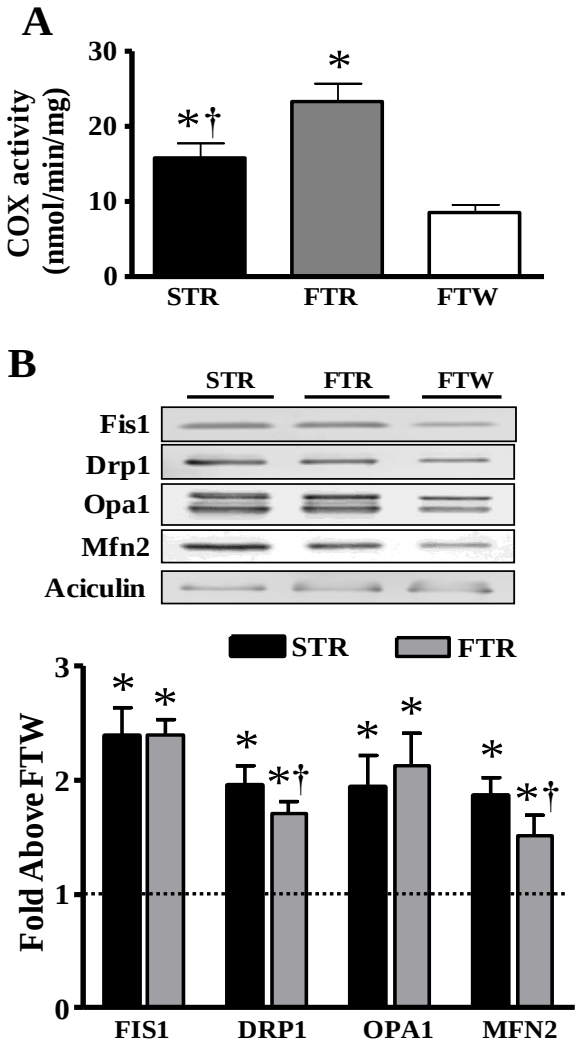

Figure 1: Expression of mitochondrial morphology proteins and COX activity from skeletal muscle of different oxidative capacities (STR, FTR, FTW). A) Cytochrome c oxidase (COX) enzyme activity of muscles of varying oxidative capacity from 3-month old Sprague-Dawley rats (STR, soleus; FTW, red gastrocnemius and quadriceps; and FTW, white gastrocnemius and quadriceps; n = 9-10; *$P < 0.05$ vs FTW, $^{\dagger}P < 0.05$ vs FTR). B) Images are representative of 8 separate experiments illustrating the response of mitochondrial morphology proteins in varying fiber types, values compared with FTW. Opa1 was quantified by summing all bands resulting from splice variants of the protein (*$P < 0.05$ vs FTW, $^{\dagger}P < 0.05$ vs STR).

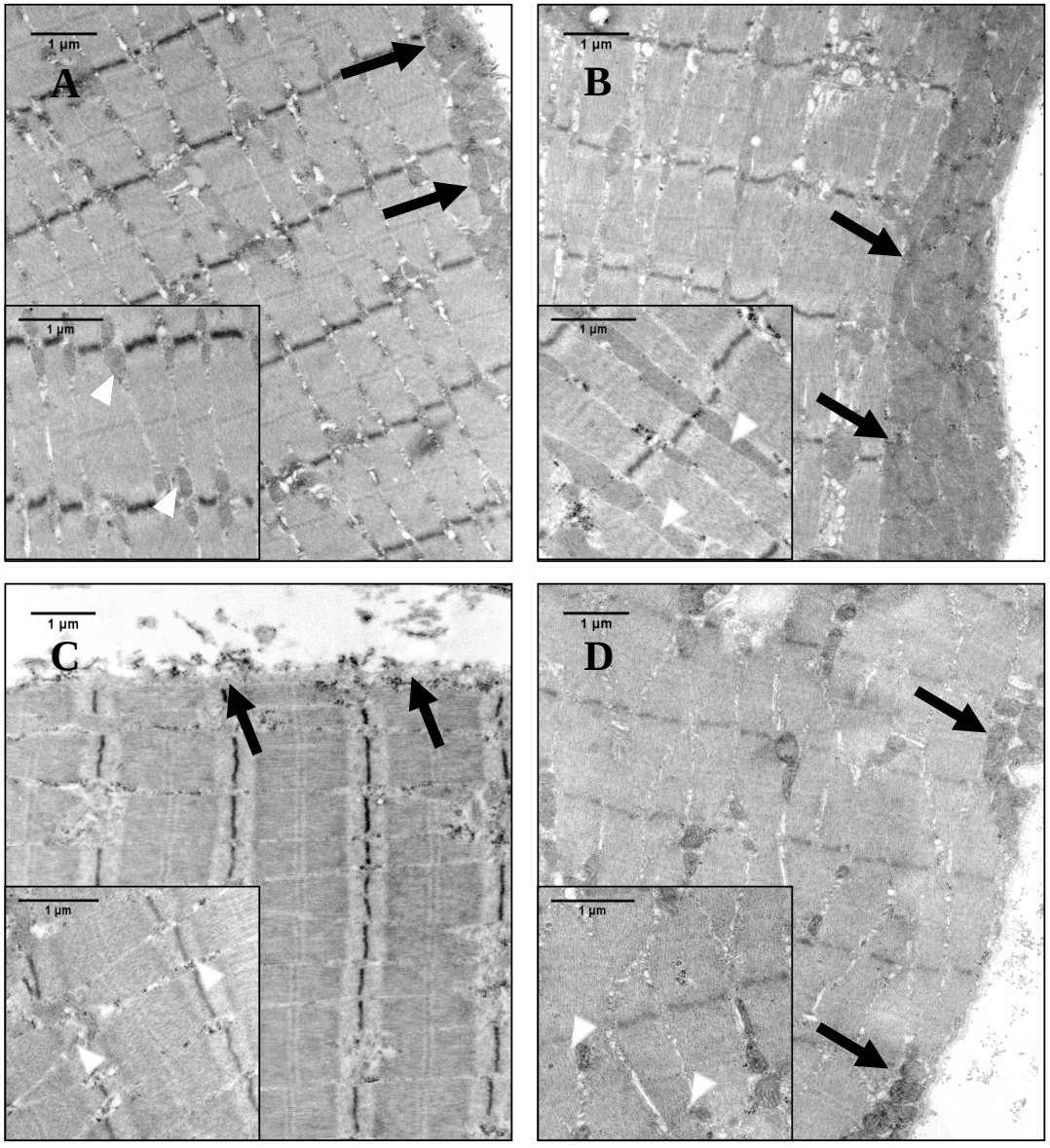
A
B
C
D
1 µm

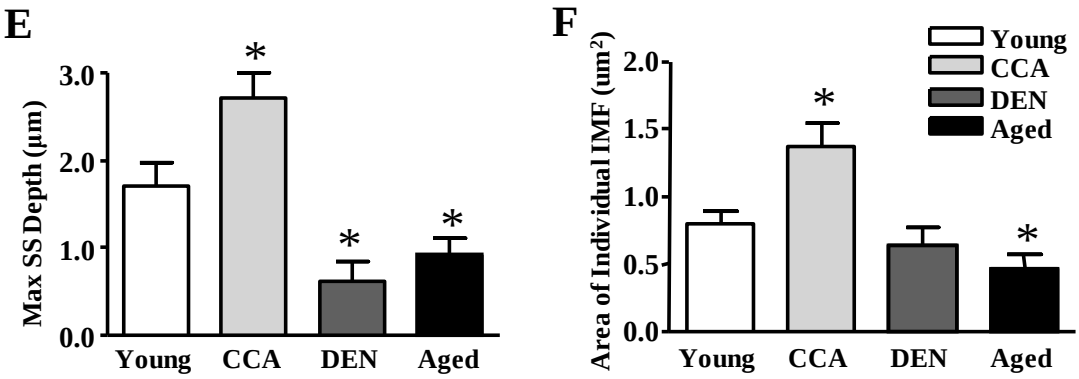
E
Max SS Depth (µm)
3.0
2.0
1.0
0.0
Young
CCA
DEN
Aged
F
Area of Individual IMF (um²)
2.0
1.5
1.0
0.5
0.0
Young
CCA
DEN
Aged

Figure 2: Electron micrographs of skeletal muscle under conditions of altered mitochondrial biogenesis in Fischer 344 Brown Norway rats in: A) control, B) chronic stimulated, C) denervated, and D) aged samples. Subsarcolemmal and intermyofibrillar mitochondrial populations are located below the sarcolemmal membrane (black arrows) and between the myofibrils (white arrow heads). Morphological alterations in mitochondria are depicted by these representative images taken at a magnification of 10,000X. E) Quantification of the maximal depth of SS mitochondria and F) the average area of individual IMF mitochondrial in control, CCA, DEN, and aged conditions (*$P < 0.05$ vs control).

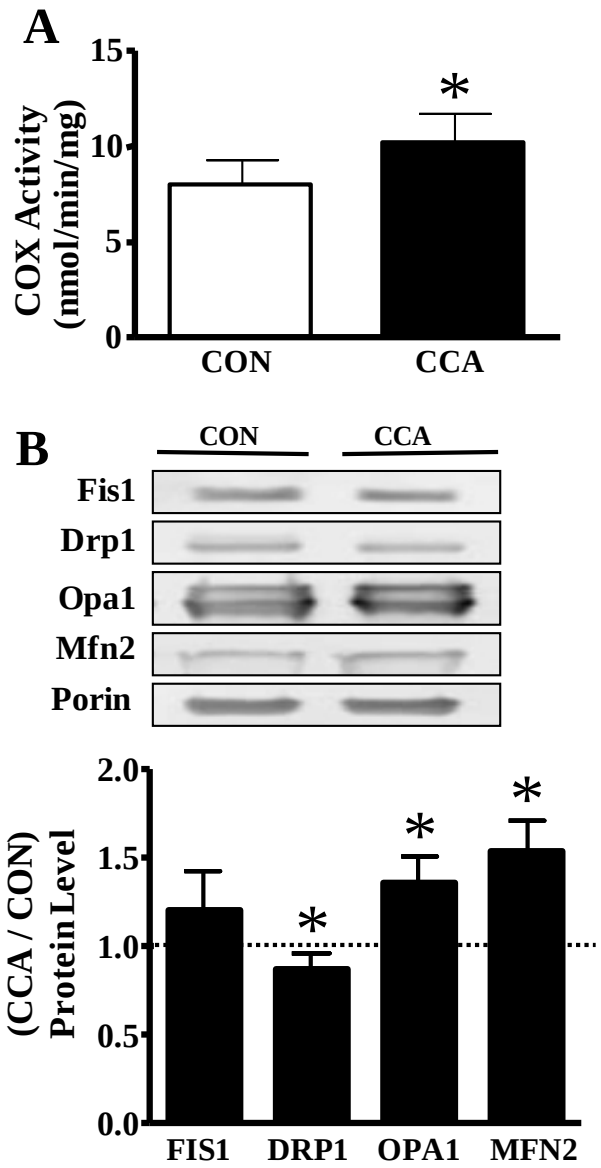

Figure 3: Effect of 7-days of chronic contractile activity (CCA) on mitochondrial morphology proteins and COX activity. A) COX enzyme activity from chronically contracted (CCA) and control (CON) muscle of 6-month old Sprague-Dawley rats (n = 8; *P < 0.05 vs control). B) Fis1, Drp1, Opa1, Mfn2 protein levels in SS mitochondrial or cytosolic fractions. Expression of the morphology proteins was corrected using the loading control Porin, and expressed as fold over control. Representative Western blots are shown for each indicated protein, with graphical quantification depicted below (n =7, *P < 0.05 vs control).

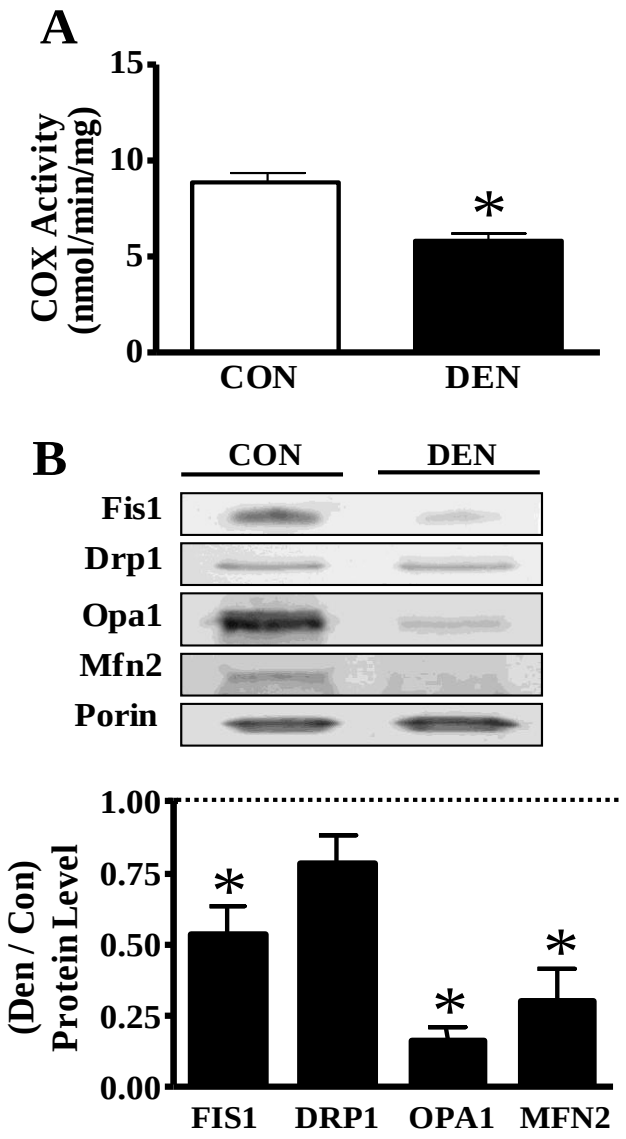

Figure 4: Expression of mitochondrial morphology protein levels and COX activity in control and 7-day denervated (DEN) muscle. A) COX enzyme activity from denervated and control muscle of 6-month old Sprague-Dawley rats (n = 9; *P < 0.05 vs control). B) Representative Western blots of Fis1, Drp1, Opa1, Mfn2 protein expression (*top*), with graphical quantification (*bottom*) expressed as fold over control. Fis1, Opa1 and Mfn2 were determined in SS mitochondrial fractions, whereas Drp1 was assessed in cytosolic fractions. Expression of the morphology proteins was corrected using the loading control Porin, and expressed as fold over control. (n = 8, *P < 0.05 vs control).

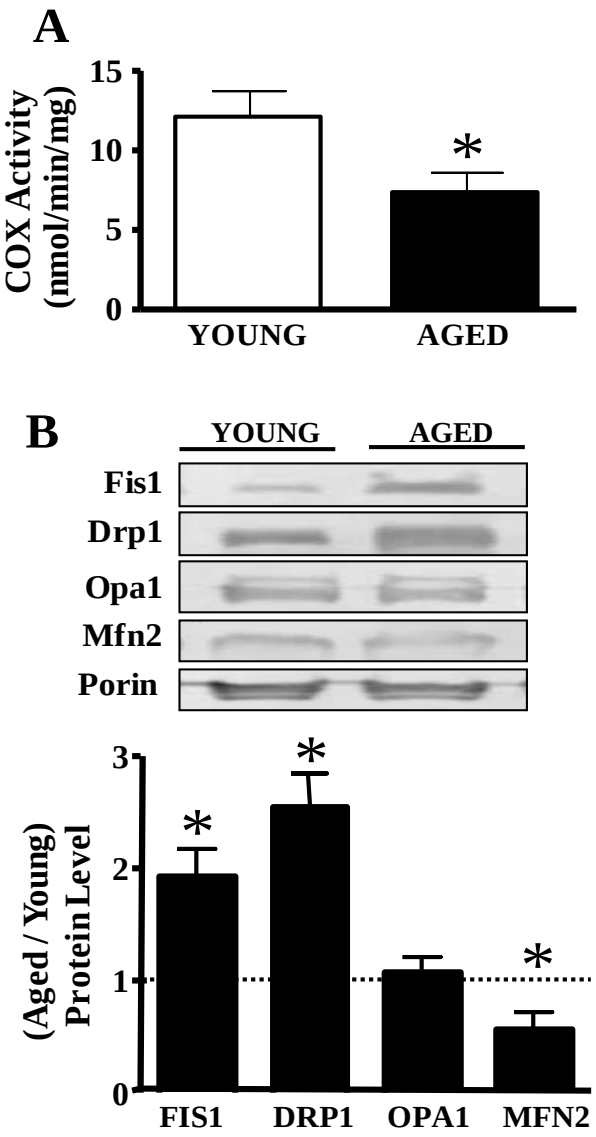

Figure 5: Fission and fusion morphology protein expression and COX activity in young and aged muscle. A) COX enzyme activity from young (5 month) and aged (35 month) old Fisher 344 Brown Norway rats (n = 5; *P < 0.05 vs aged). B) Representative images of Fis1, Drp1, Opa1, Mfn2 protein content (*top*), with graphical quantification (*bottom*) expressed as fold over young in SS mitochondrial or cytosolic fractions. Fis1, Opa1 and Mfn2 were determined using SS mitochondrial fractions, whereas Drp1 was assessed in cytosolic fractions. Expression of the morphology proteins was corrected using the loading control Porin, and expressed as fold over young. (n = 6-7, *P < 0.05 vs aged).

Discussion

The structure of mitochondria within skeletal muscle has been investigated for several years. Ultrastructural studies have quantified differences between fiber types and provided detailed characterization of mitochondrial structure in skeletal muscle of differing oxidative capacities (25; 27; 33). These studies have demonstrated that mitochondrial structure and volume density are highly variable within muscle (35). Our results demonstrate that the expression of morphology machinery proteins correlates with the oxidative capacity of muscle fibers under steady state conditions.

The mitochondrial reticular network is known to expand as a result of endurance training (27). This suggests that chronic exercise shifts the expression of fission and fusion machinery towards that of enhanced fusion. In this study, we demonstrate that the expected increase in mitochondrial area resulting from CCA was accompanied by a concomitant increase in expression of the fusion proteins Mfn2 and Opa1, along with a decrease in Drp1 protein levels. These results provide a molecular basis for the drive toward more reticular organelles induced by exercise. In contrast, denervation-induced muscle disuse produced a reduction in mitochondrial content, as evident by reduced whole muscle COX activity, decreased thickness of the SS mitochondrial layer, and reduced area of individual IMF organelles. Other studies have found similar reductions in organelle size and mitochondrial percentage per fiber area in rat diaphragm muscle following denervation (32), suggesting a shift in the balance of mitochondrial dynamics towards greater fission and fragmentation. Our data coincide with morphological evidence of mitochondrial fragmentation. With denervation, we observed that the

greatest decrease in protein expression occurred in Mfn2 and Opa1. This has been shown, in part, by Wagatsuma *et al* (39), who demonstrated a decrease in Mfn2 mRNA during hindlimb unloading, and with denervation (40).

Interestingly, our data on denervation-induced muscle disuse differs from that found in aging muscle. Although mitochondrial content decreased similarly (35 to 40%) with denervation and aging, the alterations in fission and fusion proteins differed. With aging, we observed an increase in expression of the fission protein levels of Drp1 and Fis1. In agreement with our study, Koltai *et al* also found that Fis1 protein expression increased with age (28). Thus, the underlying stimuli for changes in gene expression differ between denervation and aging, despite the fact that muscle disuse is a common feature of both conditions. Clearly, muscle disuse is only 1 component of the stimuli which results in the aging muscle phenotype. Nonetheless, the end result of this divergent pattern of gene expression is similar, with an increased tendency for organelle fission, rather than fusion.

What are the potential mechanisms involved in these changes in gene expression? The alterations in mitochondrial biogenesis are driven, in part, by PGC-1α, a major regulator of mitochondrial biogenesis (19). Mice deficient in PGC-1α have reduced expression of Mfn2 mRNA (43). Conversely, up-regulation in PGC-1α, from a single bout of cycling exercise stimulated ERRα binding at the -413/-398 motifs on the Mfn2 promoter, resulting in an increase in Mfn2 mRNA during the recovery phase (8). Similar observations were seen by Ding *et al* (15), whereby Mfn2 mRNA content increased during recovery from acute exercise. In this study, we chose to avoid the transient nature

of mRNA expression and measured the levels of fission and fusion components at the protein level under more stable adaptation conditions. We have previously reported that PGC-1α is upregulated by CCA (21), and downregulated by denervation (2) and aging (9). In support of our findings, Garnier *et al* (18) also found a coordinated increase in mitochondrial biogenesis, specifically PGC-1α, and Mfn2 transcriptional levels. Although this is certainly consistent with PGC-1α as a regulator of Mfn2 expression under these conditions, it is important to note that PGC-1α is only 1 component of the process and that additional mechanisms controlling these events have not yet been fully elucidated.

Changes in mitochondrial network formation or organelle fragmentation have physiological implications. The balance between the expression of fission and fusion proteins affects mitochondrial sensitivity to apoptotic stimuli, such that fragmented mitochondria are more prone to release pro-apoptotic proteins (37). Mitochondria obtained from aging muscle, or from muscle subjected to chronic disuse are similar, with higher rates of protein release, greater apoptotic susceptibility (2; 9), and accumulation of dysfunctional mtDNA (12). These mitochondria are likely a product of elevated rates of fission, designed to isolate the damaged portion of the mitochondrial network from its unaffected parts and to promote the selective clearance of damaged mitochondria through mitophagy (36).

In contrast, extended mitochondrial reticula may have advantages over smaller isolated mitochondria in that they can serve as an effective system for electrically-coupled power transmission throughout the cell (7). Muscle fibers are quite large in size,

and significant gradients exist for substrates within muscle (7). In such an instance, the expanded mitochondrial network may facilitate rapid delivery of O_2 and lipid-soluble substrates from regions of high to low availability. Consequently, expansion of the mitochondrial network provides physiological advantages to the cell under conditions of high metabolic demand, such as exercise.

In summary, our data show that chronic muscle use induces a shift in the balance of the regulatory proteins involved in fission and fusion toward upregulation of the fusion process. In contrast, chronic muscle disuse promotes expression of proteins which are involved in organelle fragmentation, an outcome similar to that observed in aging muscle, albeit through a divergent pathway. These changes in fission and fusion machinery components are an important part of the adaptive responses of skeletal muscle mitochondria to changes in muscle use, disuse, and aging, with physiological implications for energy production and organelle turnover.

Reference List

1. **Adhihetty PJ, Ljubicic V and Hood DA**. Effect of chronic contractile activity on SS and IMF mitochondrial apoptotic susceptibility in skeletal muscle. *Am J Physiol Endocrinol Metab* 292: E748-E755, 2007.
2. **Adhihetty PJ, O'Leary MF, Chabi B, Wicks KL and Hood DA**. Effect of denervation on mitochondrially mediated apoptosis in skeletal muscle. *J Appl Physiol* 102: 1143-1151, 2007.
3. **Adhihetty PJ, Uguccioni G, Leick L, Hidalgo J, Pilegaard H and Hood DA**. The role of PGC-1alpha on mitochondrial function and apoptotic susceptibility in muscle. *Am J Physiol Cell Physiol* 297: C217-C225, 2009.
4. **Bach D, Naon D, Pich S, Soriano FX, Vega N, Rieusset J, Laville M, Guillet C, Boirie Y, Wallberg-Henriksson H, Manco M, Calvani M, Castagneto M, Palacin M, Mingrone G, Zierath JR, Vidal H and Zorzano A**. Expression of Mfn2, the Charcot-Marie-Tooth neuropathy type 2A gene, in human skeletal muscle: effects of type 2 diabetes, obesity, weight loss, and the regulatory role of tumor necrosis factor alpha and interleukin-6. *Diabetes* 54: 2685-2693, 2005.
5. **Bach D, Pich S, Soriano FX, Vega N, Baumgartner B, Oriola J, Daugaard JR, Lloberas J, Camps M, Zierath JR, Rabasa-Lhoret R, Wallberg-Henriksson H, Laville M, Palacin M, Vidal H, Rivera F, Brand M and Zorzano A**. Mitofusin-2 determines mitochondrial network architecture and mitochondrial metabolism. A novel regulatory mechanism altered in obesity. *J Biol Chem* 278: 17190-17197, 2003.
6. **Bakeeva LE, Chentsov YS and Skulachev VP**. Ontogenesis of mitochondrial reticulum in rat diaphragm muscle. *Eur J Cell Biol* 25: 175-181, 1981.
7. **Bakeeva LE, Chentsov Y and Skulachev VP**. Mitochondrial framework (reticulum mitochondriale) in rat diaphragm muscle. *Biochim Biophys Acta* 501: 349-369, 1978.
8. **Cartoni R, Leger B, Hock MB, Praz M, Crettenand A, Pich S, Ziltener JL, Luthi F, Deriaz O, Zorzano A, Gobelet C, Kralli A and Russell AP**. Mitofusins 1/2 and ERRalpha expression are increased in human skeletal muscle after physical exercise. *J Physiol* 567: 349-358, 2005.
9. **Chabi B, Ljubicic V, Menzies KJ, Huang JH, Saleem A and Hood DA**. Mitochondrial function and apoptotic susceptibility in aging skeletal muscle. *Aging Cell* 7: 2-12, 2008.
10. **Chen H, Chomyn A and Chan DC**. Disruption of fusion results in mitochondrial heterogeneity and dysfunction. *J Biol Chem* 280: 26185-26192, 2005.
11. **Chen H, Detmer SA, Ewald AJ, Griffin EE, Fraser SE and Chan DC**. Mitofusins Mfn1 and Mfn2 coordinately regulate mitochondrial fusion and are essential for embryonic development. *J Cell Biol* 160: 189-200, 2003.
12. **Chomyn A and Attardi G**. MtDNA mutations in aging and apoptosis. *Biochem Biophys Res Commun* 304: 519-529, 2003.

13. **Cogswell AM, Stevens RJ and Hood DA**. Properties of skeletal muscle mitochondria isolated from subsarcolemmal and intermyofibrillar regions. *Am J Physiol* 264: C383-C389, 1993.
14. **De Vos KJ, Allan VJ, Grierson AJ and Sheetz MP**. Mitochondrial function and actin regulate dynamin-related protein 1-dependent mitochondrial fission. *Curr Biol* 15: 678-683, 2005.
15. **Ding H, Jiang N, Liu H, Liu X, Liu D, Zhao F, Wen L, Liu S, Ji LL and Zhang Y**. Response of mitochondrial fusion and fission protein gene expression to exercise in rat skeletal muscle. *Biochim Biophys Acta* 1800: 250-256, 2010.
16. **Fannjiang Y, Cheng WC, Lee SJ, Qi B, Pevsner J, McCaffery JM, Hill RB, Basanez G and Hardwick JM**. Mitochondrial fission proteins regulate programmed cell death in yeast. *Genes Dev* 18: 2785-2797, 2004.
17. **Frank S, Gaume B, Bergmann-Leitner ES, Leitner WW, Robert EG, Catez F, Smith CL and Youle RJ**. The role of dynamin-related protein 1, a mediator of mitochondrial fission, in apoptosis. *Dev Cell* 1: 515-525, 2001.
18. **Garnier A, Fortin D, Zoll J, N'Guessan B, Mettauer B, Lampert E, Veksler V and Ventura-Clapier R**. Coordinated changes in mitochondrial function and biogenesis in healthy and diseased human skeletal muscle. *FASEB J* 19: 43-52, 2005.
19. **Handschin C and Spiegelman BM**. Peroxisome proliferator-activated receptor gamma coactivator 1 coactivators, energy homeostasis, and metabolism. *Endocr Rev* 27: 728-735, 2006.
20. **Heath IB and Rethoret K**. Temporal analysis of the nuclear cycle by serial section electron microscopy of the fungus, Saprolegnia ferax. *Eur J Cell Biol* 21: 208-213, 1980.
21. **Irrcher I, Adhihetty PJ, Sheehan T, Joseph AM and Hood DA**. PPARgamma coactivator-1alpha expression during thyroid hormone- and contractile activity-induced mitochondrial adaptations. *Am J Physiol Cell Physiol* 284: C1669-C1677, 2003.
22. **Jagasia R, Grote P, Westermann B and Conradt B**. DRP-1-mediated mitochondrial fragmentation during EGL-1-induced cell death in C. elegans. *Nature* 433: 754-760, 2005.
23. **James DI, Parone PA, Mattenberger Y and Martinou JC**. hFis1, a novel component of the mammalian mitochondrial fission machinery. *J Biol Chem* 278: 36373-36379, 2003.
24. **Kayar SR, Claassen H, Hoppeler H and Weibel ER**. Mitochondrial distribution in relation to changes in muscle metabolism in rat soleus. *Respir Physiol* 64: 1-11, 1986.
25. **Kayar SR, Hoppeler H, Essen-Gustavsson B and Schwerzmann K**. The similarity of mitochondrial distribution in equine skeletal muscles of differing oxidative capacity. *J Exp Biol* 137: 253-263, 1988.
26. **Kelley DE, He J, Menshikova EV and Ritov VB**. Dysfunction of mitochondria in human skeletal muscle in type 2 diabetes. *Diabetes* 51: 2944-2950, 2002.

27. **Kirkwood SP, Packer L and Brooks GA**. Effects of endurance training on a mitochondrial reticulum in limb skeletal muscle. *Arch Biochem Biophys* 255: 80-88, 1987.
28. **Koltai E, Hart N, Taylor AW, Goto S, Ngo JK, Davies KJ and Radak Z**. Age-associated declines in mitochondrial biogenesis and protein quality control factors are minimized by exercise training. *Am J Physiol Regul Integr Comp Physiol* 303: R127-R134, 2012.
29. **Lee YJ, Jeong SY, Karbowski M, Smith CL and Youle RJ**. Roles of the mammalian mitochondrial fission and fusion mediators Fis1, Drp1, and Opa1 in apoptosis. *Mol Biol Cell* 15: 5001-5011, 2004.
30. **Lipman RD, Chrisp CE, Hazzard DG and Bronson RT**. Pathologic characterization of brown Norway, brown Norway x Fischer 344, and Fischer 344 x brown Norway rats with relation to age. *J Gerontol A Biol Sci Med Sci* 51: B54-B59, 1996.
31. **Meeusen S, DeVay R, Block J, Cassidy-Stone A, Wayson S, McCaffery JM and Nunnari J**. Mitochondrial inner-membrane fusion and crista maintenance requires the dynamin-related GTPase Mgm1. *Cell* 127: 383-395, 2006.
32. **Miledi R and Slater CR**. Some mitochondrial changes in denervated muscle. *J Cell Sci* 3: 49-54, 1968.
33. **Ogata T and Yamasaki Y**. Scanning electron-microscopic studies on the three-dimensional structure of mitochondria in the mammalian red, white and intermediate muscle fibers. *Cell Tissue Res* 241: 251-256, 1985.
34. **Orlander J, Kiessling KH, Larsson L, Karlsson J and Aniansson A**. Skeletal muscle metabolism and ultrastructure in relation to age in sedentary men. *Acta Physiol Scand* 104: 249-261, 1978.
35. **Picard M, White K and Turnbull DM**. Mitochondrial morphology, topology and membrane interactions in skeletal muscle: A quantitative three-dimensional electron microscopy study. *J Appl Physiol* 2012.
36. **Romanello V and Sandri M**. Mitochondrial biogenesis and fragmentation as regulators of muscle protein degradation. *Curr Hypertens Rep* 12: 433-439, 2010.
37. **Sugioka R, Shimizu S and Tsujimoto Y**. Fzo1, a protein involved in mitochondrial fusion, inhibits apoptosis. *J Biol Chem* 279: 52726-52734, 2004.
38. **Takahashi M and Hood DA**. Chronic stimulation-induced changes in mitochondria and performance in rat skeletal muscle. *J Appl Physiol* 74: 934-941, 1993.
39. **Wagatsuma A, Kotake N, Kawachi T, Shiozuka M, Yamada S and Matsuda R**. Mitochondrial adaptations in skeletal muscle to hindlimb unloading. *Mol Cell Biochem* 350: 1-11, 2011.
40. **Wagatsuma A, Kotake N, Mabuchi K and Yamada S**. Expression of nuclear-encoded genes involved in mitochondrial biogenesis and dynamics in experimentally denervated muscle. *J Physiol Biochem* 2011.
41. **Wang X, Su B, Siedlak SL, Moreira PI, Fujioka H, Wang Y, Casadesus G and Zhu X**. Amyloid-beta overproduction causes abnormal mitochondrial dynamics via

differential modulation of mitochondrial fission/fusion proteins. *Proc Natl Acad Sci U S A* 105: 19318-19323, 2008.

42. **Wicks KL and Hood DA**. Mitochondrial adaptations in denervated muscle: relationship to muscle performance. *Am J Physiol* 260: C841-C850, 1991.
43. **Zechner C, Lai L, Zechner JF, Geng T, Yan Z, Rumsey JW, Collia D, Chen Z, Wozniak DF, Leone TC and Kelly DP**. Total skeletal muscle PGC-1 deficiency uncouples mitochondrial derangements from fiber type determination and insulin sensitivity. Cell Metab 12: 633-642, 2010.

CHAPTER 3:

THE CYTOSKELETAL REGULATION OF MITOCHONDRIAL MOVEMENT WITHIN SKELETAL MUSCLE CELLS

Rationale for Manuscript #2

Mitochondria are distributed in the cell to match the energy demands, and it is their interaction with the cytoskeleton that controls their movement and displacement. Our purpose was to determine which cytoskeletal components are primary responsible for mitochondrial movement in muscle cells.

In neurons, microtubules are the primary tracks governing mitochondrial movements. Based on this knowledge, we hypothesized that microtubules, and their associated motor proteins are the main cytoskeletal filament proteins involved in mitochondrial dynamics within skeletal muscle.

SI and DAH conceived and designed the experiments, interpreted the data and wrote the manuscript. SI collected and analyzed all the data. Both authors approved the final version of the manuscript.

Cytoskeletal regulation of mitochondrial movement within skeletal muscle cells

Sobia Iqbal and David A. Hood

School of Kinesiology and Health Science, and the Muscle Health Research Centre
York University, Toronto, Ontario M3J 1P3, Canada

Running title: Mitochondrial movement in skeletal muscle cells

To whom correspondence should be addressed:
David A. Hood, PhD
School of Kinesiology and Health Science
York University, Toronto, Ontario
M3J 1P3, Canada
Tel: (416) 736-2100 ext: 66640
Fax: (416) 736-5698
E-mail: dhood@yorku.ca

Abstract

Mitochondria are distributed in the cell to match the energy demands, and it is their interaction with the cytoskeleton that controls their movement and displacement. Our purpose was to determine which cytoskeletal components are primarily responsible for mitochondrial movement in muscle cells. Live-cell imaging was used to visualize mitochondrial dynamics in myoblasts. Destabilization of microtubules (MT) reduced the total path length and average speed traveled by mitochondria by 64–74%, whereas actin disruption only reduced these variables by 37-40%. Downregulation of the microtubule motor proteins, Kif5B and dynein, by siRNA resulted in similar decreases in the average speed of mitochondrial movements, by 30-40%. We observed a reduction in mitochondrial average speed of movement (by 22-48%) under high calcium conditions. This attenuation in mitochondrial movement in the presence of calcium was negated in cells pre-treated with siRNA targeted to the microtubule motor protein adaptor, Milton, suggesting that Milton is involved in mediating mitochondrial arrest in the presence of calcium in muscle cells. By understanding mitochondrial movements we can elucidate the underlying basis for organelle interactions, leading to the formation of the mitochondrial reticulum, particularly during conditions of elevated calcium, such as exercise.

Introduction

Mitochondria are vital organelles, critical for energy supply and cell survival. Such functional versatility is paralleled by the structural complexity of the organelle. Mitochondria can compensate for alterations in energy requirements by adjusting their size and distribution within skeletal muscle (5). It is their interaction with the cytoskeleton that is used to control their position, movement and anchorage within cells (23). The three cytoskeletal elements, actin, microtubules and intermediate filaments act to vary the degree of scaffolding along which mitochondria are capable of moving.

The distribution of mitochondria to specific sites within the cell has consistently been linked to microtubules and actin. In neurons and cardiac myocytes, microtubules are the primary tracks governing mitochondrial movements (15; 26), while in *S. cerevisiae* the positioning of mitochondria is reliant on actin-based transportation (20). Intracellular transport of cargo, such as mitochondria, to specific locations within the cytoplasm involves molecular motors that bind directly to the cargo and the cytoskeletal track. Dynein and kinesins motor proteins use microtubules to transport cargo throughout the cell. In neurons, movement along microtubules occurs either towards the cell body using cytoplasmic dynein, or away, using kinesins. There are 14 kinesin superfamilies encoded by the human and mouse genomes, consisting of more than 45 members (10). In neurons, Kinesin-1 and Kinesin-3 have been identified to regulate mitochondrial movements (16; 19). Kinesin-1, also known as conventional kinesin, consists of three distinct members, Kif5A, Kif5B and Kif5C. Kif5A and Kif5C are neuron-specific, whereas Kif5B is ubiquitously expressed (1; 2). Inhibition of Kinesin-1

in *Drosophila* halts mitochondrial movement in motor axons (19), and in non-neuronal cells, whereby deletion of Kif5B alters mitochondrial positioning (23; 25). The movement of motor proteins along microtubules takes advantage of the dynamic instability of the tubulin polymer. Growth of microtubules allows for the continued expansion of the cytoskeleton, which motor proteins use as tracks. Conversely, the ability of microtubules to shrink is thought to be important for morphological changes in the cell, and in the reorientation of microtubules during the locomotion of organelles (13).

In muscle, calcium (Ca^{2+}) is a key regulator of contractile activity, but it is also an important signaling ion. Ca^{2+} has a role in the regulation of mitochondrial respiration, and it is involved in the opening of the mitochondrial permeability transition pore (mtPTP) (4). This dissipates the electrochemical proton gradient, thereby halting ATP production by oxidative phosphorylation. Calcium influx has also been found to inhibit mitochondrial movement in neurons and in cardiac myocytes (12; 24; 26). The ability of mitochondria to respond to intracellular signals such as Ca^{2+}, is mediated by motor protein/adaptor complexes. The core of this complex is composed of the Kinesin-1 motor along with two mitochondrial-specific adaptors, mitochondrial Rho GTPase (Miro) and Milton (24). Milton binds directly to Kinesin-1 (21), whereas Miro serves as an anchor linking Milton and Kinesin-1 to mitochondria (8). Elevated calcium binds to the EF-hands of Miro and induces a conformational change in the protein, resulting in the dissociation of the complex from microtubules and arresting mitochondrial movements (12; 24).

Traditionally, mitochondria have been thought to be static in nature, but are now known to be quite dynamic within cells. However, what is unknown is how the distribution of mitochondria are controlled and regulated. By understanding mitochondrial movements we can elucidate the underlying basis for organelle interactions, leading to the formation of the mitochondrial reticulum, and the distribution of energy in muscle cells.

Experimental Procedures

Cell Culture and Transfections: C_2C_{12} murine skeletal muscle cells were grown in DMEM supplemented with 10% fetal bovine serum and 1% Penicillin/Streptomycin (Growth Media, GM). Cells were cultured in custom made glass bottom culture plates and maintained at 37^o in 5% CO_2. Upon reaching a confluence of approximately 60%, mito-DsRED2 was transfected into myoblasts using Lipofectamine 2000 (Life Technologies) to visualize mitochondria. Mitochondrial movement was observed in C_2C_{12} cells using an expression vector that encodes a fusion of red fluorescence protein and the mitochondrial targeting sequence from cytochrome c oxidase subunit VIII (mito-dsRED2).

***Treatments*:** Forty-eight hours following transfection with mito-DsRed2, myoblasts were treated with microtubule and/or actin disrupting drugs, or a vehicle control (DMSO; Sigma-Aldrich). Microtubules were depolymerized using nocodazole (20μM; Toronto Research Chemicals) and colchicine (20μM; Sigma-Aldrich), while Taxol (2μM; Sigma-Aldrich) was used for stabilization. Actin was disrupted using cytochalasin D (2μM; Enzo Life Sciences). Pre-incubation with these agents was 1 hr prior to imaging.

In order to study the regulation of mitochondrial dynamics by calcium, C_2C_{12} cells were treated with either ionomycin (1μM, Sigma-Aldrich), a Ca^{2+} ionophore, or thapsigargin (1μM, Enzo Life Science), an inhibitor of the sarcoplasmic reticulum Ca^{2+}-ATPase. Ca^{2+} levels were suppressed using the chelators EGTA (5mM, Sigma-Aldrich) and BAPTA-AM (2μM, Calbiochem).

Mitochondrial Movement Analysis: Mitochondria were visualized using an inverted Nikon Eclipse TE2000-U fluorescent microscope equipped with 100x/1.5 oil objective lens, with a custom designed chamber designed to maintain a constant temperature of 37^{o}C with 5% CO_2. Mitochondrial dynamics were captured at 2 sec intervals for a total time of 5 mins using real-time imaging. Analyses were performed using the NIS Element AR 3.1 software, and was limited to regions of interest in the periphery of the cells, where individual mitochondria were readily resolved and could be used for analysis, while avoiding the confounding influence of high density mitochondrial networks.

Immunocytochemistry of Actin and Microtubules: For immunocytochemistry, the transfected cells were washed 3x with PBS at room temperature. The cells were then fixed with 3.7% formaldehyde for 7 min and washed with 3x with PBS. Cells were permeabilized with 0.1% Triton X-100 at 4 °C for 15 min and washed 3X with PBS. Subsequently, cells were stained with a FITC conjugated α-tubulin primary antibody (Abcam), or Acti-stain 488 phalloidin (Cytoskeleton Inc) for 2 hrs or 30 mins, respectively. The cells were then washed 3X with PBS and incubated with DAPI (Sigma-Aldrich) for 5 mins to stain the DNA. After washing twice with PBS, the media was replaced with GM without phenol red.

RNA Interference: Silencer Select predesigned small interfering RNA (siRNA) for Kif5B (5'-GACAUGUCGCAGUUACAATT-3'), dynein (Dynch1; 5'-GAAAGAUCCGCAACACGAATT-3'), Milton (TRAK1; 5'-GCAACGUGGUCCUCGAUAATT-3') and scrambled controls (scRNA) were used in

the knockdown experiments (Ambion). To produce knockdowns, the media was switched to pre-transfection media (DMEM and 10% FBS). The following day, the media was changed to DMEM and myoblasts were incubated with mito-DsRED2, and either 50 nM of siRNA specific for Kif**5**B or dynein, or 100 nM of siRNA for TRAK1, along with 10 μl of Lipofectamine 2000 for 6 hrs. Concomitantly, scrambled non-targeting siRNA underwent the same conditions. Forty-eight hours post-transfection, cells were used for image analysis or were collected for protein extracts.

Immunoblotting: Protein extracts from myoblasts were separated on 6–15% SDS-PAGE and subsequently transferred onto nitrocellulose membranes. Membranes were then blocked (1 hr or 1.5 hr) with a 5% skim milk in 1x TBS-Tween20 solution (Tris-buffered saline–Tween-20: 25 mM Tris–HCl, pH 7.5, 1 mM NaCl and 0.1% Tween-20) at room temperature, followed by incubation in blocking solution with antibodies directed towards Kif5B (1:500; Santa Cruz), Dynein heavy chain (1:1000; Santa Cruz), PGC-1α (1:500; Millipore), COX IV (1:250; Abcam), COX I (1:500; MitoSciences), or α-tubulin (1:2000; Calbiochem) overnight at 4°C. Subsequently, membranes were washed 3x 5 min with TBS-Tween20, followed by incubation at room temperature (1 hr) with the appropriate secondary antibody conjugated to horseradish peroxidase, and washed again 3x for 5 min each with TBS-Tween20. Membranes were developed using Western Blot Luminol Reagent (Santa Cruz). Films were subsequently scanned and quantified via densitometric analysis for the intensity of signals with SigmaScanPro software (version 5, Jandel Scientific).

Real-time PCR: Total RNA was extracted from C_2C_{12} cells 48 hrs after transfection, as previously described (18). The concentration and purity of the RNA was assessed using absorbance readings at 260 and 280 nm (Ultrospec 2100 Pro). In accordance with the manufacturer's recommendations, SuperScript® III reverse transcriptase (Invitrogen) was used to reverse transcribe the RNA into cDNA. Using sequences from GenBank, primers were designed with Primer 3 v. 0.4.0 software (Massachusetts Institute of Technology, Cambridge, MA) for Milton as the gene of interest, with glyceraldehyde-3-phosphate dehydrogenase (GAPDH) and β2-microglobulin (β2M) serving as the endogenous controls. The primers used were as follows: Milton forward: 5'-GGGAACGAGGACCACAATAA-3', Milton reverse: 5'-CCTCCGCTCAGACAGGTAGT-3', GAPDH forward: 5'-AACACTGAGCATCTCCCTCA-3', GAPDH reverse: 5'-GTGGGTGCAGCGAACTTTAT-3', β2M forward: 5'- GGTCTTTCTGGTGCTTGTCT-3', β2M reverse: 5'- TATGTTCGGCTTCCCATTCT-3'. Quantification of the gene of interest was corrected using the endogenous controls and analyzed as previously described (18).

Oxygen Consumption: Oxygen consumption was determined based on fluorescence quenching by oxygen using OxoPlates (Innovative Instruments). Cells were added to each well at a density of 8000 cells/well. The following day, cells were pre-incubated (1 hr) with the microtubules and/or actin disrupting agents. Optical oxygen sensors at the bottom of microplates contained an indicator and a reference dye. Wells containing air-saturated (100%) and oxygen-free (0%) solutions were used for calibration. Fluorescence

was assessed for 3.5 hrs in 3 min intervals in dual kinetic mode (Synergy HT microplate reader), using filter 1 (530/645 nm) and filter 2 (530/590) settings in order to detect fluorescence of the indicator and reference dyes, respectively. From these values, ratios were calculated and compared to the standard calibrations, thus allowing quantification of oxygen consumption.

Calcium Imaging: Cells were washed with GM without phenol red and incubated in the dark for 40 mins in a solution containing the calcium-sensitive dye fura-2-acetoxymethyl ester (Fura-2 AM, 5μM) and 0.02% pluronic F-127. Fura-2 AM-loaded cells were washed twice and the media was replaced with GM without phenol red for an additional 20 mins to allow the de-esterification of fura-2 AM to occur. Prior to imaging, the media was replaced. Ratiometric imaging at absorption wavelengths of 340 and 380nm (emission 510nm) was taken at 30 sec intervals. Changes in the ratio of fluorescence intensity obtained at 340 nm (fura-2-Ca^{2+} bound) to that of 380 nm (Ca^{2+} free fura-2) were used to assess Ca^{2+} levels following the addition of either ionomycin or thapsigargin to the media, to stimulate the release of calcium, and following the chelation of calcium by EGTA or BAPTA-AM.

Statistical Analyses: Data were analyzed with GraphPad 4.0 software and expressed as means ± SE. T-tests and 1-way ANOVAs were performed where appropriate, and differences were considered statistically significant if $P < 0.05$.

Results

Microtubules are the primary filaments used by mitochondria during trafficking. To elucidate which cytoskeletal elements are primarily responsible for mitochondrial motility within myoblasts, we disturbed microtubules and actin, and observed their effects on organelle movement. We examined the co-localization of actin (Fig 1A) and mitochondria (Fig 1B) in control cells (Fig 1C), and compared them to myoblasts exposed to the actin disrupting agent cytochalasin D (Fig 1D). Exposure to cytochalasin D resulted in the drastic rearrangement of actin filaments, such that they appeared disjoined and no longer extended throughout the length of the cell. Actin disruptions reduced the total path length and average speed of mitochondria by 37 and 40%, respectively (Fig 1I and 1J).

Next, we then examined the effects of microtubule disruptions on mitochondrial dynamics. Cells stained with FITC-conjugated α-tubulin antibodies and treated with colchicine or taxol, displayed alterations in the structure of microtubules compared to untreated myoblasts (Fig 1F–H). The destabilize agent, colchicine, resulted in enhanced depolymerization of microtubules (Fig 1G). Conversely, the stabilizer, taxol is known to block microtubule disassembly. As depicted in Figure 1H, taxol preventing normal polymerization of the filaments.

In response to depolymerization of microtubules using nocodazole and colchicine, the total path length of mitochondria was reduced by 64–72% (Fig 1I), similar reductions were observed in the average speed traveled by the organelles (68–74%, Fig 1J). In addition, the stabilization of microtubules by taxol also significantly altered

mitochondrial motility, albeit to a lesser degree (Fig 1I and 1J). To deduce the effects that microtubule and actin disruption would have in combination, we co-incubated myoblasts with nocodazole and cytochalasin D. Changes in mitochondrial motility were similar to the results observed with nocodazole treatment alone. We then ascertained whether disruptions in the cytoskeleton and mitochondrial movement had any effect on oxygen utilization. No significant effects on oxygen consumption were observed (Fig 1K).

Treatment with microtubule disrupting drugs arrested mitochondria to a greater extent than actin depolymerization. Given the effects that cytoskeletal disruption had on mitochondrial speed, it was of interest to examine whether this reduction was due to slower movements, or to an overall greater percentage of time that mitochondria remained stationary. By transfecting mito-dsRED2 to visualize mitochondria (Fig 2A), we determined the percentage of time that mitochondria spent in motion. To analyze the movement characteristics of individual *mitochondria, kymographs* were generated from the live-cell imaging videos to document the dynamic properties of the organelles. We determined that mitochondria remained in constant motion, and frequently changed their direction (Fig 2), as reflected by horizontal deviations in the kymograph tracings. The addition of microtubule disrupting agents reduced the motility of mitochondria, as depicted by decreased horizontal deviations in the kymograph tracings over the 5 min recording period with the addition of colchicine, nocodazole, or taxol. Interestingly, the kymograph data generated from treatment with cytochalasin D was comparable to control

conditions. Quantification of organelle motility revealed that alterations in microtubules increased the percentage of time that mitochondria were stopped by 1.6 – 2.7-fold (Fig 2C). However, changes to the structure of actin filaments using by cytochalasin D treatment had no significant effect on the amount of time mitochondria were in motion in these myoblasts.

Knockdown of microtubule motor proteins attenuates mitochondrial dynamics. For mitochondria to bind to cytoskeletal elements, motor proteins are required. The transfection of siRNA probes against Kif5B and dynein in C_2C_{12} myoblasts resulted in significant reductions in their protein levels by 59 and 40%, respectively (Fig 3A and 3B). The reduction in Kif5B was specific, and did not alter levels of mitochondrial biogenesis markers (Fig 3A) or mitochondrial morphology proteins Mfn2, Opa1, Fis1, or Drp1 (unpublished observations). Reductions in both Kif5B and dynein resulted in similar significant decreases in the average speed of mitochondrial movements, by 30–40%, as well as in the total path length travelled by the organelles (decreased by 28–37%, Fig 3C and 3D).

Cytosolic calcium regulates mitochondrial movement in myoblasts. Calcium is an important signaling molecule in skeletal muscle, and as such we were interesting in examining its effects on mitochondrial motility. The Ca^{2+} ionophore, ionomycin, triggered an increase in Ca^{2+} levels that was suppressed by the addition of EGTA, as assessed by Fura2-AM ratiometric analysis (Fig 4A and 4B). The rising phase of the

cytosolic Ca^{2+} spike was accompanied by decreases in organelle motility in myoblasts (Fig 4B and 4C). The total path length and average speed traveled by mitochondria were attenuated by 42 and 48%, respectively. The addition of EGTA permitted the recovery of mitochondrial movement, which coincided with reductions in the amount of cytosolic Ca^{2+}, (Fig 4A-C). Similar effects were observed with the incubation of thapsigargin, a SERCA inhibiting agent. The addition of thapsigargin significantly reduced the total path length and average speed of mitochondria by 19 and 22%, respectively (Fig 4E and F). Mitochondrial motility and Ca^{2+} levels returned to resting levels with the addition of the Ca^{2+} chelator BAPTA-AM (unpublished observations).

The mechanisms by which Ca^{2+} exerts its effects are still under investigation. Milton is thought to be involved, since in neurons, Milton links mitochondria to Kif5B motor proteins, allowing mitochondria to move along microtubules in a Ca^{2+}-dependent manner (12; 24). Thus, we reduced the level of Milton in myoblasts and observed its influence under conditions of elevated Ca^{2+} in the presence of thapsigargin (Fig 4G). The decrease in mitochondrial speed of movement observed with thapsigargin treatment alone was negated in cells pre-treated with Milton siRNA, suggesting that Milton is involved in mediating mitochondrial arrest in the presence of Ca^{2+}.

Figure 1

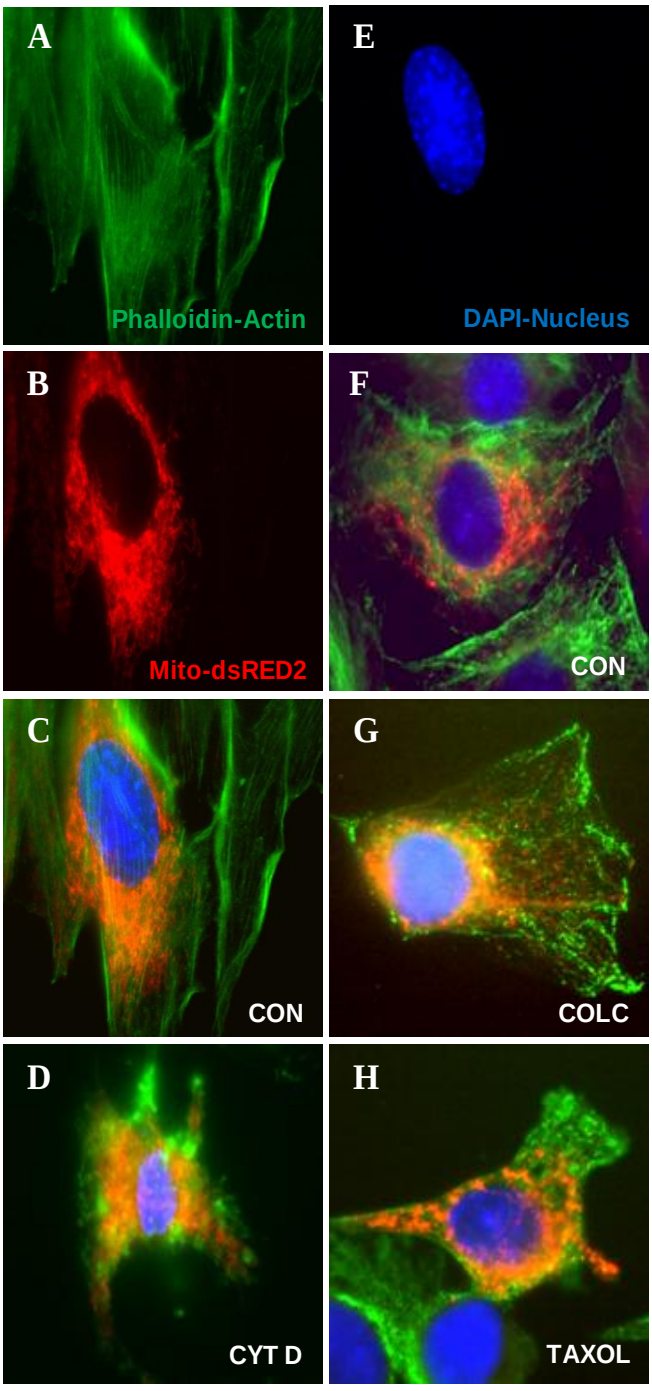
A
Phalloidin-Actin
E
DAPI-Nucleus
B
Mito-dsRED2
F
CON
C
CON
G
COLC
D
CYT D
H
TAXOL

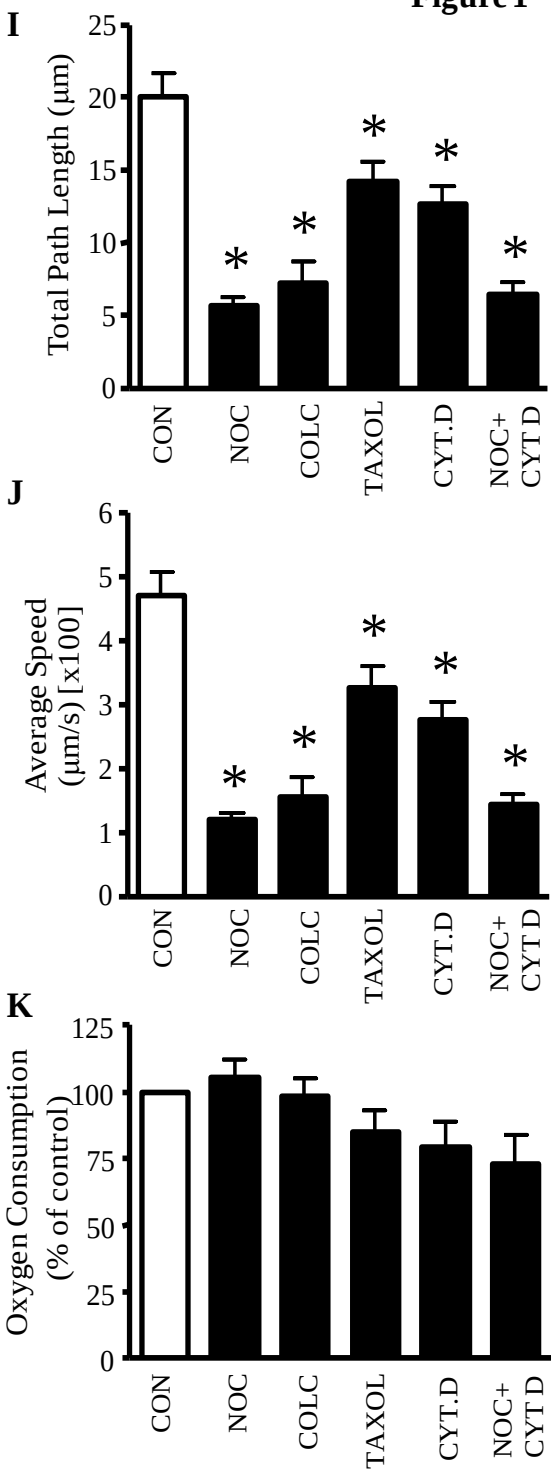
I
Total Path Length (µm)
25
20
15
10
5
0
CON
NOC
COLC
TAXOL
CYT.D
NOC+ CYT D
J
Average Speed (µm/s) [x100]
6
5
4
3
2
1
0
K
Oxygen Consumption (% of control)
125
100
75
50
25
0

Figure 1: Microtubules are the primary filaments used by mitochondria during trafficking. A: Myoblasts stained with phalloidin (green) alone, B: transfected with Mito-dsRED2 (red), or E: stained with DAPI for nuclei (blue). C: Merged images are overlays of phalloidin, Mito-dsRED2 and DAPI. Non-treated cells exhibited normal morphology of actin filaments. D: After 1 hr of treatment with cytochalasin D (CYT D), myoblasts presented cells with actin disruptions. F: Additionally, untreated myoblasts display normal microtubule (green, GFP-tubulin), mitochondria (red, Mito-dsRED2) and nuclei (blue, DAPI) organization. G: Myoblasts pre-treated with the microtubule disrupting agents Colchicine (COLC) and H: TAXOL for 1 hr exhibited alterations in the microtubule structure. COLC and Taxol were successful at disrupting microtubules, as indicated by the images above. I: Quantification of the total path length and J: the average speed traveled by mitochondria over the 5 min capturing time. Movement of mitochondria was determine from an average of n=36–72 mitochondria from 9 separate cells. K: Oxygen consumption was assessed in myoblasts with microtubule and/or actin disruptions using the microtubule disruptors Nocodazole (NOC), COLC, Taxol, and/or the actin disrupting agent CYT D, along with a control treatment (CON, DMSO). Values are expressed as averages ± SEM, N=6. *Significantly different from CON, $P < 0.05$.

Figure 2

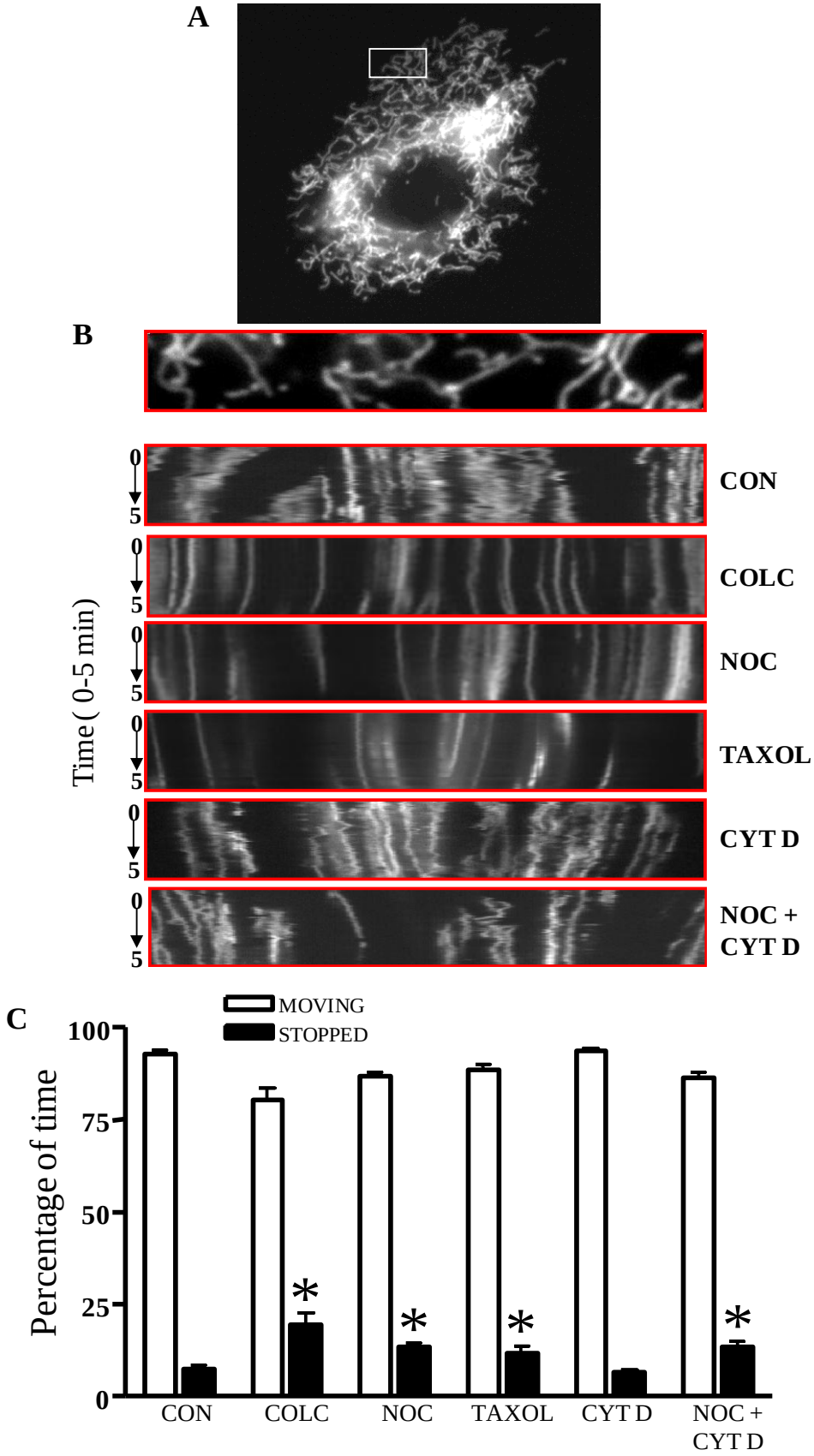
A
B
Time (0-5 min)
0
5
CON
COLC
NOC
TAXOL
CYT D
NOC +
CYT D
C
MOVING
STOPPED
Percentage of time
100
75
50
25
0
CON
COLC
NOC
TAXOL
CYT D
NOC +
CYT D

Figure 2: Treatment with microtubule disrupting drugs arrested mitochondria to a greater extent than actin depolymerization. A: Mitochondrial movement in a representative myoblast transfected with mito-DsRed2. B: The first frame in a live-cell imaging series is displayed above with representative kymographs generated from the movies from control (CON, DMSO) Nocodazole (NOC), Colchicine (COLC), Taxol, Cytochalasin D (CYT D), or NOC + CTY D treatments. Time (0-5 min) progresses from the top to bottom in the kymograph. Whereas, the x-axis represents mitochondrial position. Vertical white lines correspond to stationary mitochondria, and horizontal deviations (vibrations from the vertical) depict moving mitochondria. C: The percentage of time that mitochondria spent in motion as a result of microtubule and actin disruptions was determined by monitoring the position of the organelle throughout the capturing time. Mitochondria were considered in motion if movement was greater than 0.01μm in the 2 sec of capturing time. Movement of mitochondria was determined and averaged from n=36-72 mitochondria from 9 separate cells. Error bars represent mean ± SEM, $*P < 0.05$ vs. CON.

Figure 3

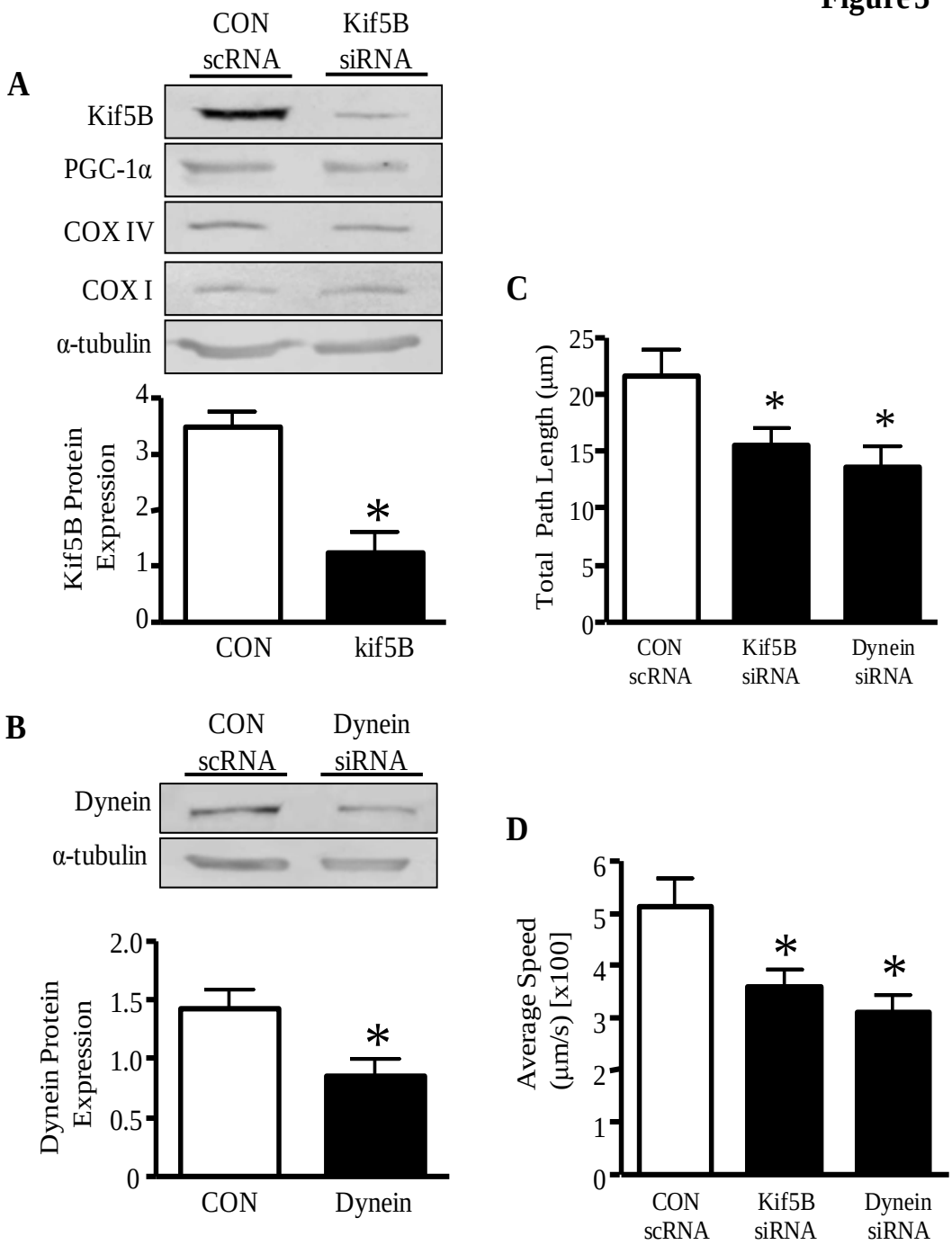
A
CON scRNA
Kif5B siRNA
Kif5B
PGC-1α
COX IV
COX I
α-tubulin
Kif5B Protein Expression
CON
kif5B
B
CON scRNA
Dynein siRNA
Dynein
α-tubulin
Dynein Protein Expression
CON
Dynein
C
Total Path Length (μm)
CON scRNA
Kif5B siRNA
Dynein siRNA
D
Average Speed (μm/s) [x100]
CON scRNA
Kif5B siRNA
Dynein siRNA

Figure 3: Knockdown of microtubule motor proteins attenuates mitochondrial dynamics. A: Representative Western blots of markers of mitochondrial content in myoblasts treated with either scrambled control (scRNA CON) or siRNA for Kif5B *(above).* Quantification of protein expression of Kif5B siRNA and scRNA control *(below).* B: Representative Western blots of dynein treated with an antisense probe and its respective scRNA control *(above),* along with graphical quantification *(below).* α-tubulin was unchanged between the conditions and was used as a loading control. Experiments were repeated for 5 separate trials. C: The total path length and D: the average speed traveled by mitochondria was assessed in scRNA CON and siRNA treatment for Kif5B and dynein. Movement of mitochondria was averaged from n=20–40 mitochondria from 5 separate cells, $*P < 0.05$ vs. CON scRNA.

Figure 4

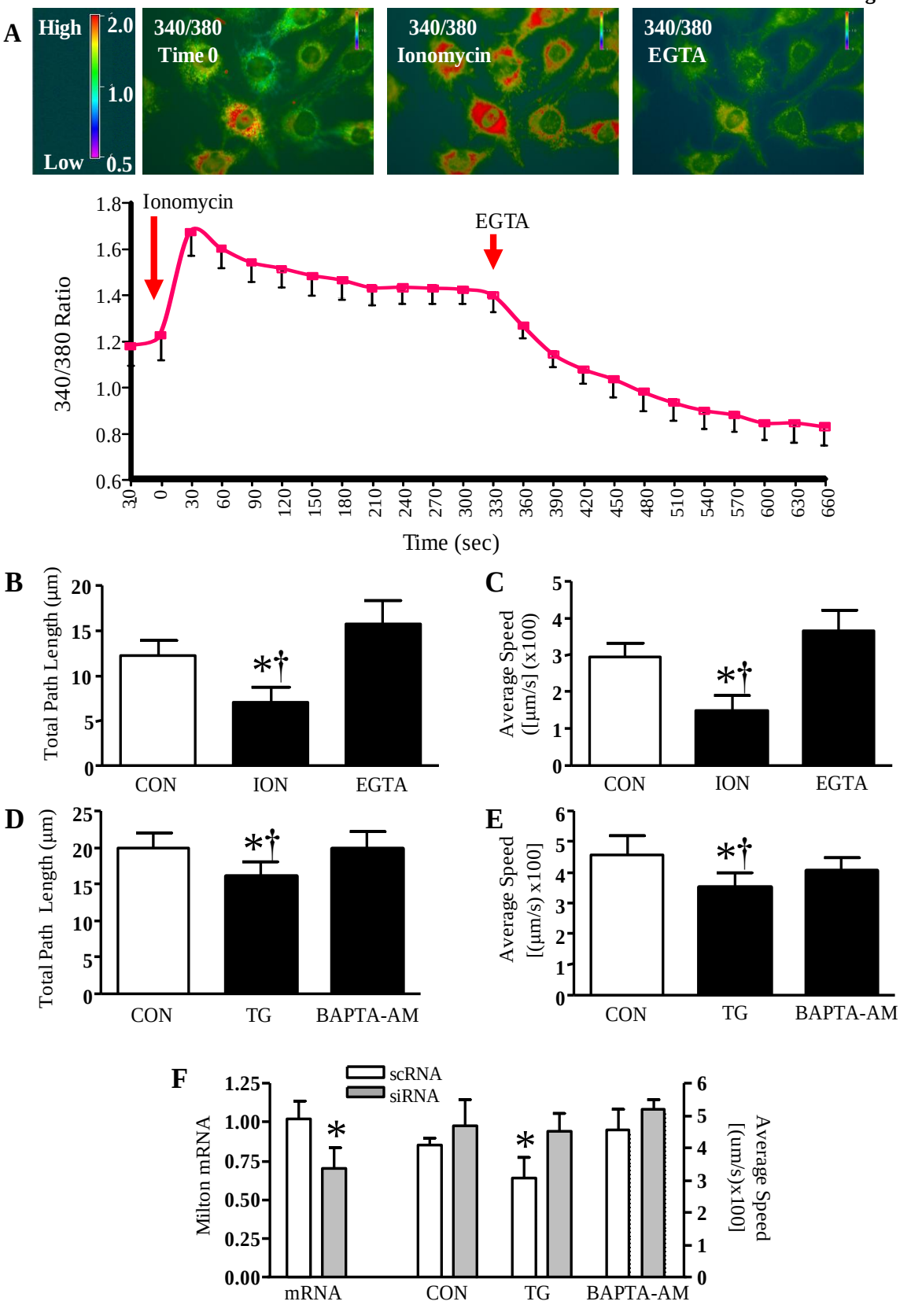
A
High
2.0
1.0
Low
0.5
340/380
Time 0
340/380
Ionomycin
340/380
EGTA
Ionomycin
EGTA
340/380 Ratio
Time (sec)
B
Total Path Length (µm)
CON
ION
EGTA
C
Average Speed ([µm/s] (x100)
D
Total Path Length (µm)
CON
TG
BAPTA-AM
E
Average Speed [(µm/s) x100]
F
scRNA
siRNA
Milton mRNA
Average Speed [(um/s)x100]
mRNA
CON
TG
BAPTA-AM

Figure 4: Cytosolic calcium regulates mitochondrial movement in myoblasts. A: Intracellular calcium levels were assessed in Fura2-AM loaded C_2C_{12} cells. Fura2 fluorescence was measured using excitation of Ca^{2+}-bound (340nm, red) and the Ca^{2+}-free form (380nm, green). Thus, elevations evoked by the addition of Ionomycin (ION) and Thapsigargin (TG) appear as increases in the red component. Elevated calcium concentrations were achieved through the addition of ionomycin and reduced by EGTA. B, C: Increased calcium attenuated mitochondrial movement, and organelle transport was recovered by the addition of EGTA. Endogenous calcium levels were elevated with Thapsigargin treatment and suppressed with BAPTA-AM. D, E: High calcium concentrations inhibited the total path length and the average velocity traveled by the organelles. (n=6–8, *P < 0.05 vs CON). F: Milton mRNA levels were assessed in myoblasts treated with 100 nM of scRNA or siRNA specific for Milton (*left*). The average speed traveled by mitochondria was determined in scRNA and siRNA transfected C_2C_{12} cells, treated with Thapsigargin and BAPTA-AM (*right*).

Discussion

In order to efficiently supply the cell with energy, mitochondria must be transported to areas of high energy demands. In neurons, mitochondria are delivered to areas where they required, and retained at sites where energy demand is high, such as growth cones, nodes of Ranvier and synapses (3; 7; 14). Within neurons, areas of high activity possess greater densities of mitochondria (11; 17). The movement of mitochondria to specific sites within the cell is dependent on a cytoskeleton-based transportation system. Moreover, environmental and physiological changes are thought to influence the positioning of organelles within the cells. Thus, our purpose was to determine which cytoskeletal components were primarily responsible for mitochondrial movement within myoblasts, and to investigate the effects of calcium on mitochondrial motility. To do so, we utilized live-cell imaging techniques to monitor the dynamics of these organelles.

To address the influence of the cytoskeleton on mitochondrial motility we assessed 1) the total path length, 2) average speed, and 3) percentage of time that organelles remained stationary. Our results indicate that microtubule disruption resulted in greater impediments in mitochondrial motility as compared to conditions in which actin polymerization was disturbed in myoblasts. Administration of microtubule depolymerizing or stabilizing agents resulted in similar effects on mitochondrial motility, yet they varied in the degree of their effects. These variations are likely due to differences in the organization of the microtubules. Microtubules are normally dynamically unstable, undergoing constant polymerization and depolymerization. The presence of taxol enhances the stability of microtubules, rendering them more susceptible

to undergoing post-translational modifications, such as acetylation, detyrosination, and polyglutamylation (9). Recently it has been found that Kinesin-1 binds preferentially to detyrosinated microtubules, and these kinesins move at slower velocities (6). These post-translational modifications may explain the disparity between the effects of taxol and nocodazole or colchicine treatments.

Since kinesin and dynein motors drive the movement of mitochondria along microtubules, we speculated that the downregulation of these components would alter organelle transport. By reducing the levels of Kif5B, a member of the Kinesin-1 family, we observed decreased mitochondrial motility. It has previously been reported that the deletion of similar kinesin-1 family members in fungus and mouse neurons, led to altered mitochondrial distribution (23; 25). Analyses in the Drosophila nervous system support the concept that the primary motors for mitochondrial movement are Kinesin-1, in coordination with dynein, which moves mitochondria in the opposite direction (12).

Calcium influx has been found to inhibit mitochondrial movement in neurons and cardiac myocytes using motor protein/adapter complexes (17; 19). However, the influences of Ca^{2+} within skeletal muscle, as well as the mechanism by which Ca^{2+} exerts its effects are still under investigation. Our results indicate that elevations in Ca^{2+} exert a negative effect on mitochondrial movement, and cause an inhibition of motility. Linker proteins coordinate the movement of mitochondria with environmental signals, and are necessary for proper localization of the organelle. In neurons, HEK293 and COS-7 cells, Milton acts as a mitochondrial-specific linker that redistributes the organelle to appropriate regions within the cell, in response to increases in Ca^{2+} (14; 15; 17).

Mutations in the protein result in mitochondrial trafficking defects, while other organelles retain their normal distribution (15). In this context, it is interesting that we observed Milton to also have a vital role in mitochondrial movement when Ca^{2+} levels were elevated in myoblast cells. Inhibition of Milton disrupted Ca^{2+}-induced mitochondrial transport. Thus, Milton may mediate associations between Kinesin-1 and mitochondria in muscle cells.

We next wanted to examine the effect that chronic changes in motility might have on mitochondrial content. Argyropoulos *et al* previously found that inhibition of the motor protein, Kif5B, reduced cytochrome b mRNA (2). Therefore, we speculated that reductions in Kif5B would alter the expression of proteins involved in mitochondrial biogenesis. We observed no change when we examined the prominent regulator of mitochondrial biogenesis, PGC-1α, as well as the mitochondrially- and nuclear-encoded proteins COXI and COXIV, respectively. Therefore, our data are not consistent with a role for changes in motor protein expression on mitochondrial biogenesis.

In summary, mitochondria primarily move along microtubules tracks. In myoblasts, mitochondria can pause, change their direction, and their velocity of movement. Displacement within myoblasts is regulated by physiological signals, such as Ca^{2+}, which inhibits mitochondrial movements in a Milton-dependent manner. By understanding mitochondrial movements and the signaling events that regulate their dynamics, we can elucidate the underlying basis for organelle interactions, leading to the formation of the mitochondrial reticulum and the distribution of energy in muscle cells. Mitochondrial transport is important not only during organelle biogenesis, but also for

recycling and degradation of cellular components. Whether these events happen in fully mature skeletal muscle, in which physical constraints are imposed by the presence of myofibril proteins, remains to be established. It is known that mitochondria form a dense network when they form myotubes, but their motility has never been analyzed. Future studies examining this possibility, and even extrapolating to contracting muscle fibres will be important for understanding how mitochondrial biogenesis and the reticulum form during conditions of increased oxidative capacity.

Reference List

1. **Adhihetty PJ, O'Leary MF, Chabi B, Wicks KL and Hood DA**. Effect of denervation on mitochondrially mediated apoptosis in skeletal muscle. *J Appl Physiol* 102: 1143-1151, 2007.
2. **Balaban RS, Nemoto S and Finkel T**. Mitochondria, oxidants, and aging. *Cell* 120: 483-495, 2005.
3. **Barsoum MJ, Yuan H, Gerencser AA, Liot G, Kushnareva Y, Graber S, Kovacs I, Lee WD, Waggoner J, Cui J, White AD, Bossy B, Martinou JC, Youle RJ, Lipton SA, Ellisman MH, Perkins GA and Bossy-Wetzel E**. Nitric oxide-induced mitochondrial fission is regulated by dynamin-related GTPases in neurons. *EMBO J* 25: 3900-3911, 2006.
4. **Bleazard W, McCaffery JM, King EJ, Bale S, Mozdy A, Tieu Q, Nunnari J and Shaw JM**. The dynamin-related GTPase Dnm1 regulates mitochondrial fission in yeast. *Nat Cell Biol* 1: 298-304, 1999.
5. **Brooks C, Cho SG, Wang CY, Yang T and Dong Z**. Fragmented mitochondria are sensitized to Bax insertion and activation during apoptosis. *Am J Physiol Cell Physiol* 2010.
6. **Carter HN and Hood DA**. Contractile activity-induced mitochondrial biogenesis and mTORC1. *Am J Physiol Cell Physiol* 303: C540-C547, 2012.
7. **Cassidy-Stone A, Chipuk JE, Ingerman E, Song C, Yoo C, Kuwana T, Kurth MJ, Shaw JT, Hinshaw JE, Green DR and Nunnari J**. Chemical inhibition of the mitochondrial division dynamin reveals its role in Bax/Bak-dependent mitochondrial outer membrane permeabilization. *Dev Cell* 14: 193-204, 2008.
8. **Chabi B, Ljubicic V, Menzies KJ, Huang JH, Saleem A and Hood DA**. Mitochondrial function and apoptotic susceptibility in aging skeletal muscle. *Aging Cell* 7: 2-12, 2008.
9. **Chang CR and Blackstone C**. Cyclic AMP-dependent protein kinase phosphorylation of Drp1 regulates its GTPase activity and mitochondrial morphology. *J Biol Chem* 282: 21583-21587, 2007.
10. **Chen H, Chomyn A and Chan DC**. Disruption of fusion results in mitochondrial heterogeneity and dysfunction. *J Biol Chem* 280: 26185-26192, 2005.
11. **Cribbs JT and Strack S**. Reversible phosphorylation of Drp1 by cyclic AMP-dependent protein kinase and calcineurin regulates mitochondrial fission and cell death. *EMBO Rep* 8: 939-944, 2007.
12. **De Vos KJ, Allan VJ, Grierson AJ and Sheetz MP**. Mitochondrial function and actin regulate dynamin-related protein 1-dependent mitochondrial fission. *Curr Biol* 15: 678-683, 2005.
13. **Fan X, Hussien R and Brooks GA**. H2O2-induced mitochondrial fragmentation in C2C12 myocytes. *Free Radic Biol Med* 49: 1646-1654, 2010.
14. **Fannjiang Y, Cheng WC, Lee SJ, Qi B, Pevsner J, McCaffery JM, Hill RB, Basanez G and Hardwick JM**. Mitochondrial fission proteins regulate programmed cell death in yeast. *Genes Dev* 18: 2785-2797, 2004.

15. **Frank M, Duvezin-Caubet S, Koob S, Occhipinti A, Jagasia R, Petcherski A, Ruonala MO, Priault M, Salin B and Reichert AS**. Mitophagy is triggered by mild oxidative stress in a mitochondrial fission dependent manner. *Biochim Biophys Acta* 1823: 2297-2310, 2012.
16. **Frank S, Gaume B, Bergmann-Leitner ES, Leitner WW, Robert EG, Catez F, Smith CL and Youle RJ**. The role of dynamin-related protein 1, a mediator of mitochondrial fission, in apoptosis. *Dev Cell* 1: 515-525, 2001.
17. **Frezza C, Cipolat S and Scorrano L**. Organelle isolation: functional mitochondria from mouse liver, muscle and cultured fibroblasts. *Nat Protoc* 2: 287-295, 2007.
18. **Horibe T and Hoogenraad NJ**. The chop gene contains an element for the positive regulation of the mitochondrial unfolded protein response. *PLoS One* 2: e835, 2007.
19. **Iqbal S, Ostojic O, Singh K, Joseph AM and Hood DA**. Expression of mitochondrial fission and fusion regulatory proteins in skeletal muscle during chronic use and disuse. *Muscle Nerve* 2013.
20. **Jagasia R, Grote P, Westermann B and Conradt B**. DRP-1-mediated mitochondrial fragmentation during EGL-1-induced cell death in C. elegans. *Nature* 433: 754-760, 2005.
21. **Jendrach M, Mai S, Pohl S, Voth M and Bereiter-Hahn J**. Short- and long-term alterations of mitochondrial morphology, dynamics and mtDNA after transient oxidative stress. *Mitochondrion* 8: 293-304, 2008.
22. **Jendrach M, Pohl S, Voth M, Kowald A, Hammerstein P and Bereiter-Hahn J**. Morpho-dynamic changes of mitochondria during ageing of human endothelial cells. *Mech Ageing Dev* 126: 813-821, 2005.
23. **Lee YJ, Jeong SY, Karbowski M, Smith CL and Youle RJ**. Roles of the mammalian mitochondrial fission and fusion mediators Fis1, Drp1, and Opa1 in apoptosis. *Mol Biol Cell* 15: 5001-5011, 2004.
24. **Pellegrino MW, Nargund AM and Haynes CM**. Signaling the mitochondrial unfolded protein response. *Biochim Biophys Acta* 1833: 410-416, 2013.
25. **Smirnova E, Shurland DL, Ryazantsev SN and van der Bliek AM**. A human dynamin-related protein controls the distribution of mitochondria. *J Cell Biol* 143: 351-358, 1998.
26. **Strack S and Cribbs JT**. Allosteric modulation of Drp1 mechanoenzyme assembly and mitochondrial fission by the variable domain. *J Biol Chem* 287: 10990-11001, 2012.
27. **Takeyama N, Miki S, Hirakawa A and Tanaka T**. Role of the mitochondrial permeability transition and cytochrome C release in hydrogen peroxide-induced apoptosis. *Exp Cell Res* 274: 16-24, 2002.
28. **Twig G, Elorza A, Molina AJ, Mohamed H, Wikstrom JD, Walzer G, Stiles L, Haigh SE, Katz S, Las G, Alroy J, Wu M, Py BF, Yuan J, Deeney JT, Corkey BE and Shirihai OS**. Fission and selective fusion govern mitochondrial segregation and elimination by autophagy. *EMBO J* 27: 433-446, 2008.
29. **Zuchner S, Mersiyanova IV, Muglia M, Bissar-Tadmouri N, Rochelle J, Dadali EL, Zappia M, Nelis E, Patitucci A, Senderek J, Parman Y, Evgrafov O, Jonghe PD, Takahashi Y, Tsuji S, Pericak-Vance MA, Quattrone A, Battaloglu**

E, Polyakov AV, Timmerman V, Schroder JM and Vance JM. Mutations in the mitochondrial GTPase mitofusin 2 cause Charcot-Marie-Tooth neuropathy type 2A. *Nat Genet* 36: 449-451, 2004.

CHAPTER 4:

THE INFLUENCE OF ROS ON MITOCHONDRIAL DYNAMICS

Rationale for Manuscript #3

Mitochondria are dynamic organelles, continuously undergoing cycles of fission and fusion, resulting in alterations in their morphology and function, however the mechanisms governing these changes have yet to be fully elucidated. Hence, we sought to determine the effects of oxidative stress on mitochondrial dynamics.

The connection between oxidative stress and mitochondrial morphology has previously been shown in endothelial cells and neurons, and recently in C2C12 myoblasts. Whereby, exposure to high levels of ROS induces mitochondrial fragmentation. Based on these finding, we hypothesized that an increase in oxidative stress would fragment the mitochondrial network and reduce mitochondrial motility.

SI and DAH conceived and designed the experiments, interpreted the data and wrote the manuscript. SI collected and analyzed all the data. Both authors approved the final version of the manuscript.

Oxidative stress-induced mitochondrial fragmentation and movement in skeletal muscle cells

Sobia Iqbal and David A. Hood

School of Kinesiology and Health Science, and the Muscle Health Research Centre
York University, Toronto, Ontario M3J 1P3, Canada

Running title: Oxidative-stress induced mitochondrial fragmentation

To whom correspondence should be addressed:
David A. Hood, PhD
School of Kinesiology and Health Science
York University, Toronto, Ontario
M3J 1P3, Canada
Tel: (416) 736-2100 ext: 66640
Fax: (416) 736-5698
E-mail: dhood@yorku.ca

Abstract

Mitochondria are dynamic organelles, continuously undergoing cycles of fission and fusion, resulting in alterations in their morphology and function, however the mechanisms governing these changes have yet to be fully elucidated. Hence, we sought to determine the effects of oxidative stress on mitochondrial dynamics in mouse myoblasts. We demonstrated that acute exposure to oxidative stress with H_2O_2 resulted in a 41% increase in fragmentation of the mitochondrial reticulum within 3 hours of exposure, an effect that was preceded by a reduction in membrane potential. Using live-cell imaging, we monitored mitochondrial motility and found that oxidative stress resulted in a 30% reduction in the total path length and average velocity travelled by mitochondria within myoblasts. This attenuation in mitochondrial movement was abolished by the addition of N-acetylcysteine, a reactive oxygen species scavenger. To investigate whether H_2O_2-induced fragmentation was mediated by the action of Drp1, we incubated cells with mDivi1, an inhibitor of Drp1 translocation to mitochondria. mDivi1 attenuated oxidative stress-induced mitochondrial fragmentation by 27%. Thus, the observed oxidative stress-induced mitochondrial fragmentation was mediated, in part, by Drp1. Moreover, we demonstrated that exposure to oxidative stress activated the ER-unfolded protein response prior to the initiation of mitophagy and the mitochondrial-unfolded protein response pathways. These findings indicate that oxidative stress is a vital signaling mechanism in the regulation of mitochondrial morphology and motility.

Introduction

Mitochondria are essential organelles for the life and death of eukaryotic cells. They play key roles in aerobic energy production, apoptosis, mitophagy and cellular signaling. These versatile organelles were once thought to be static and rigid structures. More recently, mitochondria have been appreciated for their dynamic nature. They can change their distribution by moving along cytoskeletal tracks, or change their overall morphology. The maintenance and appropriate networking of mitochondria within the cell is mediated by fusion and opposing fission processes. Fusion involves the mixing of mitochondrial material, whereas fission divides the organelle into smaller components. Disruptions in either of these opposing events can lead to developmental defects and disease (29), suggesting that the proper maintenance of mitochondrial morphology is critical for normal cell function.

Mitochondrial fission is orchestrated, in part, by Drp1 (4; 25), a protein that is a GTPase of the dynamin family. All dynamin members are structurally similar, but functionally diverse GTP-binding proteins. Drp1 assists in mitochondrial fission by polymerizing into a ring-like structure around the organelle. The cross-bridging of the GTPase domains of adjacent Drp1 proteins results in GTP hydrolysis, constriction, and the ultimate severing of mitochondria (26). It is the phosphorylation status of Drp1 that determines its localization and consequently its effect on mitochondrial structure. Ser^{637} phosphorylation results in inhibition Drp1 GTPase activity, preventing the protein from translocating from the cytosol to the sites of mitochondrial division, thereby inhibiting organelle fission (9; 11).

Mitochondria are the primary source of reactive oxygen species (ROS) generation. Within these organelles, low levels of ROS are constantly produced during normal respiration when the O_2 consumed undergoes a one-electron reduction. In skeletal muscle subject to conditions of chronic muscle disuse (1) and aging (8), an increased production of ROS from mitochondria occurs, and this coincides with an increased incidence of mitochondrial fragmentation (19). More direct connections between oxidative stress and mitochondrial morphology have previously been shown in endothelial cells and neurons, and recently in C_2C_{12} cells, whereby exposure to high levels of hydrogen peroxide, a major contributor to oxidative stress, induces mitochondrial fragmentation (3; 5; 21).

To promote proper functioning of mitochondria in the face of ROS-induced damage, the cell has quality control mechanisms in place. The endoplasmic reticulum (ER) and mitochondria (mt) are exposed to newly synthesized protein and are responsible for their proper folding and assembly. Homeostasis is achieved by balancing the nascent protein load with the folding capacity of the organelle. When the ability to do so is compromised, ER and mitochondrial stress ensues. The adaptive responses to this imbalance, termed the ER-unfolded protein response (UPR) and mt-UPR, coincide with the upregulation of molecular chaperones allowing for the increased folding capacity of the cell. If the cellular stress is too extensive and cannot be alleviated, the UPR activates cell destructive responses including apoptosis and the mitophagy pathway (24).

Mitochondria are dynamic organelles, continuously moving and undergoing cycles of fission and fusion, resulting in alterations in their displacement, morphology,

and function, however the mechanisms governing these changes have yet to be fully elucidated. Hence, we sought to determine the effects of ROS on mitochondrial dynamics in myoblasts and to establish the interplay between mitochondrial morphology and stress responses during conditions of oxidative stress.

Experimental Procedures

Cell Culture and Treatments: C_2C_{12} murine skeletal muscle cells were plated into 6-well dishes and allowed to proliferate in DMEM supplemented with 10% fetal bovine serum and 1% Penicillin/Streptomycin (Growth Media, GM). Upon reaching a confluence of approximately 60%, the mito-DsRED2 plasmid was transfected into myoblasts using Lipofectamine 2000 (Life Technologies), thus allowing for the visualization mitochondria.

Mitochondrial movement was observed in C_2C_{12} cells using an expression vector that encodes a fusion of red fluorescence protein and the mitochondrial targeting sequence from cytochrome c oxidase subunit VIII (mito-dsRED2). Forty-eight hours following transfection with mito-DsRed2, cells were treated with either vehicle (H_2O or DMSO) or 20mM N-acetylcysteine (NAC) for 60 mins, while incubated with H_2O_2. Mdivi-1 (25μM, Tocris) was used as a selective inhibitor of Drp1, due to its suppression of Drp1 GTPase activity, thus blocking the self-assembly of the protein (7). Imaging of Drp1 occurred by transfection of the pEYFP-C1-Drp1 plasmid (Addgene) into myoblasts.

Mitochondrial Movement Analysis: Mitochondria were visualized using an inverted Nikon Eclipse TE2000-U fluorescent microscope equipped with 100x/1.5 oil objective lens, while a custom designed chamber maintained a constant temperature of 37^{o}C with 5% CO_2. Mitochondrial dynamics were captured at 2 sec intervals for a total time of 5 mins using real-time imaging. Analyses were performed using the NIS Element AR 3.1 software, and was limited to regions of interest in the periphery of the cells, where

individual mitochondria were readily resolved and could be used for analysis while avoiding the confounding influence of high density mitochondrial networks.

The percentage of time that mitochondria spent in motion with and without the addition of H_2O_2 was determined by monitoring the position of the organelle throughout the 5 min capturing time. Mitochondria were considered in motion if movement was greater than 0.01μm in the 2 second capturing frames, and taken as a percentage over the 5 minute time course for each movie.

The number of fission and fusion events was determined in a 7x7 μm area over the time course of 5 mins. The average from 3 – 5 squares, placed in a non-overlapping fashion, were used to determine the number of fission and fusion events, from 6 – 10 separate cells. A fusion event occurred when a mitochondrion extended its projection and merged with a neighbouring mitochondrion, and black pixels no longer separated the organelles. Whereas a fission event consist of a break of the mitochondrial filament, whereby black pixels separate the once continuous mitochondrial network.

Mitochondrial Isolation: Mitochondria were isolated using an adapted protocol (6; 17). Briefly, the medium was removed from myoblasts and washed with ice-cold PBS. Cells were gently scraped in mitochondrial isolation buffer containing 10% 0.1 M Tris-MOPS, 1% EGTA-Tris, and 20% 1 M sucrose (pH 7.4). Subsequently, cells were subjected to differential centrifugation and mitochondria were resuspended in mitochondrial isolation buffer. Mitochondrial fractions were used for immunoblotting of mitophagy marker proteins.

Immunoblotting: Protein extracts from myoblasts and isolated mitochondria fractions were separated on 6–12% SDS-PAGE and subsequently transferred onto nitrocellulose membranes. Membranes were blocked for 1 hr with a 5% skim milk in 1x TBST (Tris-buffered saline–Tween-20: 25 mM Tris–HCl, pH 7.5, 1 mM NaCl and 0.1% Tween-20) solution at room temperature, followed by incubation in blocking solution with antibodies directed towards P-Drp1 (1:250; Cell Signaling), Drp1 (1:500; BD Transduction Laboratories), LC3 (1:500; Cell Signaling), p62 (1:5000; Sigma-Aldrich), Porin (1:3000; Abcam), mtHSP60 (1:500; Enzo Life Sciences), mtHSP70 (1:1000; Enzo Life Sciences), cpn10 (1:500; Enzo Life Sciences), CHOP (1:1000; Cell Signaling), P-eIF2α (1:500; Invitrogen), eIF2α (1:500; Cell Signaling), or α-tubulin (1:5000; Calbiochem) overnight at 4°C. Subsequently, membranes were washed 3x 5 min with TBST, followed by incubation at room temperature (1 hr) with the appropriate secondary antibody conjugated to horseradish peroxidase, and washed again 3x for 5 min each with TBST. Membranes were developed using Western Blot Luminol Reagent (Santa Cruz), and films were subsequently scanned and quantification via densitometric analysis for the intensity of signals with SigmaScanPro software (version 5, Jandel Scientific, San Rafael, CA, USA).

Membrane Potential: Tetramethylrhodamine ethyl ester (TMRE) is a cationic dye that is rapidly accumulated by mitochondria due to their $\Delta\Psi$. Depolarization of mitochondria results in a decrease in $\Delta\Psi$ and failure to sequester TMRE. To determine membrane potential, cells were washed 2x with PBS. Subsequently, cells were incubated with TMRE (50 nM, Invitrogen) for 45 minutes. After washing twice with PBS, the media

was replaced with GM without phenol red and imaged. TMRE fluorescence was measured in the dark using a fluorescence microscope at 60X magnification, and light exposure was kept to the minimum to insure accurate measurements. The change in fluorescence observed after the addition of H_2O_2 (300μM) was determined and compared relative to untreated cells. The mean from 13-18 cells in 6 separate experiments was used for analysis.

Oxygen Consumption: Oxygen consumption was determined based on fluorescence quenching by oxygen using OxoPlates (Innovative Instruments). Cells were added to each well at a density of 8000 cells/well. The following day, H_2O_2 (300 μM) was added to the wells containing C_2C_{12} cells and oxygen consumption was assessed at 0, 1, 3, and 5 hrs. Optical oxygen sensors at the bottom of microplates contained an indicator and a reference dye. Wells containing air-saturated (100%) and oxygen-free (0%) solutions were used for calibration. Fluorescence was assessed for 3.5 hrs in 3 min intervals in dual kinetic mode (Synergy HT microplate reader), using filter 1 (530/645 nm) and filter 2 (530/590) settings in order to detect fluorescence of the indicator and reference dyes, respectively. From these values, ratios were calculated and compared to the standard calibrations, thus allowing for quantification of oxygen consumption.

Statistical Analyses: Data were analyzed with GraphPad 4.0 software and expressed as means ± SE. T-tests and 1-way ANOVAs were performed where appropriate, and differences were considered statistically significant if $P < 0.05$.

Results

Oxidative stress halts mitochondrial movement in C_2C_{12} cells. We examined the influence of oxidative stress on mitochondrial dynamics by live-cell imaging of cultured myoblasts. By transfecting mito-dsRED2 to visualize mitochondria (Fig 1A), we determined the percentage of time that mitochondria spent in motion, their total path length, and the average speed traveled by the organelles. To analyze the movement characteristics of individual mitochondria, kymographs were generated from the live-cell imaging videos. The side-to-side horizontal oscillations visible over the 5 min duration of data collection reveal the dynamic properties of the organelles (Fig 1B). We observed that mitochondria remained in constant motion, and frequently changed their direction. The addition of H_2O_2 inhibited mitochondrial movements. Quantification of organelle motility revealed a 44% increase in the percentage of time that mitochondrial remained stationary (Fig 1C). Moreover, H_2O_2 exposure was able to reduce the total path length (*above*) and the average speed (*below*) traveled by mitochondria by 31 and 33%, respectively (Fig 1D). The reduction in mitochondrial movement is attributed to oxidative stress, since the addition of NAC, the free radical scavenger, was able to negate the effects observed with H_2O_2 alone (Fig 1D).

Oxidative stress induces mitochondrial fragmentation, as well as reductions in membrane potential and oxygen consumption. Mitochondrial movement is speculated to be associated with alterations in the morphology of the organelle as a result of fission and fusion events (Fig 2A). Thus, we investigated whether oxidative stress would change the

frequency of fission and fusion. Exposure to H_2O_2 for 5 mins significantly reduced the number of fusion and fission events occurring within C_2C_{12} myoblasts by 5.6– and 4.7–fold, respectively (Fig 2B). Interestingly, the removal of reactive oxygen species by NAC restored the rate of fission, but enhanced the number of fusion events, both in the presence and absence of H_2O_2.

At early time points following the addition of H_2O_2 (1 hr) the morpology of mitochondria was not altered (Fig 3A and 3B). After 3 hrs of exposure, H_2O_2 resulted in an increased percentage of fragmented mitochondria relative to the total area of the cell (Fig 3B). In cells exposed to H_2O_2 for 5 hrs, the extent of fragmentation was enhanced by 3.6–fold (Fig 3B). These changes in mitochondrial morphology were not due to an increase in apoptosis, as cell viability was unaltered up to 5 hrs following the addition of 300μM H_2O_2 (unpublished observations).

Next we sought to determine the functional implications resulting from acute exposure to oxidative stress. H_2O_2 (300μM) induced membrane depolarization, as indicated by reductions in the fluorescence of TMRE, beginning at 1 hr following treatment (Fig 3C). TMRE fluorescence continued to decline to 57% of control values at 5 hrs. Since, alterations in membrane potential often result in changes in oxygen consumption, we evaluated the effect of H_2O_2 on C_2C_{12} oxygen consumption at 0, 1, 3, and 5 hrs of treatment (Fig 3D). One hr following exposure to H_2O_2 (300μM), oxygen consumption was reduced by 48%, and continued to decline up to 5 hrs, at which time point respiration was reduced by 90% compared to initial values.

Oxidative stress-induced mitochondrial fragmentation is mediated by Drp1. To examine the importance of Drp1 during oxidative stress-induced mitochondrial fragmentation, we reduced the activity of Drp1 using Mdivi-1. When myoblasts were exposed to 100μM H_2O_2 for 3 hrs, Mdivi-1 attenuated the amount of fragmented mitochondria by 27% (Fig 4A). These findings indicate that Drp1 activation is responsible, in part, for oxidative stress-induced mitochondrial fragmentation. Next, we examined the expression and translocation profile of Drp1 following H_2O_2 exposure. In control untreated cells, and at 1 hr following H_2O_2 exposure, Drp1 was visualized throughout the cytosol, as observed by the diffuse yellow fluorescence in the cell (Fig 4B). Following 3 – 5 hrs of H_2O_2 exposure, Drp1 was recruited from the cytosol, concentrated to areas nearby mitochondria, and was revealed as an accumulation of Drp1-positive puncta in mitochondrial regions (Fig 4B). Concomitantly H_2O_2 treatment resulted in the dephosphorylation (and activation) of Drp1, which was inhibited by Mdivi-1 (Fig 4C). This occurred in the absence of a change in total Drp1 expression.

Acute oxidative stress specifically induces the ER-UPR response, without affecting the mt-UPR or mitophagy. Alterations in mitochondrial morphology have been found to correspond to an increased incidence of mitophagy (28). Thus, we sought to determine whether the oxidative stress-induced fragmentation was also affecting mitophagy. During 5 hrs of exposure to 300μM H_2O_2 the levels of the mitophagy markers, LC3 and p62 were unaltered in mitochondrial fractions of C_2C_{12} myoblasts. However, longer

treatments with H_2O_2 (24 hrs) were sufficient to evoke an increase in the localization of these mitophagy markers with mitochondrial fractions (Fig 5A).

To determine whether the mitochondrial-UPR was altered by acute exposure to oxidative stress, we examined the expression of mitochondrial chaperones involved in protein folding (Fig 5B). We did not observe any significant changes in the levels of mtHSP60, mtHSP70, or cpn10 in either whole cell (Fig 5B) or mitochondrial fractions (unpublished observations) by increasing the duration of H_2O_2 treatment from 1 – 5 hrs. We next examined the effects of H_2O_2 on the expression of ER-UPR proteins. At 3 hrs of H_2O_2 exposure, a large 12–fold increase in the expression of CHOP was observed, which remained elevated at 5 hrs by 8.5–fold relative to control values (Fig 5C). Similarly, the phosphorylation of eIF2α was significantly upregulated by 32% in the presence of oxidative stress (Fig 5D).

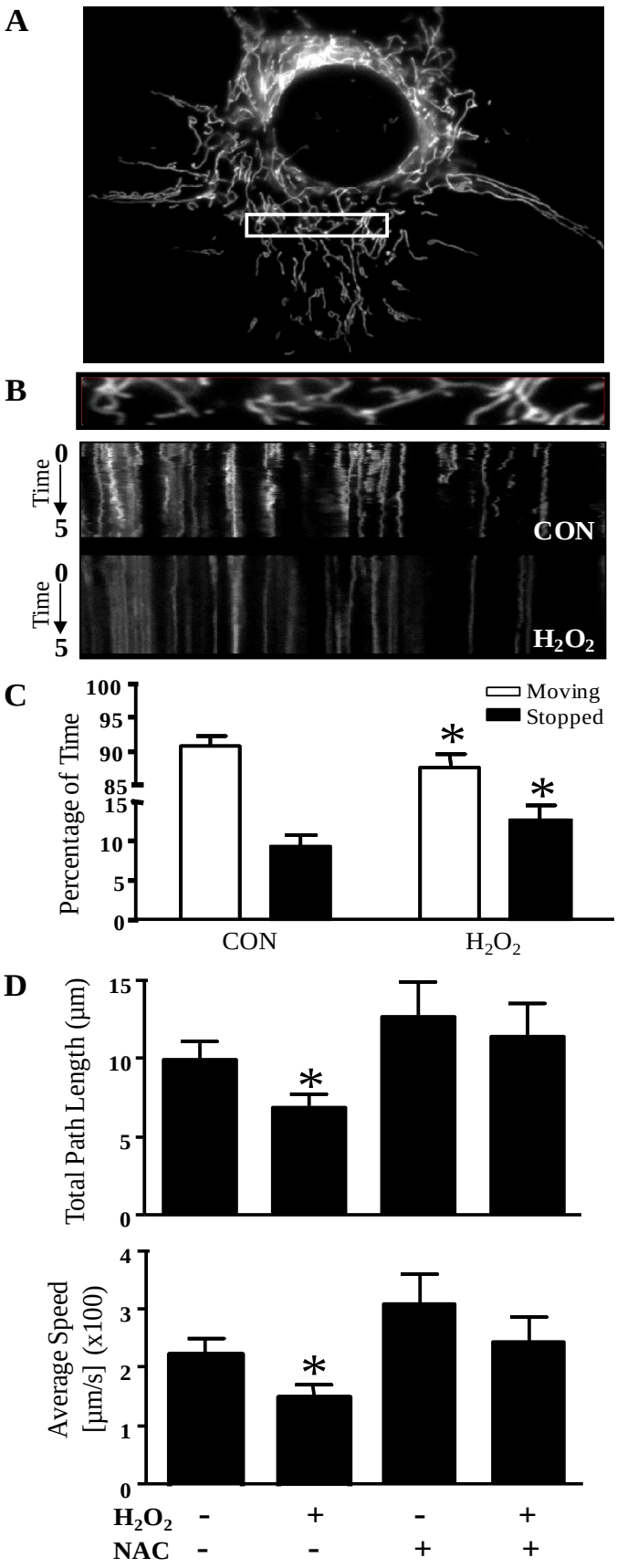
A
B
Time
0
5
CON
Time
0
5
H2O2
C
100
95
90
85
15
10
5
0
Percentage of Time
Moving
Stopped
*
*
CON
H2O2
D
15
10
5
0
Total Path Length (µm)
*
4
3
2
1
0
Average Speed
[µm/s] (x100)
*
H2O2 - + - +
NAC - - + +

Figure 1

Figure 1: Oxidative stress halts mitochondrial movement in C_2C_{12} myoblasts. A: Representative myoblast co-transfected with mito-DsRED2. B: The upper panel is the first frame in a live-cell imaging series with representative kymographs generated from the videos of untreated and treated 300μM H_2O_2 myoblasts displayed below. Time (0-5 min) progresses from the top to bottom in the kymograph. Whereas, the x-axis represents mitochondrial position. Vertical white lines correspond to stationary mitochondria, and horizontal deviations (vibrations from the vertical) depict moving mitochondria. C: The percentage of time that mitochondria spent in motion with and without the addition of 300μM H_2O_2 was determined by monitoring the position of the organelle throughout the 5 min capturing time in 10 separate experiments. D: Quantification of the total path length (*above*) and the average speed (*below*) traveled by mitochondria was assessed in control and 300μM H_2O_2 treated myoblasts, with or without the presence of N-acetyl cysteine (NAC, 60 min pre-treatment). Movement of mitochondria was determined and averaged from n=18 – 80 mitochondria from 6 – 10 separate cells. All values are expressed as averages ± SEM, $*P < 0.05$ vs. CON.

Figure 2

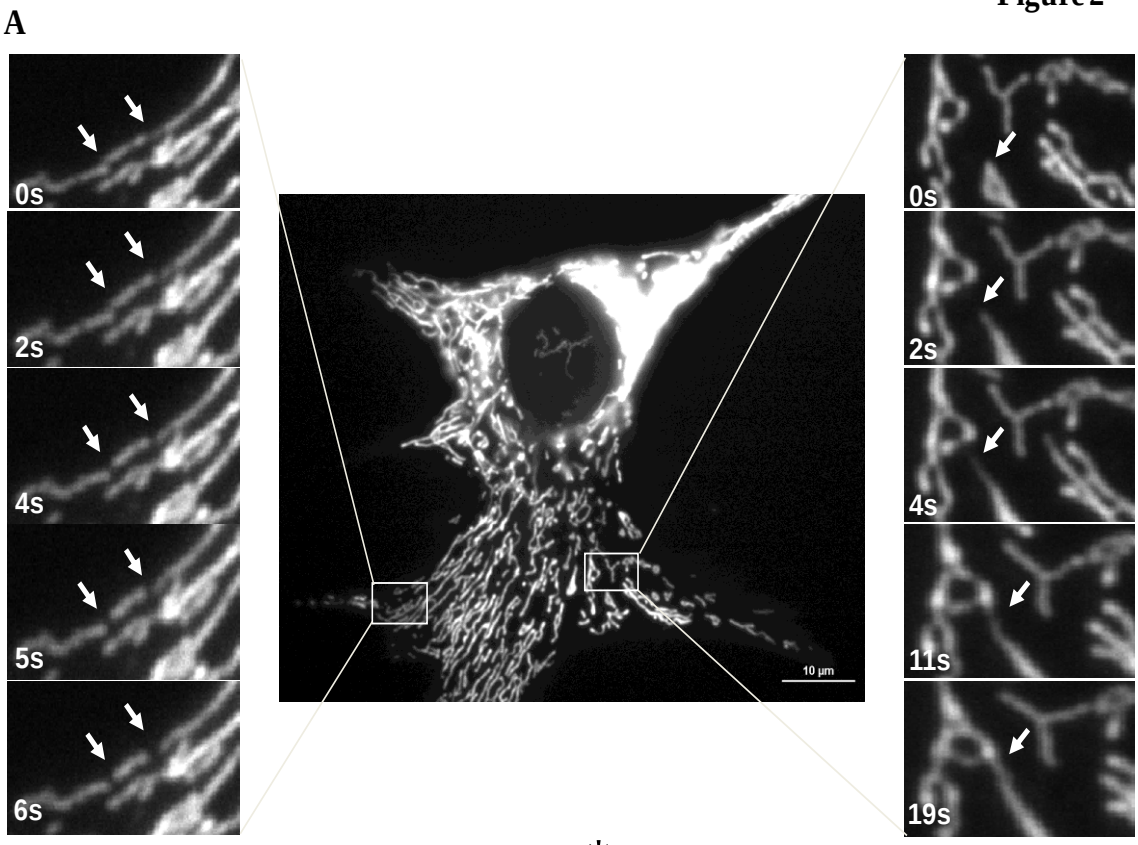
A
0s
2s
4s
5s
6s
10 µm
0s
2s
4s
11s
19s
B
No. of Events in 7x7µm Area in 5 min
0
1
2
3
4
5
6
7
*
*
*
*
H2O2 - + - + - + - +
NAC - - + + - - + +
Fusion
Fission

Figure 2: Oxidative stress results in changes to mitochondrial dynamics. A: The first frame from a live-cell imaging series of a representative myoblast *(centre)*, with time-lapse images of myoblasts expressing mito-DsRed2. The left panel displays representative images of a 6 sec time-lapse series of a myoblast undergoing mitochondrial fission. The arrows indicate sites of mitochondrial division. The right panel of images displays sequential events of mitochondrial fusion monitored over 19 secs. The arrow denotes the extension of a mitochondrial filament, resulting in a fusion event. B: The number of mitochondrial fission and fusion events was determined in a 7x7 μm area over the time course of 5 mins, from 6 – 10 separate cells. The number of fission and fusion events was determined in control and H_2O_2 (300μM) treated myoblasts, with or without NAC. Values are expressed as averages ± SEM, $*P < 0.05$ vs. CON (without H_2O_2 and NAC).

A **Figure 3**

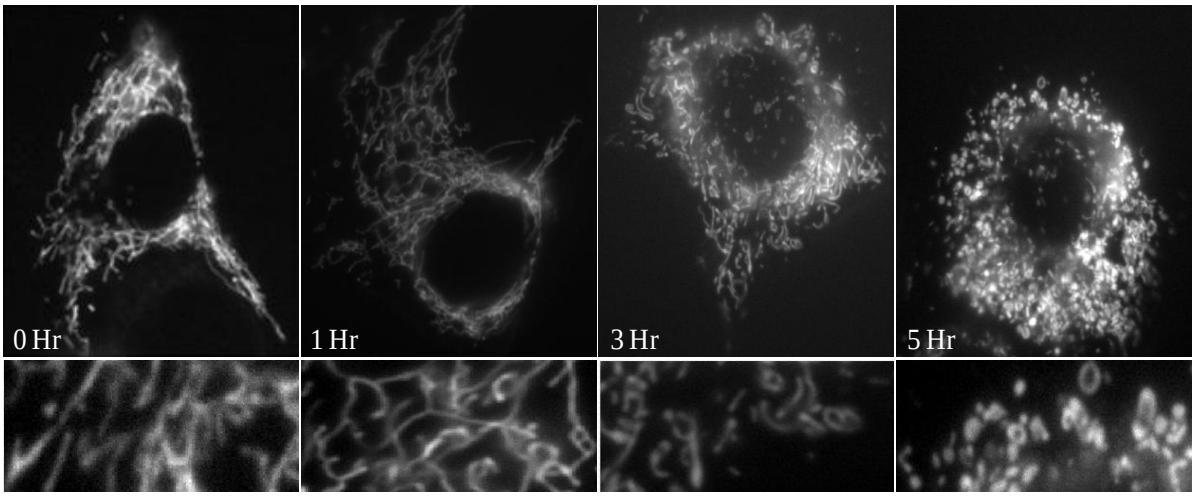
0 Hr
1 Hr
3 Hr
5 Hr

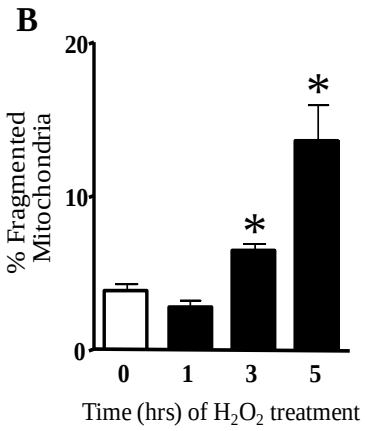
B
% Fragmented Mitochondria
20
10
0
*
*
0
1
3
5
Time (hrs) of H2O2 treatment

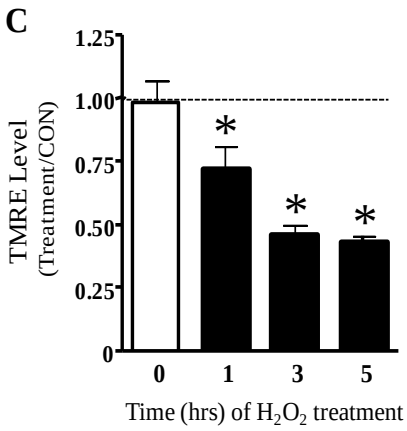
C
TMRE Level (Treatment/CON)
1.25
1.00
0.75
0.50
0.25
0
*
*
*
0
1
3
5
Time (hrs) of H2O2 treatment

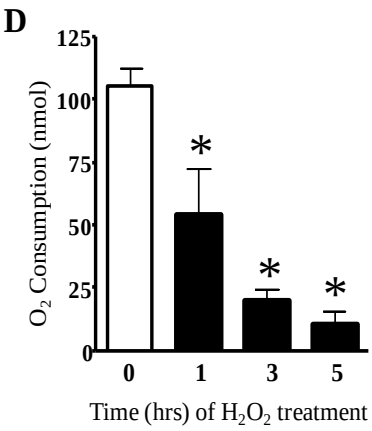
D
O2 Consumption (nmol)
125
100
75
50
25
0
*
*
*
0
1
3
5
Time (hrs) of H2O2 treatment

Figure 3: Oxidative stress induces mitochondrial fragmentation, as well as reductions in membrane potential and oxygen consumption. Myoblasts were treated with 300μM H_2O_2 for 5 hours, transfected with Mito-dsRED2 for visualization of mitochondria and imaged immediately or after 1, 3, or 5 hours of incubation. Mitochondrial morphology was assessed as the percentage of the cell occupied by either fragmented or network mitochondria. A: Representative images for each time point *(top)*, with magnified images of the mitochondrial network are displayed under each condition. H_2O_2 altered the morphology of mitochondria, such that more fragmented organelles were observed beginning at 3 hrs post-treatment. B: The percentage (mean ± SEM) of total cell area displaying fragmented mitochondria from six separate experiments. C: Membrane potential was analyzed by assessing the fluorescence of TMRE. The mean fluorescence intensity of each condition was expressed as a percentage of the untreated control. Mean percentage ± SEM of 13-18 cells are shown. D: O_2 consumption was determined in C_2C_{12} cells treated with 300 μM for a total time of 5 hrs. N=4; *Significantly different from 0 hour, $P < 0.05$.

Figure 4

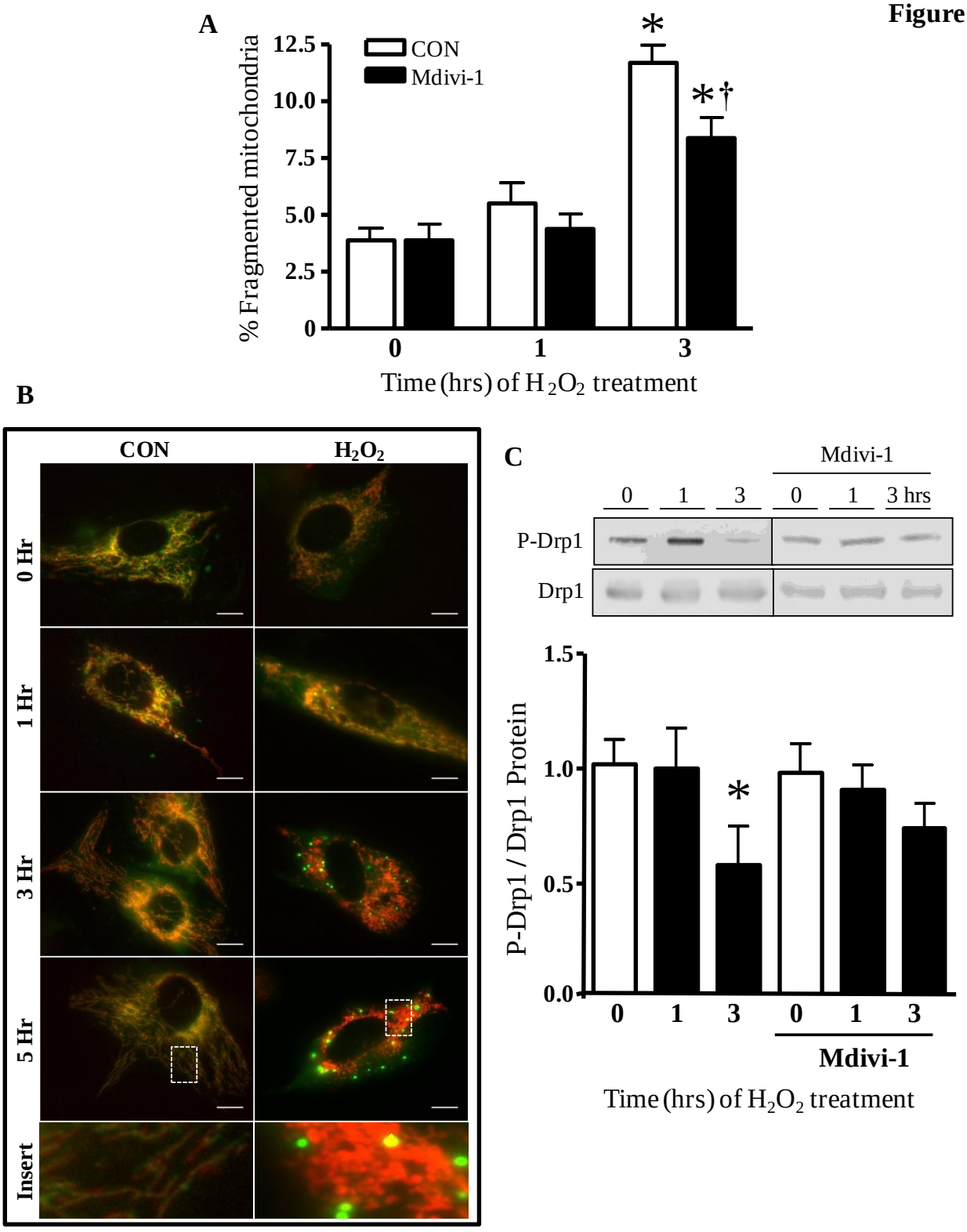
A
% Fragmented mitochondria
12.5
10.0
7.5
5.0
2.5
0
CON
Mdivi-1
*
*†
0
1
3
Time (hrs) of H2O2 treatment
B
CON
H2O2
0 Hr
1 Hr
3 Hr
5 Hr
Insert
C
Mdivi-1
0
1
3
0
1
3 hrs
P-Drp1
Drp1
P-Drp1 / Drp1 Protein
1.5
1.0
0.5
0.0
*
0
1
3
0
1
3
Mdivi-1
Time (hrs) of H2O2 treatment

Figure 4: Oxidative stress-induced mitochondrial fragmentation is mediated by Drp1. Mitochondrial morphology for myoblasts expressing mito-DsRed2 after 100μM H_2O_2 exposure. A: The percentage of fragmented mitochondria were expressed relative to the total area of the cells, with (*closed bar*) or without (*open bar*) the presence of mDivi-1 (25μM, 60 min). B: C_2C_{12} myoblasts were treated with and without 300μM H_2O_2 for 5 hrs. Cells were co-transfected with Mito-dsRED2 (red) and pEYFP-C1-Drp1 (green) and imaged at 150x magnification. Visualization of control myoblasts display long, reticular mitochondria with diffuse Drp1. Whereas H_2O_2-treatment show small, fragmented mitochondria and an accumulation of Drp1-positive puncta concentrated by mitochondria, in a time-dependent manner. The hatched boxes are magnified on the right (Insert). Scale bar represents 10μm. C: Drp1 dephosphorylation compared to total Drp1 levels with 100μM H_2O_2 exposure. The expression of phosphorylated-Drp1 (Ser 637) and total Drp1 was assessed with and without 25μM mDivi-1 (60 min pre-incubation). *Significantly different from 0 hour, $P < 0.05$; † significantly difference from untreated conditions, $P < 0.05$; N=6 for each condition.

Figure 5

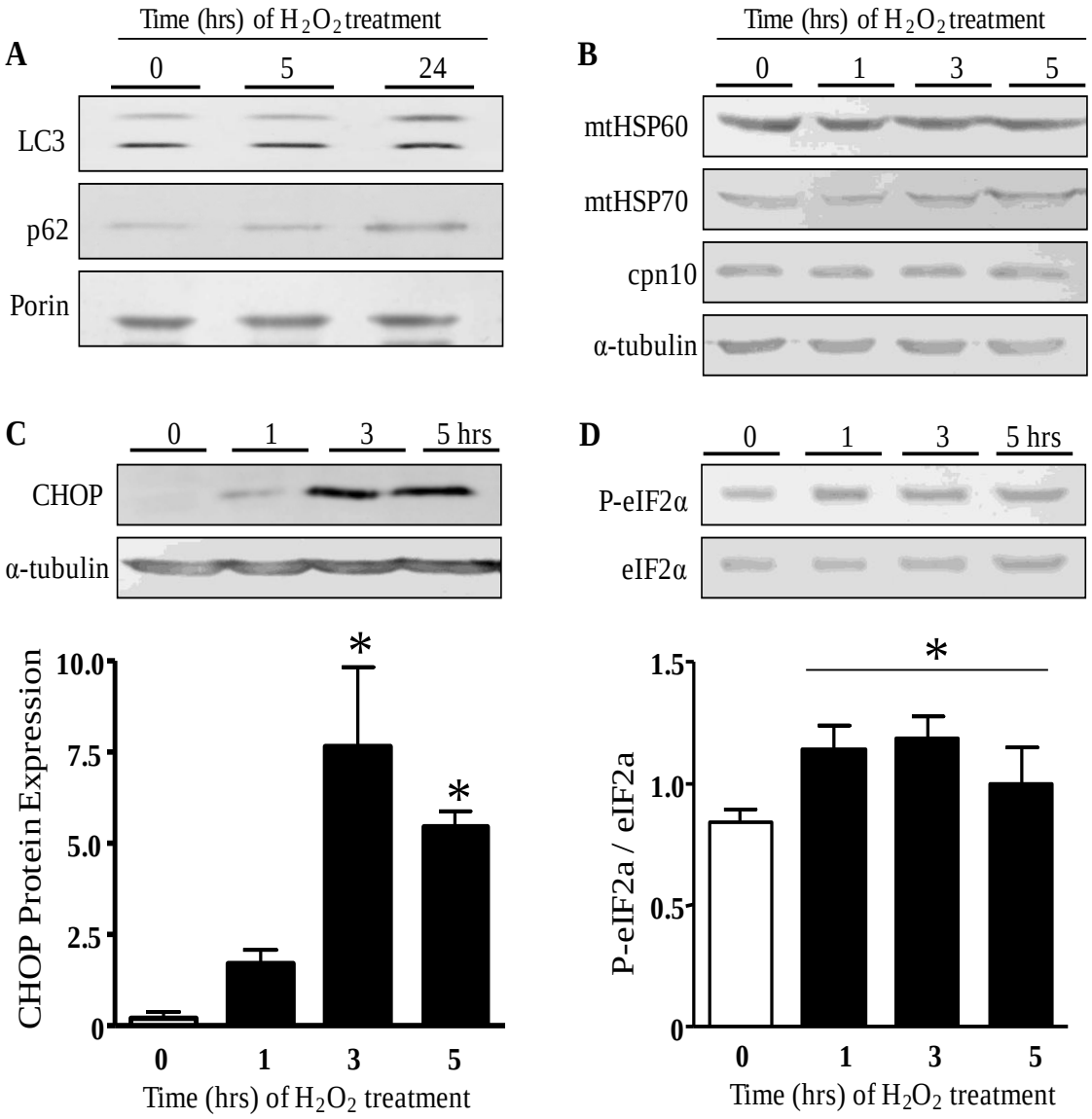
A
Time (hrs) of H2O2 treatment
0
5
24
LC3
p62
Porin
B
Time (hrs) of H2O2 treatment
0
1
3
5
mtHSP60
mtHSP70
cpn10
α-tubulin
C
0
1
3
5 hrs
CHOP
α-tubulin
CHOP Protein Expression
10.0
7.5
5.0
2.5
0
*
*
0
1
3
5
Time (hrs) of H2O2 treatment
D
0
1
3
5 hrs
P-eIF2α
eIF2α
P-eIF2a / eIF2a
1.5
1.0
0.5
0
*
0
1
3
5
Time (hrs) of H2O2 treatment

Figure 5: Acute oxidative stress specifically induces the ER-UPR response, without affecting mt-UPR or mitophagy proteins. A: The effect of oxidative stress on mitophagy. Representative western blots of the mitophagy protein markers, LC3 and p62, were assessed with acute (5 hr) and long exposure (24 hr) with 300μM H_2O_2 in mitochondrial fractions of C_2C_{12} myoblasts. Porin was used as the loading marker. B: Protein expression of markers for the mitochondrial-UPR. Levels of mtHSP60, mtHSP70, and cpn10 protein were determined in whole cell lysates after 300μM H_2O_2 exposure. Tubulin was used as the loading control. C and D: Representative western blots of the ER-UPR markers CHOP, P-eIF2α and eIF2α are displayed above, and graphical quantification is depicted below. Tubulin was unchanged between the conditions and was used as a loading control for CHOP. Values are expressed as averages ± SEM. n=6, $*P < 0.05$ vs. control.

Discussion

Mitochondria are dynamic organelles, continuously undergoing cycles of fission and fusion, resulting in alterations in their morphology and function. However the mechanisms governing these changes have yet to be fully elucidated. In the current study we examined the effects of oxidative stress on mitochondrial motility in myoblasts. To do so, we used live-cell imaging techniques to monitor the dynamics of mitochondria in cells with H_2O_2 exposure.

Hydrogen peroxide, a major contributor to oxidative damage, was shown to induce mitochondrial arrest and time dependent fragmentation. It was observed initially 3 hrs after the addition of H_2O_2, and was further elevated by 5 hrs. The delay observed between the addition of H_2O_2 and the resulting fragmentation suggests the temporal activation of a signaling response, leading to post-translational modifications of Drp1. Three hours of H_2O_2 exposure was associated with a decrease in the phosphorylation status of Drp1, thus retaining Drp1 in the cytosol and preventing its translocation to mitochondria. Since Drp1 protein expression was unaltered in the presence of oxidative stress, these results indicate that Drp1 is activated by cellular signaling, independent of a change in new protein synthesis.

To validate the importance of Drp1 in oxidative stress-induced mitochondrial fragmentation, we inhibited Drp1 dephosphorylation using the selective inhibitor Mdivi-1. Mdivi-1 administration maintained the levels of P-Drp1, concomitantly with an attenuation in H_2O_2-induced mitochondrial fragmentation. We observed comparable decreases in the number of fission and fusion events 5 mins following the addition of

H_2O_2. This is consistent with results seen in endothelial cells, whereby similar reductions in both fission and fusion were observed with H_2O_2 treatment, in a dose and time-dependent manner (21). Equivalent fission/fusion events have also been measured in senescent HUVEC cells (22), and these parallel changes suggest that mitochondrial dynamics (ie. fission and fusion) are coordinately regulated.

Mitochondria were less mobile in cells exposed to oxidative stress. This attenuation in mitochondrial movement was abolished by the addition of NAC, a reactive oxygen species scavenger. Little is known about the factors that contribute to ROS-mediated mitochondrial immobilization. We speculated that reduced mitochondrial motility could be a consequence of changes in cellular energetics. Thus, we evaluated whether oxidative-stress induced mitochondrial fragmentation and reductions in movement coincided with changes in the membrane potential and oxygen consumption of the myoblasts. In corroboration with previous reports (13; 27), our results demonstrate that acute exposure to oxidative stress resulted in fragmentation of the mitochondrial reticulum within 3 hrs of exposure, an effect that was preceded by a reduction in membrane potential and oxygen consumption, beginning after 1 hr of treatment. Twig *et al*. originally demonstrated that the decreased membrane potential in fragmented mitochondria was a prerequisite for mitophagy induction (28). In addition, Chen *et al.* reported that impaired mitochondrial fusion as a result of Mfn1/2 or Opa1 deficiency resulted in lower rates of respiration (10), resembling the effects found in our H_2O_2-treated cells. Fragmented mitochondrial structures have been observed by others, using similar stressful indicators (14; 16; 19; 20; 23). The resulting fragmented organelles

allow for the damaged portions of the mitochondrial network to be isolated from its unaffected parts. Recent findings in HeLa cells have found that mitochondrial fission is required for mitophagy induction under oxidative stress (15). We observed similar results in myoblasts, whereby mitochondrial fragmentation preceded an elevation in mitophagy.

Mitochondrial stress is speculated to result in the activation of at least three cellular responses, including mitophagy, and the mitochondrial- and ER-unfolded protein responses. The unfolded protein responses are thought to occur prior to the initiation of mitophagy. Here, we show that acute exposure to oxidative stress plays a causal role in initiating the ER-UPR without an initial effect on the mt-UPR, indicating the specificity of the UPR. CHOP has been shown to be upregulated by ER stress. CHOP is a transcription factor that binds to and activates the promoter of stress response genes, such as c- Jun N-terminal Kinase (JNK) (18). As such, it is capable of propagating the UPR signal. Additionally, it is also known that CHOP activates the transcription of mtUPR chaperone genes, such as mtHSP60 (24). We observed an increase in the expression of CHOP with oxidative stress, despite no changes in the levels of mtHSP60. Our acute treatment with H_2O_2 may not have been potent enough to elicit the mt-UPR but was sufficient to evoke the ER-UPR, in a time-dependent manner. The ER is responsible for the proper folding of vastly more proteins than that of the mitochondrion, and as a result may be under more stringent control of the protein folding environment.

Figure 6

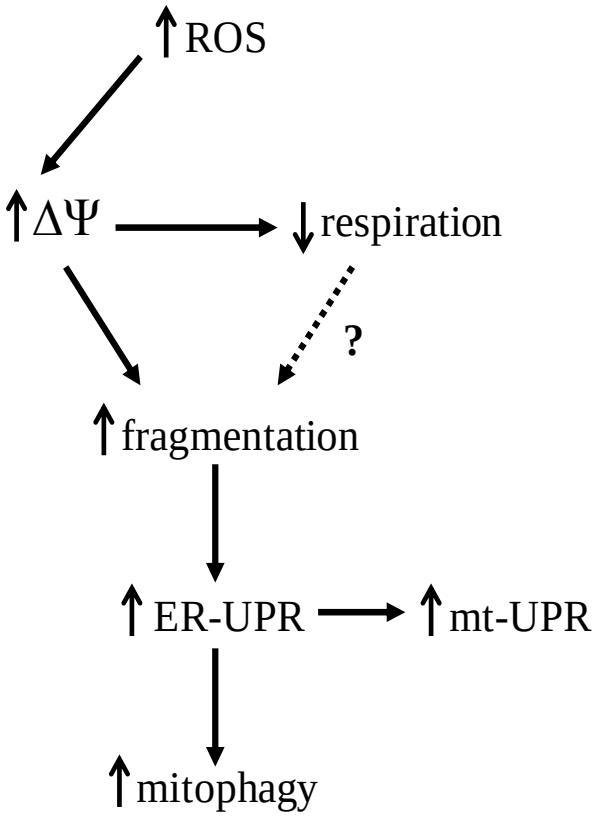

Figure 6: Summary and working hypothesis on the effects of ROS. Increased ROS results in reductions in membrane potential (*left*). Subsequently, the ROS-induced decreases in membrane potential lead to reductions in respiration, as well as enhanced mitochondrial fragmentation, mediated by Drp1. Previous work has shown that inhibition of respiratory components results in enhanced organelle fission. Moreover, these changes in mitochondrial morphology lead to increases in the ER-unfolded protein response, which then activates mitophagy and the upregulation of the mitochondrial-unfolded protein response.

Our findings indicate that elevated ROS lead to a reduction in membrane potential, an event that preceded mitochondrial fragmentation. Subsequently, the ROS-induced decrease in membrane potential lead to reductions in respiration, as well as enhanced mitochondrial fragmentation. It is conceivable that reductions in respiration result in enhanced fission (Fig 6). Previous work has demonstrated that inhibition of electron transport and ATP synthase induces mitochondrial fission and the formation of small, round mitochondria (12). We demonstrated that the mitochondrial fragmentation induced by oxidative stress is mediated, in part, by Drp1. Moreover, these changes in mitochondrial morphology lead to increases in the ER-unfolded protein response, which, when persistent, can lead to mitophagy and the activation of the mitochondrial unfolded protein responses.

In summary, our data indicate that oxidative stress is a vital signaling mechanism in the regulation of mitochondrial morphology and motility in myoblasts. ROS have been implicated in several processes underlying the aging process. Elevated levels of ROS can damage DNA, proteins, and lipids (2), and play a key role in the age-related tissue dysfunction observed. Moreover, during aging an increased incidence of mitochondrial fragmentation has been observed, with a concomitant increase in the expression of mitochondrial fission proteins (19). Our data suggest that enhanced ROS production may underlie the mitochondrial dysfunction and fragmentation observed during the aging process.

Reference List

1. **Adhihetty PJ, O'Leary MF, Chabi B, Wicks KL and Hood DA**. Effect of denervation on mitochondrially mediated apoptosis in skeletal muscle. *J Appl Physiol* 102: 1143-1151, 2007.
2. **Balaban RS, Nemoto S and Finkel T**. Mitochondria, oxidants, and aging. *Cell* 120: 483-495, 2005.
3. **Barsoum MJ, Yuan H, Gerencser AA, Liot G, Kushnareva Y, Graber S, Kovacs I, Lee WD, Waggoner J, Cui J, White AD, Bossy B, Martinou JC, Youle RJ, Lipton SA, Ellisman MH, Perkins GA and Bossy-Wetzel E**. Nitric oxide-induced mitochondrial fission is regulated by dynamin-related GTPases in neurons. *EMBO J* 25: 3900-3911, 2006.
4. **Bleazard W, McCaffery JM, King EJ, Bale S, Mozdy A, Tieu Q, Nunnari J and Shaw JM**. The dynamin-related GTPase Dnm1 regulates mitochondrial fission in yeast. *Nat Cell Biol* 1: 298-304, 1999.
5. **Brooks C, Cho SG, Wang CY, Yang T and Dong Z**. Fragmented mitochondria are sensitized to Bax insertion and activation during apoptosis. *Am J Physiol Cell Physiol* 2010.
6. **Carter HN and Hood DA**. Contractile activity-induced mitochondrial biogenesis and mTORC1. *Am J Physiol Cell Physiol* 303: C540-C547, 2012.
7. **Cassidy-Stone A, Chipuk JE, Ingerman E, Song C, Yoo C, Kuwana T, Kurth MJ, Shaw JT, Hinshaw JE, Green DR and Nunnari J**. Chemical inhibition of the mitochondrial division dynamin reveals its role in Bax/Bak-dependent mitochondrial outer membrane permeabilization. *Dev Cell* 14: 193-204, 2008.
8. **Chabi B, Ljubicic V, Menzies KJ, Huang JH, Saleem A and Hood DA**. Mitochondrial function and apoptotic susceptibility in aging skeletal muscle. *Aging Cell* 7: 2-12, 2008.
9. **Chang CR and Blackstone C**. Cyclic AMP-dependent protein kinase phosphorylation of Drp1 regulates its GTPase activity and mitochondrial morphology. *J Biol Chem* 282: 21583-21587, 2007.
10. **Chen H, Chomyn A and Chan DC**. Disruption of fusion results in mitochondrial heterogeneity and dysfunction. *J Biol Chem* 280: 26185-26192, 2005.
11. **Cribbs JT and Strack S**. Reversible phosphorylation of Drp1 by cyclic AMP-dependent protein kinase and calcineurin regulates mitochondrial fission and cell death. *EMBO Rep* 8: 939-944, 2007.
12. **De Vos KJ, Allan VJ, Grierson AJ and Sheetz MP**. Mitochondrial function and actin regulate dynamin-related protein 1-dependent mitochondrial fission. *Curr Biol* 15: 678-683, 2005.
13. **Fan X, Hussien R and Brooks GA**. H2O2-induced mitochondrial fragmentation in C2C12 myocytes. *Free Radic Biol Med* 49: 1646-1654, 2010.
14. **Fannjiang Y, Cheng WC, Lee SJ, Qi B, Pevsner J, McCaffery JM, Hill RB, Basanez G and Hardwick JM**. Mitochondrial fission proteins regulate programmed cell death in yeast. *Genes Dev* 18: 2785-2797, 2004.

15. **Frank M, Duvezin-Caubet S, Koob S, Occhipinti A, Jagasia R, Petcherski A, Ruonala MO, Priault M, Salin B and Reichert AS**. Mitophagy is triggered by mild oxidative stress in a mitochondrial fission dependent manner. *Biochim Biophys Acta* 1823: 2297-2310, 2012.
16. **Frank S, Gaume B, Bergmann-Leitner ES, Leitner WW, Robert EG, Catez F, Smith CL and Youle RJ**. The role of dynamin-related protein 1, a mediator of mitochondrial fission, in apoptosis. *Dev Cell* 1: 515-525, 2001.
17. **Frezza C, Cipolat S and Scorrano L**. Organelle isolation: functional mitochondria from mouse liver, muscle and cultured fibroblasts. *Nat Protoc* 2: 287-295, 2007.
18. **Horibe T and Hoogenraad NJ**. The chop gene contains an element for the positive regulation of the mitochondrial unfolded protein response. *PLoS One* 2: e835, 2007.
19. **Iqbal S, Ostojic O, Singh K, Joseph AM and Hood DA**. Expression of mitochondrial fission and fusion regulatory proteins in skeletal muscle during chronic use and disuse. *Muscle Nerve* 48: 963-970, 2013.
20. **Jagasia R, Grote P, Westermann B and Conradt B**. DRP-1-mediated mitochondrial fragmentation during EGL-1-induced cell death in C. elegans. *Nature* 433: 754-760, 2005.
21. **Jendrach M, Mai S, Pohl S, Voth M and Bereiter-Hahn J**. Short- and long-term alterations of mitochondrial morphology, dynamics and mtDNA after transient oxidative stress. *Mitochondrion* 8: 293-304, 2008.
22. **Jendrach M, Pohl S, Voth M, Kowald A, Hammerstein P and Bereiter-Hahn J**. Morpho-dynamic changes of mitochondria during ageing of human endothelial cells. *Mech Ageing Dev* 126: 813-821, 2005.
23. **Lee YJ, Jeong SY, Karbowski M, Smith CL and Youle RJ**. Roles of the mammalian mitochondrial fission and fusion mediators Fis1, Drp1, and Opa1 in apoptosis. *Mol Biol Cell* 15: 5001-5011, 2004.
24. **Pellegrino MW, Nargund AM and Haynes CM**. Signaling the mitochondrial unfolded protein response. *Biochim Biophys Acta* 1833: 410-416, 2013.
25. **Smirnova E, Shurland DL, Ryazantsev SN and van der Bliek AM**. A human dynamin-related protein controls the distribution of mitochondria. *J Cell Biol* 143: 351-358, 1998.
26. **Strack S and Cribbs JT**. Allosteric modulation of Drp1 mechanoenzyme assembly and mitochondrial fission by the variable domain. *J Biol Chem* 287: 10990-11001, 2012.
27. **Takeyama N, Miki S, Hirakawa A and Tanaka T**. Role of the mitochondrial permeability transition and cytochrome C release in hydrogen peroxide-induced apoptosis. *Exp Cell Res* 274: 16-24, 2002.
28. **Twig G, Elorza A, Molina AJ, Mohamed H, Wikstrom JD, Walzer G, Stiles L, Haigh SE, Katz S, Las G, Alroy J, Wu M, Py BF, Yuan J, Deeney JT, Corkey BE and Shirihai OS**. Fission and selective fusion govern mitochondrial segregation and elimination by autophagy. *EMBO J* 27: 433-446, 2008.
29. **Zuchner S, Mersiyanova IV, Muglia M, Bissar-Tadmouri N, Rochelle J, Dadali EL, Zappia M, Nelis E, Patitucci A, Senderek J, Parman Y, Evgrafov O, Jonghe PD, Takahashi Y, Tsuji S, Pericak-Vance MA, Quattrone A, Battaloglu**

E, Polyakov AV, Timmerman V, Schroder JM and Vance JM. Mutations in the mitochondrial GTPase mitofusin 2 cause Charcot-Marie-Tooth neuropathy type 2A. *Nat Genet* 36: 449-451, 2004.

CHAPTER 5:

DISSERTATION SUMMARY

FUTURE WORK

DISSERTATION SUMMARY

Classic textbook depictions of mitochondria portray these organelles to be static bean-shaped structures. However the mitochondrial population is quite heterogeneous, and cells they can form small individual organelles or extended reticula throughout muscle. This morphological plasticity is controlled by fission and opposing fusion events. Our laboratory and others (3) have found that chronic muscle use affects the morphology of mitochondria, such that as the mitochondrial content increases, so too does the occurrence of reticular structures. In contrast, chronic muscle disuse, induced through denervation, has been shown to reduce mitochondrial content, and organelle size (1; 4). Similar results have been observed with age, whereby mitochondrial volume density decreases with age without a change in organelle number (5), reflecting greater mitochondrial fragmentation. This implies that mitochondrial fission and fusion machinery components are involved in regulating the architecture of the organelle during muscle disuse. However the influence that oxidative capacity has on the expression of these proteins has yet to be thoroughly investigated. In Manuscript #1 we examined the expression of the proteins that regulate mitochondrial morphology and electron micrographs of their structures during conditions of altered oxidative capacity. We hypothesized that chronic activity would induce changes in the expression of mitochondrial fission and fusion machineries, such that fusion protein expression would outweigh the expression of fission machinery components; conversely we speculated that chronic disuse would favour the expression of fission protein components. We first

assessed the steady state expression of mitochondrial morphology proteins within fibre types of different oxidative capacities. We observed that the FTR and STR fibres possessed the highest expression of both fission and fusion proteins, compared to FTW fibres, suggesting more rapid mitochondrial turnover in highly oxidative fibres. To evoke mitochondrial biogenesis and to assess the effects of muscle use, animals underwent chronic contractile activity. To validate that mitochondrial biogenesis occurred with CCA we assessed COX activity, a marker of mitochondrial content. With CCA, mitochondrial content increased, and the organelles became reticular in size, along with concomitant increases in the fusion proteins. Next, we induced muscle disuse through denervation for 7-days. We observed fragmented mitochondria following denervation, along with significant decreases in mitochondrial content and the expression of fusion proteins. To elucidate the role that aging has on mitochondrial morphology, young (5 month) and aged (35 month) Fisher 344 Brown Norway rats were used. Aged animals also possessed smaller, fragmented mitochondria. However, the expression pattern of morphology machinery differed between aging and denervation, since aged animals displayed an increased expression of the fission proteins. This study provides us with an understanding of how mitochondrial morphology protein expression varies in response to altered organelle biogenesis.

We next examined the regulation of mitochondrial movement within muscle cells for Manuscript #2. Our focus was to determine which cytoskeletal elements were responsible for mitochondrial movement within myoblasts. A live-cell imaging approach was used, where we fluorescently labelled mitochondria, allowing us to visualize their

movement within myoblasts. The cells were exposed to microtubule and actin stabilizing and destabilizing agents in order to establish which cytoskeletal element is primarily responsible for mitochondrial movement within skeletal muscle cells. We found that microtubule disruption resulted in the greatest decreases to mitochondrial speed and path length. We next targeted the microtubule motor proteins, Kif5B and dynein, and reduced their protein expressions. Down-regulation of Kif5B and dynein resulted in similar decreases in the average speed of mitochondrial movements, as well as in the total path length travelled by the organelles. In neurons, displacement of mitochondria is regulated by calcium, whereby mitochondrial movements are inhibited through the microtubule motor protein adapter, Milton. We investigated the influence that Milton has on calcium-induced mitochondrial movement. We observed decreases in mitochondrial speed of movement under high calcium conditions, and this effect was negated in cells pre-treated with Milton siRNA, suggesting that Milton is involved in mediating mitochondrial arrest in the presence of Ca^{2+} in muscle cells. This study provides an understanding of mitochondrial movements and the signalling events that regulate their dynamics, allowing us to elucidate the underlying basis for organelle interactions.

Our laboratory has demonstrated that oxidative stress increases under conditions of chronic muscle disuse (1) and aging (2). Our purpose for Manuscript #3 was to determine the influence that oxidative stress would have on mitochondrial dynamics and to establish the interplay between mitochondrial morphology and stress responses during conditions of oxidative stress. Once again we used live-cell imaging techniques to visual mitochondria over time. We found that oxidative stress halts mitochondrial movement

and induces mitochondrial fragmentation in myoblasts. The observed oxidative stress-induced mitochondrial fragmentation is mediated by Drp1. Moreover, we demonstrated that unfolded protein responses are activated prior to the initiation of mitophagy during oxidative stress. This study determined that oxidative stress is a vital signalling mechanism in the regulation of mitochondrial morphology and motility in myoblasts.

The overall goal of this Dissertation was to understand the molecular signaling and the proteins involved in mediating mitochondrial dynamics in skeletal muscle. Both *in vivo* and cell culture studies were employed to address this goal. Specifically, these Manuscripts will 1) further our understanding of the role of mitochondrial morphology during conditions altered organelle biogenesis, 2) provide insight into the cytoskeletal regulation of the mitochondrial movement in muscle cells, and 3) elucidate some of the signalling mechanisms governing mitochondrial movement. Further knowledge into these areas will help us understand the molecular basis of mitochondrial dynamics (ie. fission, fusion, and movement) during conditions of increased (eg. exercise) or decreased (eg. aging) organelle biogenesis.

FUTURE WORK

1. Does AMP-activated kinase (AMPK) signaling alter mitochondrial dynamics in muscle cells?

Major signaling pathways that regulate mitochondrial content in skeletal muscle include AMPK, calcium, and ROS. This Dissertation examined the effects of calcium and ROS signaling on mitochondrial dynamics, however the influence of AMPK has yet to be explored. The activation of AMPK could be achieved by the addition of AICAR to C2C12 myoblasts. To determine whether AICAR successfully activated AMPK, the phosphorylation of AMPK at the Thr^{172} and downstream targets (i.e. ACC) could be assessed. Live-cell imaging techniques could be used to monitor the movement of mitochondria in order to elucidate whether organelle motility is affected by AMPK activation.

2. Are mitochondrial dynamics altered during myoblast differentiation?

Mitochondria undergo drastic alterations during myogenesis to meet the increased requirements of the cell, including the enhanced level of energy consumption by myotubes. The process of differentiation, from myoblast to myotubes, involves phenotypic modification not only in the whole cell, but also in their mitochondria. It is known that mitochondria form a dense network when they form myotubes, but their motility has never been analyzed.

The time periods at which differentiation could be examined are the myoblast, early, and late myotube formation phases. These time periods correspond to

approximately day 0, 3, and 5 of differentiation. Whole cell lysates would be collected at the same time periods to ensure that mitochondrial biogenesis takes place, using cytochrome c oxidase activity as an indicator. In addition, Mfn2, Opa1, Fis1 and Drp1 protein expression levels could be assessed at the three periods that we identified. This would allow us to relate mitochondrial movements with the expression of proteins involved in organelle dynamics during mitochondrial biogenesis.

3. Can ROS-induced mitochondrial fragmentation be offset by Drp1 inhibition under conditions of high ROS production?

ROS have been implicated in several processes underlying the aging process. Moreover, during aging an increased incidence of mitochondrial fragmentation has been observed, with a concomitant increase in the expression of mitochondrial fission proteins. Thus, by inhibiting a key mitochondrial morphology regulator, Drp1, we propose that fragmentation would be reduced and the mitochondrial network can be maintained.

We would examine this question by pre-injecting aged animals with mDivi1, a Drp1 inhibitor, and determine the changes to mitochondrial morphology by measuring mitochondrial morphology protein expression and using electron microscopy. Moreover, the quality of the organelle could be elucidated by measuring COX activity and respiration in mitochondria.

CHAPTER 6

APPENDICES

APPENDIX A:
1.0 Additional data

APPENDIX B:
2.0 Laboratory Methods

APPENDIX C:
3.0 Additional Contributions

APPENDIX A
1.0 ADDITIONAL DATA

Introduction

Mitochondral morphologies vary from interconnected networks to separate punctate structures. Chronic muscle use has previously been shown to increase the mitochondrial network (2), whereas chronic disuse induced through denervation has been shown to reduce mitochondrial size (1; 3). Similar results have been observed with age, whereby mitochondrial volume density decreases with age (4). We sought to investigate whether the proteins that regulate mitochondrial morphologies where altered as a result of chronic muscle use and disuse within whole muscle samples and within mitochondrial subfractions.

Furthermore, we were also interested in the effects of p53 ablation on mitochondrial morphology, since compromised levels of p53 have previously been shown to result in an irregular mitochondrial architecture (5). Mitochondrial morphology is closely integrated with mitophagy. We sought to determine the role of p53 in regulating mitophagy within skeletal muscle.

Finally, we developed an assay that allowed us to examine the movement of organelles within myoblasts, in particular mitochondria, lysosomes, and nuclei. Organelles transport was analyzed relative to their size, to assess whether movement is dependent on organelle area.

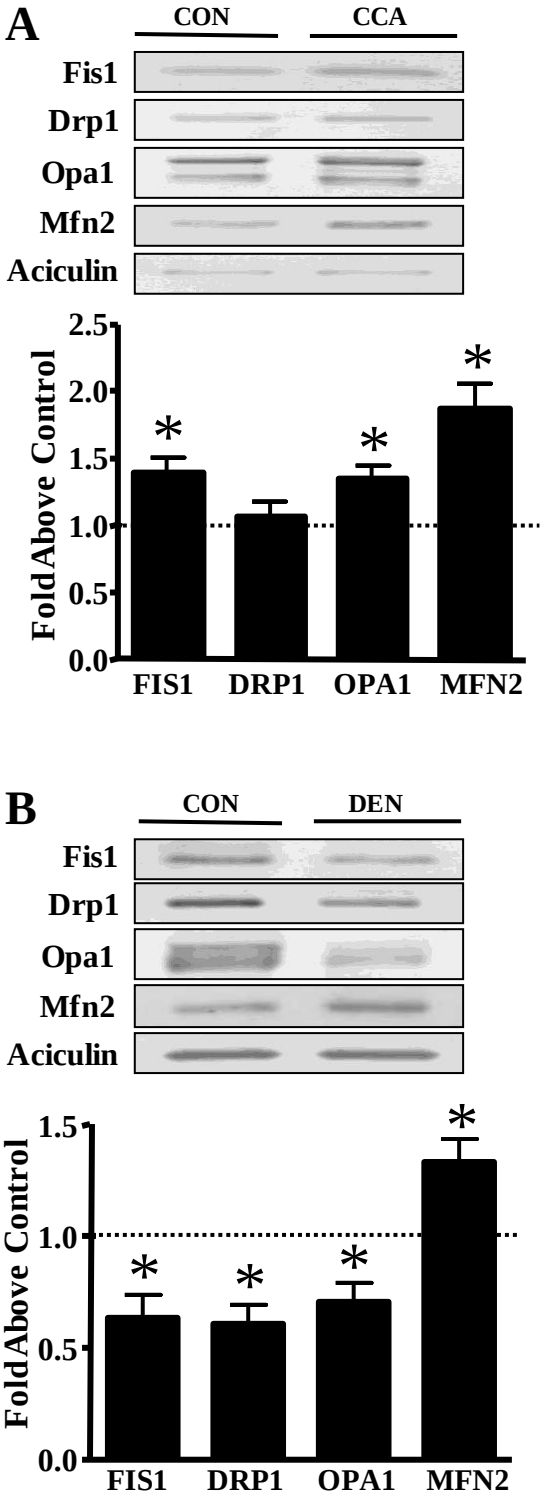
A
CON
CCA
Fis1
Drp1
Opa1
Mfn2
Aciculin
Fold Above Control
2.5
2.0
1.5
1.0
0.5
0.0
*
*
*
FIS1
DRP1
OPA1
MFN2
B
CON
DEN
Fis1
Drp1
Opa1
Mfn2
Aciculin
Fold Above Control
1.5
1.0
0.5
0.0
*
*
*
*
FIS1
DRP1
OPA1
MFN2

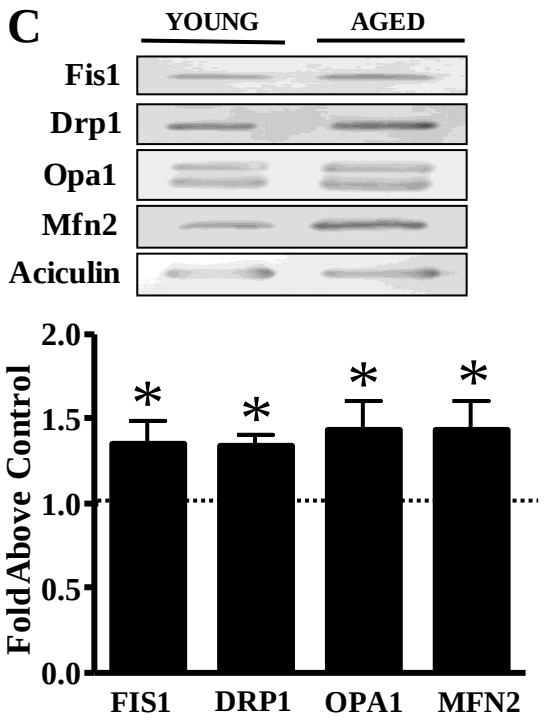

Figure 1: The effect of chronic contractile activity (CCA), denervation (DEN), and aging on mitochondrial morphology proteins. A: After 7-days of CCA the tibialis anterior muscle was extracted from the stimulated and control limbs, and used for Western blotting (n = 8). B) Mitochondrial morphology protein levels in CON and DEN whole muscle were assessed following 7-days of denervation (n = 8-9). C: Fission and fusion morphology protein expression in young and aged muscle were measured. Young (5 month) and aged (35 month) animals were used. Representative images of Fis1, Drp1, Opa1, Mfn2 protein content (*top*), with graphical quantification (*bottom*, n = 6). T-tests were used for statistical analyses (*P < 0.05). Expression of the morphology proteins was corrected using the loading control Aciculin, and expressed as fold over young.

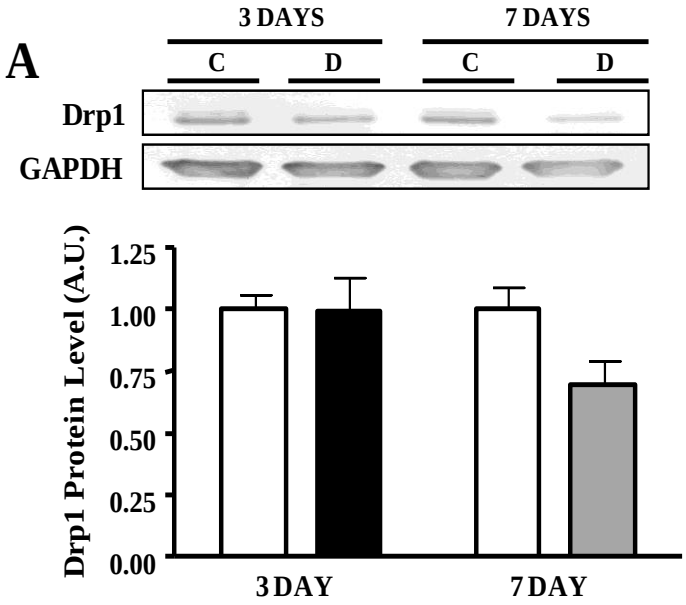
A
3 DAYS
7 DAYS
C
D
C
D
Drp1
GAPDH
Drp1 Protein Level (A.U.)
1.25
1.00
0.75
0.50
0.25
0.00
3 DAY
7 DAY

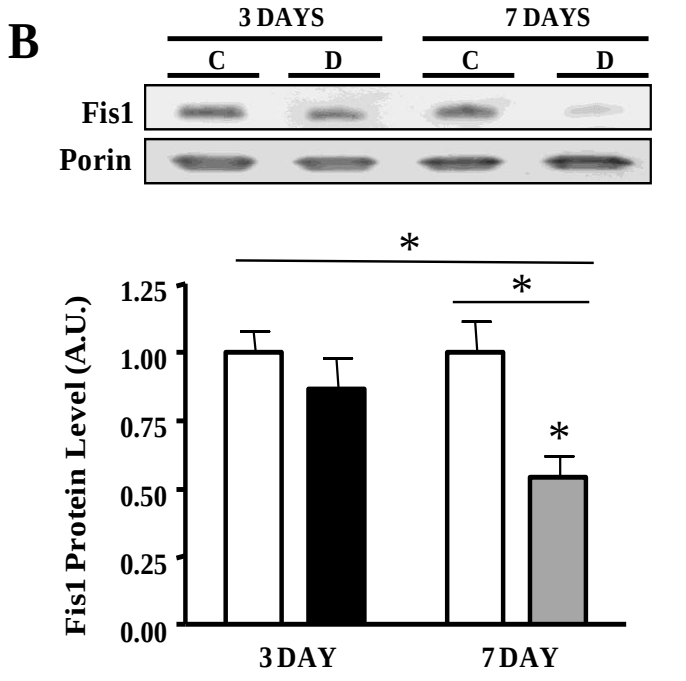
B
3 DAYS
7 DAYS
C
D
C
D
Fis1
Porin
*
*
*
Fis1 Protein Level (A.U.)
1.25
1.00
0.75
0.50
0.25
0.00
3 DAY
7 DAY

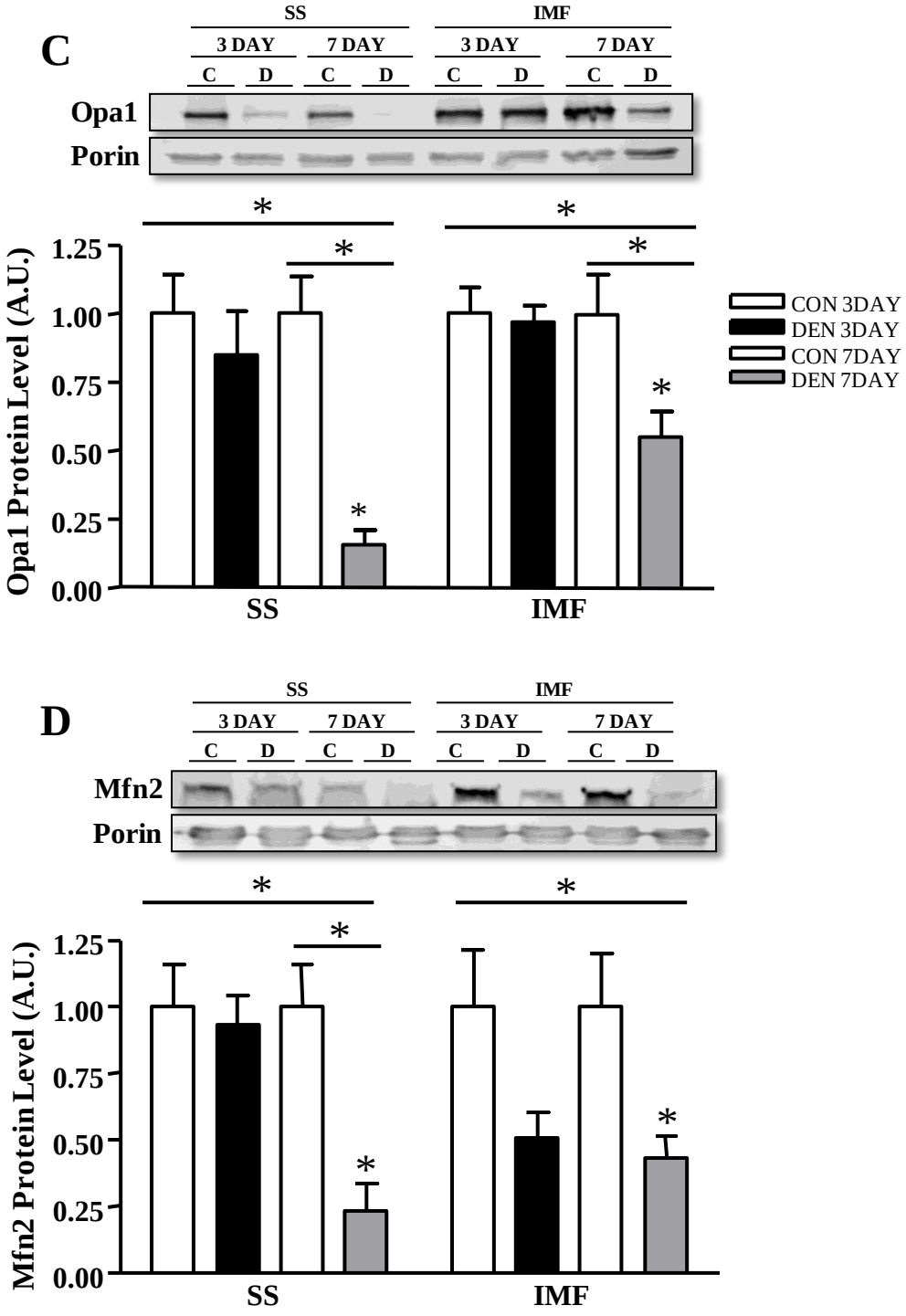
C
SS
IMF
3 DAY
7 DAY
3 DAY
7 DAY
C
D
C
D
C
D
C
D
Opa1
Porin
Opa1 Protein Level (A.U.)
1.25
1.00
0.75
0.50
0.25
0.00
SS
IMF
CON 3DAY
DEN 3DAY
CON 7DAY
DEN 7DAY
D
Mfn2
Porin
Mfn2 Protein Level (A.U.)

Figure 2: Alterations in mitochondrial morphology proteins with denervation at 3- and 7-days. Mitochondrial morphology protein levels in CON and DEN mitochondrial fractions measured for A) Drp1, B) Fis1, C) Opa1 and D) Mfn2 morphology protein expression. Representative images of Fis1, Drp1, Opa1, Mfn2 protein content (*top*), with graphical quantification (*bottom*, n = 8-9). 1-way ANOVAs were used for statistical analyses (*$P < 0.05$). Expression of the morphology proteins was corrected using the loading control Porin, and expressed as fold over control.

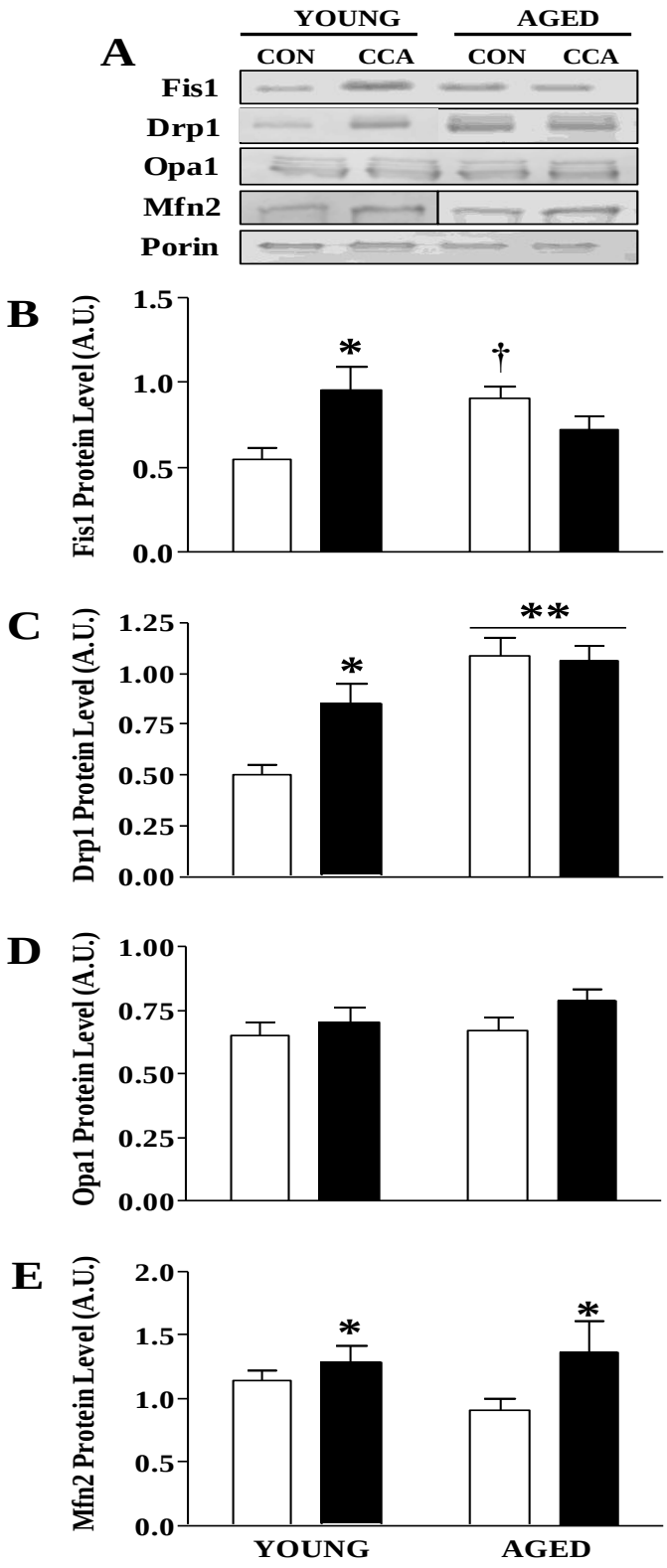
A
YOUNG
AGED
CON
CCA
CON
CCA
Fis1
Drp1
Opa1
Mfn2
Porin
B
Fis1 Protein Level (A.U.)
1.5
1.0
0.5
0.0
*
†
C
Drp1 Protein Level (A.U.)
1.25
1.00
0.75
0.50
0.25
0.00
*
**
D
Opa1 Protein Level (A.U.)
1.00
0.75
0.50
0.25
0.00
E
Mfn2 Protein Level (A.U.)
2.0
1.5
1.0
0.5
0.0
*
*
YOUNG
AGED

Figure 3: Alterations in mitochondrial morphology proteins with chronic contractile activity and aging. Young (5 month) and aged (35 month) animals were used. After 7-days of CCA the tibialis anterior muscle was extracted from the stimulated and control limbs, and used for Western blotting. A) Fis1, B) Drp1, C) Opa1, and D) Mfn2 protein levels were determined in chronically stimulated whole muscle fractions (*n* = 8-13). Representative Western blots are shown for each indicated protein and its respective loading controls, with graphical quantification depicted below. Expression of the morphology proteins was corrected using the loading control Porin. One-way ANOVA tests were used for statistical analyses (*$P < 0.05$).

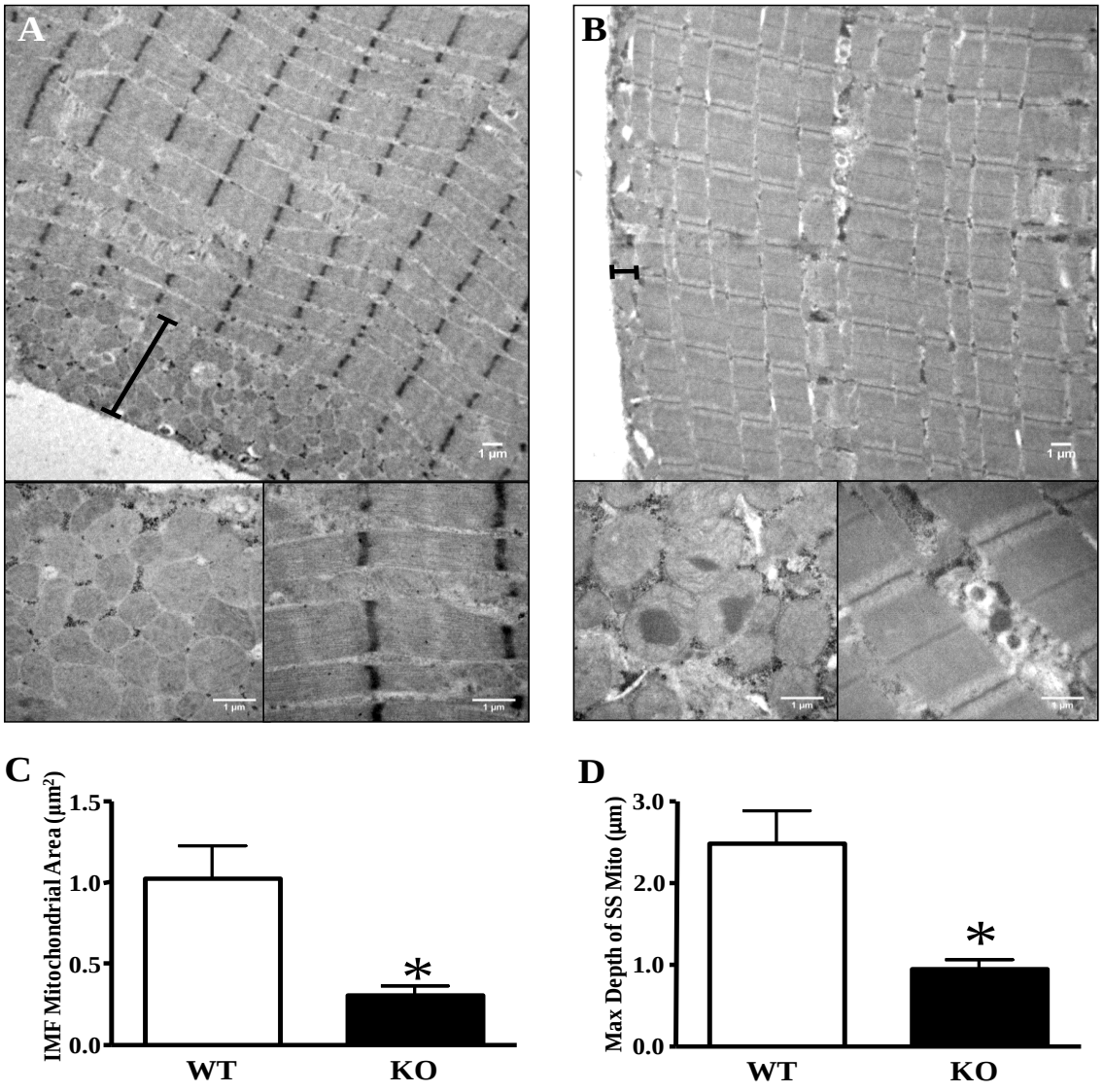

Figure 4: Electron micrographs of skeletal muscle from A) wild type (WT) and B) p53 knock out (p53 KO) mice. Morphological alterations in mitochondria are visualized by the representative images taken at a magnification of 7000X and 30, 000X (*below*). SS mitochondria are shown in the left panel, and IMF mitochondria appear to the right. C) Quantification of the maximal depth of the SS layer and D) the total area occupied by IMF mitochondria in 4 μm^2 area (n=4-7; *$P < 0.05$ vs WT).

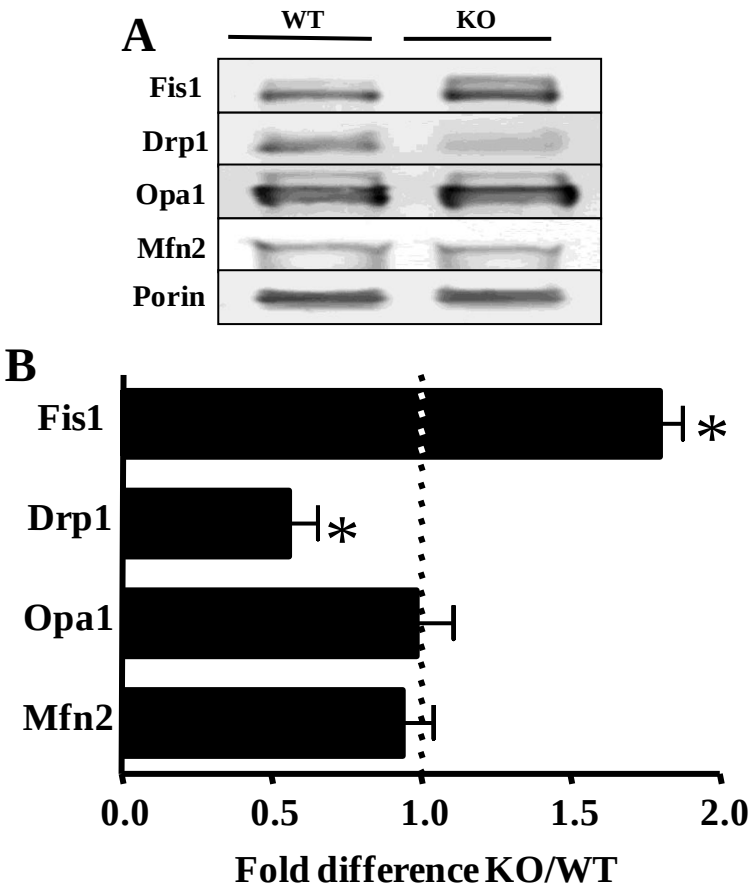

Figure 5: Fission and fusion morphology protein expression in WT and KO p53 muscle. A) Representative images of Fis1, Drp1, Opa1, Mfn2 protein content (*top*), and B) graphical quantification (*bottom*) expressed as fold over WT in SS mitochondrial or cytosolic fractions. Fis1, Opa1 and Mfn2 were determined using SS mitochondrial fractions, and corrected using the loading control Portin, whereas Drp1 was assessed in cytosolic fractions and corrected using GAPDH (n=4, *P < 0.05 vs WT).

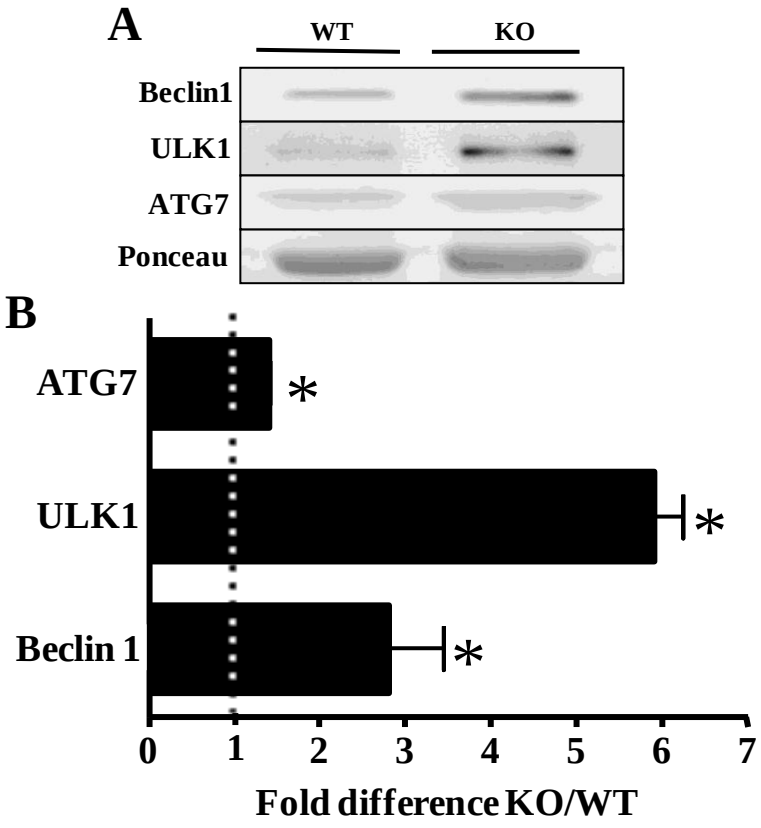

Figure 6: Expression of key autophagy and lysosomal markers from skeletal muscle of WT and KO p53 animals. A) Representative Western blots are shown for Beclin1, ULK1 and ATG7 from cytosolic fractions. B) Graphical quantification of each indicated protein depicted below (n=4, *P < 0.05 vs WT). Expression of Beclin1, ULK1, and ATG7 was corrected using the Poneau loading control and expressed as fold over WT.

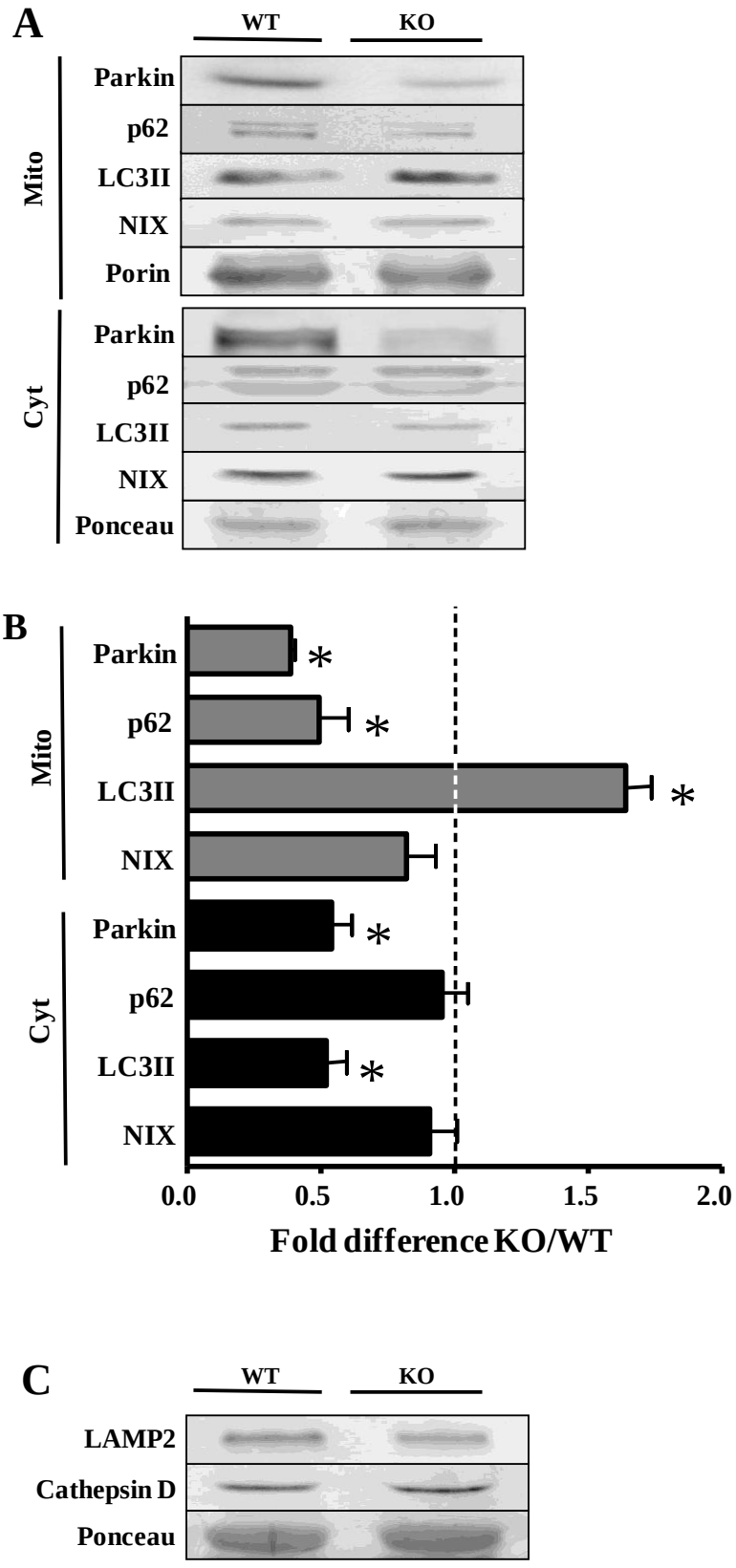
A
WT
KO
Mito
Parkin
p62
LC3II
NIX
Porin
Cyt
Parkin
p62
LC3II
NIX
Ponceau
B
Mito
Parkin
p62
LC3II
NIX
Cyt
Parkin
p62
LC3II
NIX
0.0
0.5
1.0
1.5
2.0
Fold difference KO/WT
C
WT
KO
LAMP2
Cathepsin D
Ponceau

Figure 7: Effects of p53 depletion on mitophagy. Parkin, p62, LC3II and NIX were assessed by immunoblotting. A) Representative Western blots are shown for Parkin, p62, LC3II, and NIX from mitochondrial and cytosolic subfractions. Samples were corrected for loading using the ponceau and Porin, for cytosolic and SS mitochondrial fractions, respectively. B) Graphical quantification of each indicated protein depicted below (n=4–8, $*P < 0.05$ vs WT). C) Representative Western blots are shown for LAMP2 and Cathepsin D from cytosolic fractions.

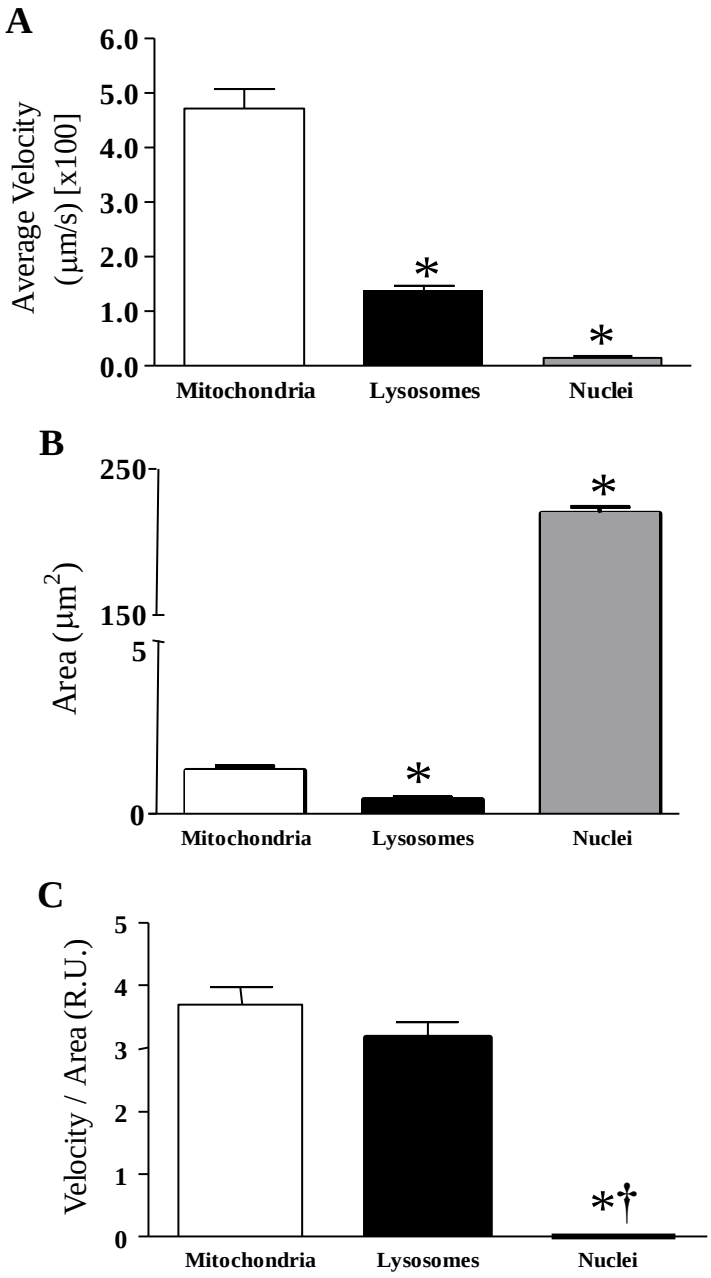

Figure 8: Organelle movement in C2C12 cells. A) The average velocity, B) area, and C) velocity/area of mitochondria, lysosomes and nuclei. * significantly different from mitochondria, from 7 separate experiments.

References

1. **Adhihetty PJ, O'Leary MF, Chabi B, Wicks KL and Hood DA.** Effects of denervation on mitochondrially mediated apoptosis in skeletal muscle. *J Appl Physiol* 102: 1143-1151, 2007.

2. **Kirkwood SP, Packer L and Brooks GA**. Effects of endurance training on a mitochondrial reticulum in limb skeletal muscle. *Arch Biochem Biophs* 255: 80-88, 1987.

3. **Miledi R and Slater CR**. Some mitochondrial changes in denervated muscle. *J Cell Sci* 3: 49-54, 1968.

4. **Orlander J, Kiessling KH, Larsson L, Karlsson J and Aniansson A.** Skeletal muscle metabolism and ultrastructure in relation to age in sedentary men. *Acta Phyiol Scand* 104: 249-261, 1978.

5. **Saleem A, Adhihetty PJ and Hood DA.** Role of p53 in mitochondrial biogenesis and apoptosis in skeletal muscle. *Physiol Genomics* 37: 58-66, 2009.

APPENDIX B
2.0 LABORATORY METHODS

2.1 MITOCHONDRIAL ISOLATION FROM SKELETAL MUSCLE

References: Cogswell et al. Am J Physiol, 1993, 264: C388-C389
Krieger et al. J Appl Physiol, 1980, 48: 23-28

Reagents

All buffers are set to pH 7.4 and stored at 4 °C

- Buffer 1
  - 100 mM KCl
  - 5 mM MgSO4
  - 5 mM EDTA
  - 50 mM Tris base

- Buffer 1 + ATP
  - Add 1 mM ATP to Buffer 1

- Buffer 2
  - 100 mM KCl
  - 5 mM MgSO4
  - 5 mM EGTA
  - 50 mM Tris base
  - 1 mM ATP

- Resuspension medium
  - 100 mM KCl
  - 10 mM MOPS
  - 0.2% BSA

- Nagarse protease (Sigma, P-4789)
  - 10 mg/ml in Buffer 2
  - Make fresh for each isolation, keep on ice

Procedure

1. Remove the tibialis anterior (TA) muscle from the rat, and put it in a beaker containing 5 ml Buffer 1, on ice immediately.
2. Place TA on a watch glass that is also on ice and trim away fat and connective tissue. Proceed to thoroughly mince the muscle sample with forceps and scissors, until no large pieces are remaining.
3. Place the minced tissue in a plastic centrifuge tube and record the exact weight of tissue.
4. Add a 10-fold dilution of Buffer 1 + ATP to the tube.
5. Homogenize the samples using the Ultra-Turrax polytron with 40% power output and 10 s exposure time. Rinse the shaft with 0.5 ml of Buffer 1 + ATP to help minimize sample loss.
6. Using a Beckman JA 25.50 rotor, spin the homogenate at a centrifuge setting of 800 g for 10 min. This step divides the IMF and SS mitochondrial subfractions. The supernate will contain the SS mitochondria and the pellet will contain the IMF mitochondria.

SS mitochondrial isolation:

7. Filter the supernate through a single layer of cheesecloth into a second set of 50 ml plastic centrifuge tubes.
8. Spin tubes at 9000 g for 10 min. Upon completion of the spin discard the supernate and gently resuspend the pellet in 3.5 ml of Buffer 1 + ATP. Since the mitochondria are easily damaged, it is important that the resuspension of the pellet is done carefully.
9. Repeat the centifugation of the previous step (9000 g for 10 min) and discard the supernate.
10. Resuspend the pellet in 200 µl of Resuspension medium, being gentle so as to prevent damage to the SS mitochondria. Some extra time is needed during this final resuspension to ensure the SS pellet is completely resuspended.
11. Keep the SS samples on ice while proceeding to islolate the IMF subfraction.

IMF mitochondrial isolation:

7. Gently resuspend the pellet (from step 6) in a 10-fold dilution of Buffer 1 + ATP using a teflon pestle.
8. Using the Ultra-Turrax polytron set at 40% power output, polytron the resuspended pellet for 10 s. Rinse the shaft with 0.5 ml of Buffer 1 + ATP.
9. Spin at 800 g for 10 min and discard the resulting supernate.
10. Resuspend the pellet in a 10-fold dilution of Buffer 2 using a teflon pestle.
11. Add the appropriate amount of nagarse. The calculation for the appropriate volume is 0.025 ml/g of tissue. Mix gently and let stand exactly 5 min.
12. Dilute the nagarse by adding 20 ml of Buffer 2.
13. Spin the diluted samples at 5000 g for 5 min and discard the resulting supernate.
14. Resuspend the pellet in a 10-fold dilution of Buffer 2. Gentle resuspension is with a teflon pestle.
15. Spin the samples at 800 g for 10 min. Upon the completion of the spin, the supernate is poured into another set of 50 ml plastic tubes (on ice), and the pellet is discarded.
16. Spin the supernate at 9000 g for 10 min. The supernate is discarded and the pellet is resuspended in 3.5 ml of Buffer 2.
17. Spin samples at 9000 g for 10 min and discard the supernate.
18. Gently resuspend the pellet in 300 µl of Resuspension medium.

2.2 BRADFORD PROTEIN ASSAY

References: Bradford M.M et al. Anal Biochem, 1876, 72:248-254

PROCEDURE

Reagents

- Extraction buffer
  - 100 mM Na/K PO_4
  - 2 mM EDTA
  - pH to 7.2

- 5 X Bradford dye
  - 250 ml 85% Phosphoric acid
  - 250 ml 100% Ethanol
  - 500 ml ddH_2O
  - 0.235 g Coomassie Brilliant Blue G250

- Bovine Serum Albumin (BSA)
  - 2 mg/ml in ddH_2O

Procedure

1. Prepare the test tubes allowing for duplicates of each sample.
2. Add 95 µl of extraction buffer to each tube.
3. Add 5 µl of sample to each tube containing the extraction buffer.
4. To generate the standard curve, add the following volumes (in µl) of extraction buffer: BSA, each in separate tubes – 100:0, 95:5, 90:10, 85:15, 80:20, 75:25.
5. Pipette 5 ml of 1 X Bradford reagent into each tube and mix by gentle vortexing.
6. In duplicate, add 0.2 ml of each test tube to 96 well plate wells.
7. Measure absorbance of wells at 595 nm with a microplate reader.
8. Calculate the protein concentration of each sample using the standard curve.

2.3 SDS Polyacrylamide Gel Electrophoresis (SDS-PAGE)

PROCEDURE

Prepare electrophoresis rack:

1) Clean glass plates thoroughly with soap followed by acetone, then distilled water.
2) Dry carefully with paper towel without touching surface.
3) Clean combs and glass plates
4) Assemble glass plates as shown:
5) Check the seal by adding a small volume of dH_2O then pour this off and let dry.

Prepare Separating Gels:

A. Mini PROTEAN 3 BIO-RAD SYSTEM

	8 %	10 %	12 %	15 %	18 %
Acrylamide	2.7 ml	3.3 ml	4.0 ml	5.0 ml	6.0 ml
Water	4.1 ml	3.5 ml	2.8 mL	1.8 ml	0.8 ml
Under Tris	3.0 ml	3.0 ml	3.0 ml	3.0 ml	3.0 ml
SDS	100 µl	100 µl	100 µl	100 µl	100 µl
APS	100 µl	100 µl	100 µl	100 µl	100 µl
TEMED	10 µl	10 µl	10 µl	10 µl	10 µl

B. Mix the contents of the separating gel as described above without adding APS or TEMED, stir.
C. Add APS and TEMED, stir.
D. Slowly pour the entire volume from the beaker into the slot between the plates, keeping the plates tilted on an angle to prevent bubbles from forming.
E. Add *tert*-Amyl alcohol to cover the top of the gel.
F. Allow ~30 min for polymerization.
G. Remove *tert*-Amyl alcohol by pouring it off quickly, and remove the remainder with a kimwipe. Rinse thoroughly with dH_20.

Prepare stacking gel:

1)

	Mini Gel (Volume/Gel)
Acrylamide	500 µl
Above Tris buffer	625 µl
ddH_2O	3.75 ml
SDS	50 µl
APS	50 µl
TEMED	7.5 µl

2) Mix the contents of the stacking gel without adding APS or TEMED, stir.
3) Add APS and TEMED, stir.
4) Using a pasteur pipette slowly pour the entire volume from the beaker into the side of the plates.
5) Add combs.
6) Allow approximately 30 min for polymerization.

Prepare samples:

1) Turn on block heater to 95°C.
2) Mix each sample with 2X Buffer and sample dye
3) Briefly spin each sample to bring the volume to bottom of tube.
4) Incubate each sample at 95°C for 5 min in a heating block to denature the proteins.
5) Briefly spin again to bring the volume to the bottom of the tube, quick cool on ice.

Sample Application:

1) Add electrophoresis buffer ensuring that bottom of plates are well covered.
2) Place the gel inside the chamber on bottom support of electrophoresis chamber.
3) Clamp the gel plates to the electrophoresis chamber. If you are only running 1 gel, a rectangular plastic plate must be clamped on the side of the chamber opposite to the gel side.
4) Remove air bubbles using a 5 ml syringe.
5) Add electrophoresis buffer in the top of the rack.
6) Remove the comb slowly and evenly using 2 hands from both sides and fix any lanes, which have been deformed using a small spatula.
7) With a kimwipe remove debris from the top of the plates, and clean out wells using a pipette.
8) Withdraw the entire volume of the sample into the pipette tip. Add it slowly into the well, injecting the sample.

Gel electrophoresis:

*Immediately following sample application:

1) Put the cover(s) on gel chamber.
2) Turn on power supply (Indicator should be set to measure Voltage not current) For small gels: Use 80-120V.
3) When the sample dyehas run to the bottom of the gel, the run is over. Turn off the power supply and remove the electrodes.
4) Remove the plates carefully from the gel and cut off a corner of the gel to remember the gel orientation. The gel is now ready for electrotransfer of proteins.

Procedure

1) Remove electrophoresis plates from chamber and separate the plates.
2) Cut away unnecessary parts of the gel using a spatula, then measure the size of the gel that remains.
3) Using a paper cutter cut 6 pieces of Whatman paper to the exact dimensions of the gel. Wearing gloves also cut a piece of nitrocellulose membrane to the dimensions of the gel.
4) Assemble the apparatus as shown:

Transfer Procedure

1) Insert the positive and negative plugs into the jacks of the electroblotter. Then plug the leads into the correct locations of the power supply.
2) Turn the power on and set to constant voltage. Transfer for 1.5 hr at 100 mA (for 8.4 x 6 cm gel). This may vary depending on the size of the protein of interest.

Removal of Transfer Membrane

1) Turn off the power supply, disconnect the negative and positive leads from the power supply, and remove the leads from the electroblotter.
2) Using gloves, carefully remove the Whatman papers, gel slab and transfer membrane to a plastic container.
3) Place the membrane in ddH_2O water to rinse.
4) Add Ponceau S stain and briefly rotate. Save the Ponceau S for reuse.
5) Rinse each blot thoroughly with ddH_2O water to decrease the red background. (If the membrane is to be cut, it should be done now while protein bands are visible).
6) Wrap in saran wrap and scan membrane.
7) Rotate membrane in Wash Buffer until the remaining Ponceau S stain is removed.
8) Incubate membrane with blocking solution for 60 min at room temperature with gentle rotation.

9) Incubate membrane with appropriate antibody diluted in blocking solution overnight at 4°C. Membrane is placed face up on a glass plate that has been covered with parafilm. The antibody is applied to membrane.
   *Note: To maintain a moist environment during an overnight incubation, wet a small Kimwipe and form it into a ball and placed on any corner of the plate. The plate is covered over with a heavy object over a plastic container.

Immunodetection

1) Wash with rotation 3 X 5 min in Wash Buffer.
2) Incubate membrane 60 min with appropriate secondary antibody diluted in blocking solution. *Note: The membrane is placed face-up onto the glass plate, which is covered with parafilm. The antibody diluted in blocking solution is applied to the face of the blot, covered in saran wrap.
3) Wash with rotation 3 X 5 min in Wash Buffer.

Enhanced Chemiluminescence Detection

1) Mix ECL fluids 1:1 ratio.
2) Apply fluid to blot and leave for 2 min.
3) Drip off the excess and place in saran wrap.
4) Expose blot to film (time will vary)
5) Develop while clipped to metal film holder (time will vary).
6) Fix for 2 min.

Stripping blots and re-probing

1) Pre-heat the rotating incubator to 50°C.
2) Place one previously probed membrane in a small hybridization tube with 20 mL of Stripping Solution. Wash in rotating incubator for 30 min at 55°C.
3) Wash membrane 3 x 10 min in wash buffer. The blot can now be blocked.

SOLUTIONS

1. Polyacrylamide Solution
   30% (w/v) Acrylamide
   0.8% (w/v) Bisacrylamide
   Filter using 15 cm Whatman circular filter paper.
   Store at 4°C

For 400 ml: Using gloves, measure out 120 g of acrylamide and 3.2 g of bisacrylamide and volume up to 400 ml with dH_2O. Suction filter.

2. Under Tris Buffer
   1 M Tris-HCl pH 8.8 (60.5 g /500 ml)

3. Over Tris Buffer
   1 M Tris-HCl, pH 6.8 (12.1 g /100 ml)
   Bromphenol Blue (for colour)

   Store at 4°C

4. Ammonium Persulfate (APS)
   10% (w/v) APS in ddH_2O (1 g/10ml)
   store at 4°C

5. Sodium Dodecyl Sulfate (SDS)
   10% (w/v) in ddH_2O (1 g/10ml)
   Store at room temperature.

6. TEMED

7. Electrophoresis Buffer pH=8.3 (10 L)

25.0 mM Tris	30.34 g
192.0 mM Glycine	144 g
0.1% (w/v) SDS	10 g

8. 6X SDS Sample Dye (10 ml; store in 1ml aliquots at -20°C)

1M Tris (pH 6.8)	3 ml
DTT	0.926 g
Bromophenol Blue	0.06 g
100 % glycerol	6 ml
SDS	1.2 g
dH_20	1 ml

9. *tert*-Amyl alcohol, 99%

REAGENTS

1. Transfer buffer

0.025M Tris HCl, pH 8.3	6.057 g
0.15M Glycine	22.52 g
20% MeOH	400 ml

*make up to 2 L with ddH_20

2. Ponceau S

Dilute contents of bottle up to 150 ml with ddH_20.

3. Wash Buffer

Tris-HCl, pH 7.5	12 g
NaCl	58.5 g
0.1% Tween20	10 ml

4. Blocking Solution

5% (w/v) Skim Milk in Wash Buffer OR
5% (w/v) BSA in Wash Buffer

5. ECL Fluid

6. Film/Developer/Fixer

7. Stripping Buffer (for 1 L)

Tris-HCl, pH=6.8	20 g
β-mercaptoethanol	7 ml
SDS	20 g

*volume up to 1 L with ddH_2O

2.4 MITOCHONDRIAL ISOLATION FROM C2C12 MYOBLASTS

References: Frezza et al. Nature Protocols, 2007, 2:287-95

SOLUTIONS:

Mitochondrial Isolation Buffer (MIB) (*make fresh)

1. 10 ml of 0.1 M Tris-MOPS (store at 0-4°C)
   - 0.1 M Tris — 6.05 g / 500 ml
   - pH to 7.4 using MOPS

2. 1 ml of 0.1 M EGTA/Tris (store at 0-4°C)
   - 0.1 M EGTA — 19.05 g / 500 ml
   - pH to 7.4 using Tris

3. 20 ml of 1 M sucrose (*make fresh)
   - 1 M sucrose — 34.33 g / 100 ml

ISOLATION PROCEDURE:

This final isolation procedure has been determined to be the optimal method for the isolation of intact mitochondria from the tissue culture of C2C12 myoblasts through differential centrifugation. The entire procedure is done at 4°C (everything to be kept on ice).

1: Set out materials (get 2 buckets of ice and chill Teflon pestle and glass potter (15 ml), centrifugation tubes, 15 ml conical tube, 200 ml of MIB and PBS on ice).

2: Remove the 10 cm plates from the incubator, and wash 2x with ice-cold PBS (keep plates on ice).

3: Add ~1.5 ml of MIB per plate, and quickly and gently scrape the plates with a rubber policeman, rotate the plate 45° and re-scrape to ensure all the cells have detached. Transfer the scraped cells into chilled pre-labelled mitochondrial isolation tube and keep on ice and cap when done. If using for mitochondrial respiration use a minimum of 10 x 10 cm plates.

---- Repeat this step for each sample ----

4: At a centrifuge setting of 600 g, with Beckman JA25.5 ROTOR, spin the samples for 10 min. Discard the supernatant and Resuspend the pellet in 3 ml of ice-cold MIB.

5: Transfer the suspension into a chilled 15 ml potter. Homogenize the cells using the Potter-Elvehjem PTFE Tissue Grinders at 800 rpm for 35 strokes (~4.5 min). Set timer to ensure consistency between samples.

6: Transfer the homogenate to a fresh tube and spin for 10 min at 600g, transfer only the supernatant gently through a falcon tube fitted with a 45 um filter, being careful to avoid the pellet.

7: Collect the supernatant and (contains mitochondria and cytosol) and transfer to a clean pre-chilled mitochondrial isolation tube. Quick spin at 600 g for 3 min to ensure that any remaining cellular debris is pelleted, now transfer only the supernatant to the last fresh tube.

8: Centrifuge the supernatant at 9,000 x g for 10 min. at 4°C.

9: Discard the supernatant and the resultant pellet is the mitochondria.

10: Gently Resuspend the pellet in 400 µl of M1B and transfer mitochondrial solution to a 1.5 ml eppendorf.

11: Spin in a microcentrifuge at 9,000 x g for 10 min. at 4°C.

12: Discard the supernatant and re-suspend the mitochondria in 80-120 µl of MIB depending on mitochondrial yield. Record the final volume and perform a Bradford assay to assess total µg of mitochondrial yield.

2.5 RNA ISOLATION

PROCEDURE:

1) Homogenize (approximately 30 sec. @ 30-40% power) tissues (200 mg) at 30% in 2 ml Tri-reagent in a 13 ml Sarstedt tube;

OR

Homogenize (approximately 30 sec. @ 30-40% power) tissues (200 mg) at 30% in 1.25 ml solution D + 1.25 ml phenol + 0.125 ml 2M sodium acetate (pH 4.0) in a 13 ml Sarstedt tube

**Note: The homogenizer must be sterilized in 0.1M NaOH and rinsed in sterile water prior to use. Rinse in sterile water between samples.

2) Let stand for 5 min at room temperature;

3) Add 0.4 ml chloroform and shake vigorously for 15 sec, let stand for 2-3 min at room temperature;

4) Spin at 12,000 *g* for 15 min at 4°C;

5) Transfer aqueous phase to 13 ml Sarstedt tube;

6) Add 1 ml isopropanol, gently shake, and allow precipitation of RNA for 5-10 min at room temperature;

7) Spin at 12,000 *g* for 10 min at 4°C;

8) Remove supernatant and add 0.7 ml 75% ethanol;

9) Transfer RNA to eppendorf tube;

10) Rinse 13 ml Sarstedt tube with 0.3 ml 70% ethanol, add to eppendorf tube and mix by vortexing;

11) Spin 5 min in eppendorf centrifuge at 4°C;

12) Discard supernatant;

13) Dry pellet under a vacuum in dessicator (DO NOT DRY PELLET WITH CENTRIFUGATION UNDER A VACUUM);

14) Dissolve pellet in 50-200 µl sterile distilled DEPC water and measure absorbance at 260 nm and 280 nm.

REAGENTS:

1. *Solution D (Denaturing solution)*

4 M Guanidinium Thiocyanate	125 g
25 mM of 1 M stock NaCitrate (pH 7.0)	6.6 ml
N-Lauroyl Sarcosine;Sigma L-5125 (0.5% Sarcosyl)	1.32 g
ddH_2O	160 ml

**Note: make up solution D and store at RT for up to 3 months. On the day of the experiment, mix 50 ml of Solution D with 0.36 ml of beta-Mercaptoethanol (0.1 M b-MEtOH)

2. *Phenol (Nucleic acid grade)*
   a) Melt solid phenol at 68 °C (cap loose) in H_2O;
   b) Add 0.25 g 8-hydroxyquinoline to 250 ml of phenol, mix;
   c) Add 250 ml 1.0 M Tris HCl (pH 8.0) and stir overnight at 4 °C covered in foil
   d) Remove supernatant;
   e) Add 250 ml 0.1 M Tris-HCl containing 0.2 % b-MEtOH (0.178 ml/100 ml for S.G. = 1.12) and mix thoroughly;
   f) Allow solution to settle and remove supernatant;
   g) Repeat 2 more times as above or until pH of phenol is > 7.6 (test with pH paper).
   h) Store in 25-50 ml aliquots at -20 °C.

3. *2.0 M Na Acetate* (pH 4.0)
   10.88 g/100 ml sterile H_2O

4. *75% ethanol in sterile H_2O*
   (75 ml ethanol + 25 ml dH_2O)

2.6 REVERSE TRANSCRIPTION, FIRST STRAND cDNA SYNTHESIS

First-strand cDNA synthesis is performed following the manufacturer's recommendations that are outlined below:

REAGENTS:

1. total RNA (isolated as described)
2. Oligo$(dT)_{12-18}$
3. 10 mM dNTPs (dATP, dTTP, dCTP, dGTP; 10 mM each)
4. Sterile ddH_20
5. RNAse OUT (40 units/ µl)
6. 0.1 M DTT
7. 5X First-strand Buffer
8. SuperScript II RT

*Note: All reagents except RNA are supplied with the SSII kit from Invitrogen.

PROCEUDRE:

1. Add following components to a nuclease/ RNA-free 500 µl eppendorf:

Oligo$(dT)_{12-18}$	1µl
1 µg of RNA	x µl
dNTP mix	1 µl
Sterile ddH_20	to 20 µl

2. Heat mixture to 65°C for 5 minutes and quick chill on ice. Collect the contents with a quick spin in a tabletop microcentrifuge and then add:

5X First-strand buffer	4 µl
0.1 M DTT	2 µl
RNAse OUT	1 µl

3. Mix contents of tube gently and incubate at 42°C for 2 minutes.
4. Add 1 µl (200 units) of Superscript II RT and mix by pipetting gently up and down.
5. Incubate at 42°C for 50 minutes.
6. Inactivate the reaction by heating at 70°C for 15 minutes.
7. cDNA is ready for use in PCR amplification.

2.7 POLYMERASE CHAIN REACTION (PCR)

1) 2 ug of RNA is converted to 2 ug of cDNA (STOCK cDNA)

2) We dilute STOCK cDNA to 1:30 (2 uL STOCK cDNA added to 58 uL nuclease-free ddH_2O)

3) We add 4 μL of diluted cDNA, thus loading 10 μg cDNA per well

4) For SYBR Green analyses, primers were optimized, diluted and mixed with PerfeCTa SYBR® Green SuperMix, ROX Master Mix and nuclease-free ddH_2O

5) Total reaction volumes were always 25 μL

6) Samples must be duplicated to ensure accuracy.

7) Use negative wells to monitor contamination, using nuclease-free ddH_2O in place of cDNA.

8) Check for nonspecific amplification and primer dimers by analyzing melt curves

2.8 WHOLE CELL RESPIRATION WITH OXOPLATE

EQUIPMENT REQUIRED:

- 96-well Flat Bottomed OxoPlate – OP96C
  Manufacturer – PreSens (http://www.presens.de/)
  North American Distributor – Innovative Instruments Inc.
  (http://www.3i-usa.com/)
- Fluorescence Plate Reader
- 96-well plate sealing film

SOLUTIONS REQUIRED:

1. 0% O_2 Standard
2. 100% O_2 Standard
3. Growth Media – Phenol Red Free

SOLUTION PREPARATION:

Adapted from OxoPlate Manual

0% O_2 Standard:

1. Add 150mg of sodium sulfite (Na_2SO_3) to a 15 mL screw top tube.
2. Add 15 mL of ddH_2O and seal tube
3. Vortex and allow >1 minute for oxygen to be depleted from solution

Notes:

- Must use a screw top lid and use enough ddH_2O to almost entirely fill container. This will minimize any dissolving of O_2 from the air in the tube.
- DO NOT REPLACE ddH_2O with Growth Media
- Shelf life is ~24 hours

100% O_2 Standard:

1. Aliquot 25 mL of Phenol Red Free Growth Media into a 50 mL screw top tube.
2. Shake vigorously for 2 minutes.
3. Loosen screw top and gently rotate tube to decrease foaming and prevent oversaturation of solution.

Notes:

- Shelf life is ~24 hours

PROTOCOL:

1. Day 1:
    a. All conditions must be performed as a minimum of 3 replicates.
    b. Perform all work in darkness and protect the OxoPlate from light at all times.
    c. Plate 8,000 cells/well into wells to be used for experiment.
        i. DO NOT PLATE CELLS IN WELLS FOR STANDARDS
        ii. A sample plan is included below.
    d. Cover plate, protect from light, and incubate
        i. Incubate long enough for cells to adhere (recommended 24 hours)

2. Day 2:
    a. Prepare standards (0% O_2 Standard and 100% O_2 Standard)
    b. Warm all cell culture media and drugs prior to beginning.
    c. Add 400 µL of standards to at least 3 empty wells per standard. Do not allow mixing.
    d. Carefully aspirate all cell culture media from wells containing cells
    e. Add 400 uL pre-warmed Phenol Red Free Growth Media or Phenol Red Free Growth Media with drug treatment quickly to each well.
    f. Seal with 96-well plate sealing film
    g. Immediately read on fluorescent plate reader with the parameters listed below.
    h. If required, correct for differences in cell number.

Fluorescence Plate Reader Settings:

- Reading Type: Kinetic
- Reader: Synergy HT-I on: Fluorescence
- Filer Set: 2
- Excitation: 530/25 (for both)
- Emission: 645/40 and 590/35
- Optics Position: Bottom (for both)
- Sensitivity: 50 (for both)
- Click Options (same for both)
    - Nb Samples per Well: 20 – *Can decrease reading time by reducing this number*
    - Delay before Sampling: 300 msec – *Can decrease reading time by reducing this number*
    - Delay between samples: 1 msec
- Select: Kinetic…
    - Run Time: 03:30:00
    - Click Minimum

    - Interval should be 00:02:51 with above settings
    - Check Allow Well Zoom during read
- Temperature Control: Yes
- Check Pre-Heating
- Temperature: 37ºC
- Lag time: 00:00:00
- Change First and Last well depending on number of wells being used with less wells you can go back to the Kinetic… options and click minimum and the time interval will reduce.

2.9 CYTOCHROME C OXIDASE (COX) ASSAY FOR MICROPLATE READER

Cell extract containing cytochrome c oxidase is added to the test solution containing fully reduced cytochrome c. The rate of cytochrome c oxidation is measured over time as a reduction in absorbance at 550 nm. The reaction is carried out at 30^{o} C.

REAGENTS

1. Horse Heart Cytochrome c (Sigma, C-2506)
2. Sodium Dithionite
3. 100 mM K-Phosphate Buffer (KPO_4; pH to 7.0)
   -make and mix equal proportions of 0.1 M KH_2PO_4 and 0.1 M $K_2HPO_4.3H_2O$
4. 10 mM K-Phosphate Buffer
   -dilute 100 mM K-Phosphate Buffer 1:10 with ddH_2O

PROCEDURE

1. Immediately following the completion of the enzyme extraction protocol from cells, proceed to making Test Solution. Add the following to a scintillation vial:

- weigh out 20 mg of horses heart cytochrome c
- add 1 ml of 10 mM KPO_4 buffer and fully dissolve cytochrome c
- make up a small volume of 10 mg/ ml sodium dithionite- 10 mM KPO_4 stock solution (Note: make fresh each experiment and use within 20 minutes)
- add 40 µl of dithionite stock solution to the Test Solution and observe the red to orange colour change
- add 8 ml of ddH_2O
- add 1 ml of 100 mM KPO_4 buffer (Note: the Test Solution becomes light sensitive at this step; make sure to the cover vial with aluminum foil).

2. Add 300 µl of Test Solution into 4-8 wells of a 96-well microplate and incubate at 30°C for 10 minutes to stabilize the temperature and absorbance.

3. Open KC4 plate reader program. Select CONTROL icon, then PRE-HEATING tab, enter 30°C and select ON (Do not run assay until KC4 temperature has reached 30°C).
4. Set-up of COX activity protocol on computer.

5. Select WIZARD icon, then READING PARAMETERS icon.

- Select Kinetic for Reading Type.
- Select Absorbance for Reader and 550 nm for wavelength (drop-down).
- Select Sweep for Read Mode.
- Select 96 Well Plate (default) for Plate Type.
- Enter first and last well to be read (eg. A1 and A4 if reading 4 samples simultaneously).
- Select Yes and Pre-heating and enter 30 for Temperature Control.
- For Shaking enter 0 for both intensity and duration (shaking is not necessary and it will delay the first reading).
- Do not select either of the two options for Pre-reading.
- Click on the KINETIC… rectangular tile to open the Kinetic window.
- Enter run time (1 minute is recommended) and select MINIMUM for Interval time (under these conditions the minimum Interval time should be 3 seconds).
- Select Allow Well Zoom During Read to see data in real time (optional).
- Under Scales, checkmarks should appear for both Auto check boxes. Do not select Individual Well Auto Scaling.
- Press OK to return to Reading Parameters window. Press OK to return to Wizard window. Press OK. Do not save the protocol.

6. Set the micropipette to 225 µl and secure 4-8 tips on the white projections (make sure they are on tight and all the same height).

7. In a second, clean 96 well plate, pipette samples into 4-8 empty wells (start with A1). *Recommended volumes:* 65 µl of enzyme extract from C2C12 cells.

8. Remove microplate with Test Solution from the incubator (as long as it has been incubating for 10 minutes). Place this plate beside the plate with the sample extracts in it.

9. On KC4 program, select the READ icon and press the START READING icon, then press the READ PLATE button. A box will appear that says, "Insert plate and start reading". Do not press OK yet, but move the mouse so that the cursor hovers over the OK button.

10. Using the micropipette (set to 225 µl) carefully draw up the Test Solution. Make sure the volume is equal in all the pipette tips, and that no significant air bubbles have entered any of the tips.

11. Pipette the Test Solution into the wells with the sample extracts (the second plate). As soon as all the Test Solution has been expelled from the tips (do not wait for the second push from the multipipette), place the plate onto the tray of the plate reader and with the other hand on the mouse, press the OK button. (Speed at

this point is paramount, as there is an unavoidable latency period between the time of pressing the OK button and the time of the first reading.)

12. If desired, add 5 μl KCN to one of the wells to measure any absorbance changes in the presence of the CYTOX inhibitor.

13. Once reading is complete, hold the CTRL key on the keyboard, and use the mouse to click once on each of the squares corresponding to a well that had sample in it. Once all the desired wells have been highlighted by a black square (up to a maximum of 8 wells), let go of the CTRL key and a large graph will appear with lines on it representing each sample.

14. To obtain the rate of change of absorbance over different time periods, select Options and enter the amount of time for which you would like a rate of change of absorbance to be calculated. The graph, along with one rate (at whichever time interval is selected) for each sample can be printed on a single sheet of paper, and the results can be saved.

15. The delta absorbance will appear in units of mOD/min and the number given will be negative. Convert this to OD/min by dividing by 1000 and omit the negative sign in the calculation. (eg. if Mean V: -394.8 mOD/mn, then use 0.395 OD/min)

CALCULATION:

$$\text{CYTOX activity} = \frac{\text{mean dealta absorbance/ minute x total volume (ml) x 1000}}{\text{18.5 (µmol/ml extinction coeff.) x sample volume (ml) x total µg/ well}}$$

Example Calculation:

55 µl of enzyme extraction
230 µl of Test Solution
Mean V: -584.30 mOD/mn
Protein concentration: 3.023 µg/ µl
Total µg/ well: 151.15

$$\text{COX activity} = \frac{(0.5843)(0.285)(1000)}{(18.5)(0.055)(3.023 \times 55)}$$

COX activity = 0.967 nmol/min/µg protein

2.10 FURA-2-AM CA2+ IMAGING

All the media used is DMEM without phenol red.

1. Wash each chamber 2X with media. Add 500 uL DMEM without phenol red to each chamber.

2. Add 5uL of Fura-2-AM (Invotrogen) and 5uL of pleuronic acid (Invitrogen) to 1mL of DMEM. Add 500 uL per chamber and incubate at 37^{o}C for 45 minutes.

3. Wash 2X with DMEM, and add fresh media. Incubate for 20 min to allow de-esterification to occur i.e. Fura-2AM doesn't exit.

4. Imaging is carried out by using 340 and 380 excitation filters.

APPENDIX C
3.0 ADDITIONAL CONTRIBUTIONS

During my Doctorial tenure, I made contributions to the following publications not included in my Dissertation:

1. A Saleem*, **S. Iqbal***, Y. Zhang , D.A. Hood. The Role of p53 in regulating Mitochondrial Morphology, Mitophagy, Protein Import and assembly within Skeletal Muscle. (* contributed equally, in preparation)

2. Y. Zhang, G. Uguccioni, V. Ljubicic, I Irrcher, K. Singh, **S Iqbal**, S. Ding, D.A. Hood. Contractile activity-induced intracellular signaling on PGC-1α gene expression in skeletal muscle cells. (in preparation)

3. Y. Zhang, **S. Iqbal**, M. O'Leary, K.J. Menzies, A. Saleem, S. Ding, D.A. Hood. Non-apoptotic Functions of Bax and Bak:Role in Mitochondrial Protein Import in Skeletal Muscle. American Journal of Physiology, 2013 Sep: 305(5): C502-11.

4. M.F.N. O'Leary, A. Vainshtein, **S. Iqbal**, O. Ostojic and D.A. Hood. Adaptive plasticity of autophagic proteins to denervation in aging skeletal muscle. American Journal of Physiology:Cell Physiology, 2013 Mar;304(5):C422-30

5. D.A. Hood and **S. Iqbal.** *Invited Editorial* – Muscle mitochondrial ultrastructure: New insights into morphological divergences. Journal of Applied Physiology, 2013 Jan: 114(2): 159-160.

6. D.A. Hood, O. Ostojic, A. Saleem, H. Carter, A. Vainshtein, **S. Iqbal**. Chapter 14: Molecular Basis of Exercise Training Adaptations in Skeletal Muscle. Exercise Physiology in Canada (B.M. MacIntosh, Editor), 2012.

7. A. Saleem, H. Carter, **S. Iqbal**, and D.A. Hood. Role of p53 within the regulatory network controlling muscle mitochondrial biogenesis. Exercise and Sport Sciences Reviews, 2011 Oct;39(4):199-205.

8. J.H. Huang, V. Ljubicic, A.M. Joseph, **S. Iqbal,** D.A. Hood. Effect of age on the processing and import of matrix-destined mitochondrial proteins in skeletal muscle. Journal of Gerontology: Biological Sciences, 2010 Feb; 65 (2):138-46.

During my Doctorial tenure, I made the following contributions to conference abstracts:

1. **S. Iqbal** and D.A. Hood. Oxidative stress-induced mitochondrial fragmentation and movement in skeletal muscle cells. Canadian Exercise and Physiology Conference, Toronto, Canada, 2013 **(Poster Presentation)**

2. J.M. Memme, M.J. Crilly, L.D. Tryon, **S. Iqbal** and D.A. Hood. Denervation-induced adaptations in autophagy and mitochondrial morphology proteins. MHAD, Toronto, Canada, 2013

3. **S. Iqbal** and D.A. Hood. The regulation of mitochondrial movement within skeletal muscle. Experimental Biology Conference, Boston, USA, 2013 **(Poster Presentation)**

4. **S. Iqbal** and D.A. Hood. Muscle Mitochondria Morphology in Skeletal Muscle. Kinesiology and Health Science Seminar, Toronto, Canada, 2012 **(Oral Presentation)**

5. H.N. Carter, M.F.N. O'Leary, **S. Iqbal,** A. Vainshtein, O. Ostojic, S.F. Pastore, D.A. Hood. Profiling Mitochondrial Turnover in Aged Skeletal Muscle: Mitophagy Arrested? MHAD, Toronto, Canada2012.

6. Y. Zhang, M.F.N. O'Leary, K.J. Menzies, A. Saleem **S. Iqbal**, D.A. Hood. Mitochondrial Protein Import in Skeletal Muscle of Wild Type (WT) and Bax/Bak knockout (DKO) mice: The non-apoptotic role of Bax and/or Bak. MHAD, Toronto, Canada, 2012.

7. **S. Iqbal** and D.A. Hood. Alterations in Mitochondrial Fission and Fusion Proteins with Chronic Muscle Use and Disuse. Experimental Biology Conference, Washington, USA, 2011 **(Poster Presentation)**

8. **S. Iqbal** and D.A. Hood. Skeletal Muscle Mitochondria Along Microtubules. Canadian Exercise and Physiology Conference, Toronto, Canada, 2010 **(Oral Presentation)**

9. **S. Iqbal** and D.A. Hood. Analysis of mitochondrial dynamics in C2C12 myoblasts. Muscle Health Awareness Day, Toronto, Canada, 2010 **(Poster Presentation)**

10. **S. Iqbal** and D.A. Hood. Quantification of Dynamic Mitochondrial Morphologies in Myoblasts. Experimental Biology Conference, Anaheim, USA, 2010 **(Poster Presentation)**

11. **S. Iqbal** and D.A. Hood. Mitochondrial Fission and Fusion Among Fibre Types and in Myoblasts. Ontario Exercise Physiology Conference, Barrie, Canada, 2010 **(Oral Presentation)**

12. **S. Iqbal** and D.A. Hood. Fission and Fusion of Mitochondria in Skeletal Muscle. Kinesiology and Health Science Seminar, York University, Toronto, Canada, 2009 **(Oral Presentation)**

13. **S. Iqbal**, V. Ljubicic, and D.A. Hood. Electron Microscopic Evaluation of Mitochondria and Aged Muscle: Effect of Chronic Contractile Activity. International Biochemistry of Exercise Conference, Guelph, Canada, 2009 (**Poster Presentation)**

14. **S. Iqbal**, A.M. Joseph, and D.A. Hood. Molecular Basis of Mitochondrial Morphology in Aging Skeletal Muscle. Ontario Exercise Physiology Conference, Barrie, Canada, 2009 **(Oral Presentation)**